ARSENIC REMOVAL FROM WATER USING PURE AND METAL DOPED TITANIA NANOPARTICLES

BY

MUHAMMAD IHSAN DANISH

(2010-NUST-MS PhD-Env S-05)

A thesis submitted in partial fulfillment of

the requirements for the degree of

Master of Science

in

Institute of Environmental Sciences and Engineering (IESE)
School of Civil and Environmental Engineering (SCEE)
National University of Sciences and Technology (NUST)
Islamabad, Pakistan
(2012)

It is certified that the contents and form of the thesis entitled

ARSENIC REMOVAL FROM WATER USING PURE AND METAL DOPED TITANIA NANOPARTICLES

Submitted by

MUHAMMAD IHSAN DANISH

have been found satisfactory for the requirements of the degree of
Master of Science in Environmental Science

Supervisor: _____
Dr. Ishtiaq A. Qazi
Associate Dean & Professor
IESE, SCEE, NUST

Member:_____
Dr. Zahir-ud-Din Khan
Associate Professor
IESE, SCEE, NUST

Member:_____
Dr. Muhammad Ali Awan
Assistant Professor
IESE, SCEE, NUST

External Member: _____
Dr. Amir Habib
Assistant Professor
SCME, NUST

In the name of Allah the most beneficent and the most merciful

DEDICATION

I would like to dedicate this thesis to my beloved parents. For all their support, financially and emotionally; I will remain ever indebted to them.

ACKNOWLEDGEMENTS

This thesis is the end of my journey in obtaining my MS. I have not travelled in vacuum in this journey. This thesis has been kept on track and been seen through to completion with the support and encouragement of numerous people including my well wishers, my friends, colleagues and my institution.

I am indebted to my supervisor, **Prof. Dr. Ishtiaq A. Qazi** for all his guidance and support throughout the complete MS journey. His dedication to research is highly inspiring. Without his guidance it would have been difficult to present the thesis in its current form.

I would like to thank **Dr. Amir Habib** and **Mr. Akif Zeb** who were instrumental in providing valuable suggestions and inputs during the entire duration of the project.

I would also like to take this opportunity to thank **Dr. Zahir-ud-din Khan** and **Dr. Ali Awan** for their valuable time and suggestions.

I cannot find words to express my gratitude to my parents and my youngest sister for their endless love, prayers and encouragement.

Last, but by no means least, I thank all my colleagues who in any way helped me achieving the desired outcomes from this project. To those who indirectly contributed in this research, your kindness means a lot to me. Thank you very much.

For any errors or inadequacies that may remain in this work, of course, the responsibility is entirely my own

Muhammad Ihsan Danish

TABLE OF CONTENTS

LIST OF ABBREVIATIONS

AB	Arsenobetaine
AC	Arsenocholine
As(III)	Arsenite
As(V)	Arsenate
Ag-TiO_2	Silver doped titania
AAS	Atomic absorption spectrophotometer
Cr- TiO_2	Chromium doped titania
DMA	Dimethylarsonate
EC	Electrical conductivity
EDS	Energy dispersive x-ray spectroscopy
eV	Electron volt
Fe- TiO_2	Iron doped titania
HOMO	Highest occupied molecular orbital
LD50	Lethal dosage 50
LI	Liquid impregnation
LUMO	Lowest unoccupied molecular orbital
MCA	Maximum contaminant level
MMA	Monomethylarsonate
PCRWR	Pakistan Council for Research in Water Resources
PDWQS	Pakistan Drinking Water Quality Standards
RO	Reverse osmosis
TiO_2	Titanium dioxide
XRF	X-ray fluorescence
XRD	X-ray diffraction
SEM	Scanning electron microscope
UV	Ultra violet

LIST OF SYMBOLS

Symbol	Description	Unit
B	Langmuir constant	Dimensionless
C	Speed of light	cm/sec
C_o	Initial arsenic concentration	mg/L
C_f	Final arsenic concentration	mg/L
C_t	Arsenic concentration after time t	mg/L
e^-	Electron	Dimensionless
Eg	Band gap	eV
H	Initial adsorption rate	mg/g min
h^+	Hole	Dimensionless
Hν	Incident light	eV
K	Pseudo-second order rate constant	g mg^{-1} min^{-1}
K_F	Freudlich	
K_T	Thomas rate constant	ml/min mg
k_{YN}	Yoon-Nelson rate constant	L/min
M	Mass of nanoparticles	Grams
N	Freudlich	
q_m	Arsenic adsorbed per unit weight	mg/g
R_L	Langmuir constant	Dimensionless
V	Effluent volume	L
λ	Wavelength	nm
θ	Effluent flow rate	L/min
τ	50% breakthrough time	min
α	Absorption coefficient	cm^{-1}
$\beta_{1/2}$	Full width of a diffraction line at one half of maximum intensity	Radians

LIST OF TABLES

Chapter 2

Chapter 4

LIST OF FIGURES

ABSTRACT

Nanosized metal oxide, Titania provides high surface area and specific affinity for the adsorption of heavy metals, including Arsenic (As), which is posing a great threat to world population due to its carcinogenic nature. In this study As(III) adsorption was studied on Pure and metal (Ag and Fe) doped Titania nanoparticles which were synthesized by liquid impregnation method with some modifications, with doping level of 1 atom-% weight. These nanoparticles were characterized by X-ray diffraction (XRD), X-ray florescence (XRF), UV/Vis diffuse reflectance spectroscopy and scanning electron microscopy (SEM). The crystallite sizes of the synthesized nanoparticles were in the range of 30 to 40 nm. Band gap was calculated using Kubelka-Munk function it was found that metal doping shifted the absorption band into visible region. Effect of operational parameters like dose of nanoparticles, initial As(III) concentration and pH were evaluated at 25^{o}C. The data obtained gave a good fit with Langmuir and Freundlich isotherms and the adsorption was found to conform to pseudo second order Kinetics. In batch studies over 90% of arsenic removal was shown by both Fe and Cr-doped Titania nanoparticles from a solution containing up to 2ppm of the heavy metal. The synthesized nanoparticles were coated on glass beads by Heat Attachment Method. Fixed bed columns of nanoparticles coated on glass beads were made for As(III) removal under different operating conditions. Thomas and Yoon-Nelson models were applied to predict the breakthrough curves and to find the characteristic column parameters useful for process design. The theoretical curves based on model parameters gave a good fit with the practically observed results. The exhausted columns were regenerated by using 10 % NaOH solution. After regeneration, only a loss of less than 9% in the removal efficiency of the columns was observed.

CHAPTER 1

INTRODUCTION

1.1 BACKGROUND

To meet the demands of fast growing world population for drinking water, there is an increasing pressure on both surface and ground water resources. In some parts of the world, this has resulted in utilization of ground waters that are highly contaminated with heavy metals including Arsenic. In earth crust arsenic is ranked as the 20th most abundant element (Gulledge, 1973). In water it is mostly found in inorganic form, namely arsenite [As(III)] and arsenate [As(V)]. The source of these two ions in water is either natural or byproducts of industrial waste.

Arsenic is well known for its toxic and carcinogenic nature from a very long time. Severe health effects (both cancer and non-cancer) results from ingestion of inorganic arsenic (NRC, 1999). Due to its carcinogenic nature it is classified as Class A carcinogen by USEPA. Continues exposure to low arsenic concentration has been associated to some serious health problems, like cancer of skin, kidney, lungs and bladder. Human population is exposed to arsenic contamination from different sources but the most direct exposure results from drinking water contaminated with arsenic. The exposure of human population to arsenic has been enhanced since people have started using underground water (more contaminated with arsenic) in preference to surface water (contaminated with microbes). Due to its toxic nature the USEPA in January 2006, has reduced the maximum contaminant level (MCL) of arsenic in drinking water from 50μg/L to 10μg/L. The drinking water industry has to come up with new and advance treatment methods to meet this new standard.

A lot of research has been done on the removal of arsenic from water. Many technologies have been applied, like coagulation/flocculation, ion exchange resins, reverse osmosis and adsorption. Among adsorbents, activated carbon, activated alumina, iron oxide, zeolites and some natural products have been used. The old

arsenic contamination level of 50 ppb can be achieved easily with the conventional techniques such as reverse osmosis, coagulation, activated alumina and ion exchange; however the new maximum contamination level (MCL) of 10 ppb need the use of more advanced technologies.

Arsenic shows a high affinity for adsorption on Titania nanoparticles. The use of titania nanoparticles for arsenic adsorption is not a very old technique. Titania because of its chemical and physical stability, porous and non corrosive nature, lower cost and no toxicity finds enormous applications in the field of environment. Titania has enormous affinity for arsenic and adsorbs it over a wide range of pH (2-14). Like other adsorbents, Titania also has strong affinity towards As(V) for adsorption. But unlike others Titania is a strong photocatalyst, it oxidizes the more toxic As(III) to less harmful As(V) and then adsorbs it. This photocatalytic reaction needs UV light, which is only 5% of the incident sunlight. In this research both the sorptive and photocatalytic properties of Titania are enhanced by doping it with some metalas, like silver, chromium and iron. Metal doping shifts the absorption band into visible region thus enabling Titania to use a broad spectrum of light.

The pure and metal doped Titania nanoparticles were then coated on glass beads and packed in column. Column studies were conducted to evaluate the As(III) removing potential of the columns.

1.2 RESEARCH OBJECTIVES

The objectives of this research are;

- To determine the adsorption potential of Titania based nanoparticles for arsenic removal
- To find which metal doping can give excellent results for arsenic removal
- Optimization of pH for arsenic removal
- Establishing the kinetics of arsenic removal by TiO_2
- To conduct column studies and find the different column capacities
- To determine the effect of various parameters on column performance

CHAPTER 2

LITERATURE REVIEW

2.1 ARSENIC OCCURRENCE

Naturally occurring elemental arsenic is ubiquitous. It is the 20th most abundant in earth's crust, 14th in seawater and 12th in the human body (Deedar et al., 2009; Mandal and Suzuki, 2002). Although it is present in air, water and soil, the most direct source to which human population is exposed is drinking water contaminated with arsenic. The presence of arsenic, even at a very high concentration, does not cause any change in odor, taste or visible appearance of water. Therefore it is very difficult to detect the presence of arsenic in drinking water without complex analytical techniques. The increase in arsenic level in drinking water has become a serious environmental concern worldwide. High concentration of arsenic in drinking water has been noticed in many countries of the world, including Argentina, Bangladesh, Canada, Chile, China, Hungary, India, Japan, Mexico, Poland, Taiwan and USA (Jain and Ali, 2000). About, 60-100 million individuals are currently exposed to arsenic contaminated drinking water in India and Bangladesh (Ng et al., 2003).

Ground water contamination with arsenic is believed to be geological, mainly caused by the arsenic bearing sediments releasing arsenic into groundwater aquifers (Pena, M. et al., 2006). Arsenic is never found in free state, it is found largely in combination with oxygen, sulphur and iron (Brewstar, 1994; Jain and Ali, 2000). Naturally over 200 different mineral forms of arsenic are occurring, of which Arsenates are about 60%, sulfides and sulfosalts makes 20% and arsenides, arsenates, oxides, silicates and elemental arsenic makes the remaining 20% (Onishi, 1969; Mandal and Suzuki, 2002). Anthropogenic sources exceed the natural sources of arsenic by 3:1 (Mandal and Suzuki, 2002). The major man-made sources of arsenic contamination are arsenial pesticides, fertilizers, dust of burning fossil fuel, animal and industrial waste disposal (Mandal and Suzuki, 2002).

Arsenic in nature is present in two forms; inorganic and organic. Organic form is mainly found in foodstuff as monomethyl arsenic acid, dimethyl arsenic acid and arseno sugars. Inorganic form occurs in two oxidation states, Arsenate [As(III)] and Arsenite [As (III)]. In natural water As(III) is mainly found as arsenious acid (H_3AsO_3), and As(V) occur as anionic species ($HAsO_4^{2-}$ and $H_2AsO_4^-$) (Clifford and Lin, 1995). Natural water is mostly contaminated with the more toxic inorganic form rather than organic one. Ground water mainly contains As(III) due to the prevailing reducing conditions, while As(V) is mainly found in the more oxidized surface waters. Inorganic arsenic has been made the top priority pollutant by USEPA (Ng et al., 2003).

2.2 CHEMISTRY OF ARSENIC

The metalloid, Arsenic (As) having an atomic number 33 and atomic mass of 74.9216 is a member of group VA of the periodic table. Arsenic speciation in environmental materials is very important due to the different level of toxicity shown by various species. It is found in four different oxidation states (i.e; -3, 0, 3 and 5), which encompasses all the major arsenic species that are present in clinical and environmental samples, like arsenite [As(III)], arsenate [As(V)], arsenic acids ($HAsO_4^{-2}$, $H_2AsO_4^-$ and H_3AsO_4), arsenious acids (including H_3AsO_3, $H_2AsO_3^-$ and $HAsO_3^{-2}$) monomethylarsonate (MMA), dimethylarsonate (DMA), arsenocholine (AC) and arsenobetaine (AB). However, among all these arsenic species arsenite is of particular interest. It is almost 10 times as toxic as As(V) and near 70 times as toxic as the methylated species, MMA and DMA. Both MMA and DMA are moderately toxic, while AB and AC are non-toxic (Kumaresan and Riyazuddin, 2001). In general, inorganic arsenic forms are more toxic for living organisms (including plants, animals and Human beings) and more mobile than organic species (Meharg and Hartley-Whitaker, 2002). These reasons make it necessary to remove As(III) from drinking water.

Arsenic is a redox sensitive element, which means that it can change its form through gain (Reduction) or loss (Oxidation) of electrons. The occurrence, speciation, mobility

and distribution of arsenic depends on many geochemical factors like pH, redox conditions, presence of other ionic species, water chemistry and activity of microbes (Shih, 2005). Arsenate, As(V), is used in agriculture pesticides, glass making and refining of Cu (Conner, 1990; Dutré et al., 1999). Under oxidizing conditions, As(V) is the prevalent form in soils (Pongratz, 1998; Smith et al., 1998a; Turpeinen et al., 1999, 2002) and is dominant in the solid phase of the soil (Montperrus et al., 2002). On the other hand, As(III) is the primary form of As in waste environments (Dermatas et al., 2004) and under reducing condition, like soils saturated with water or soils with significant organic waste or matter (Smith et al., 1998a). As(III) is known to be more mobile and more toxic than As(V) (Panstar-Kallio and Manninen, 1997; Stronach et al., 1997).

Arsenic shows anionic behavior in water. Arsenic acid (H_3AsO_4) predominates at low pH (≤ 2) and aerobic conditions in water, in between pH value of 2 to 11 its anions ($H_2AsO_4^-$ and $H_2AsO_4^{-2}$) replace it. At mildly reduced conditions and low pH arsenious acid appears but as the pH increases it is replaced by $H_2AsO_3^-$ and when the pH value cross 12, $HAsO_3^{-2}$ appears. In the presence of sulphide and at low pH, $HAsS_2$ can arise; arsenic metal, arsine and its derivatives appear at extreme reducing conditions (Kumaresan and Riyazuddin, 2001). The arsenic speciation is shown in the pe Vs pH diagram (Fig.2.1).

Since in solution arsenic form anions, so the other common anions (like Cl^- and SO_4^{-2}) cannot give complexes with it. The complexes of anionic arsenic more act like a ligand in water. It can bind with sulfur, nitrogen and organic carbon. Sulfur and other sulfhydryl groups (cystine, organic dithiols, proteins and enzymes) react with As(III) but amine group and other organics having reduced nitrogen does not react with As(III). However, As(V) reacts in the opposite way, it reacts with reduce nitrogen groups like amines, but does not react with sulfhydryl groups. Carbon reacts with both As(III) and As(V) to from organoarsenicals. The complexation of both the arsenic species by the organic matter dissolved in water makes its sorption as well as its coprecipitation with the solid-phase inorganics and organics difficult; it actually results in an increase in the mobility of different arsenic species in water.

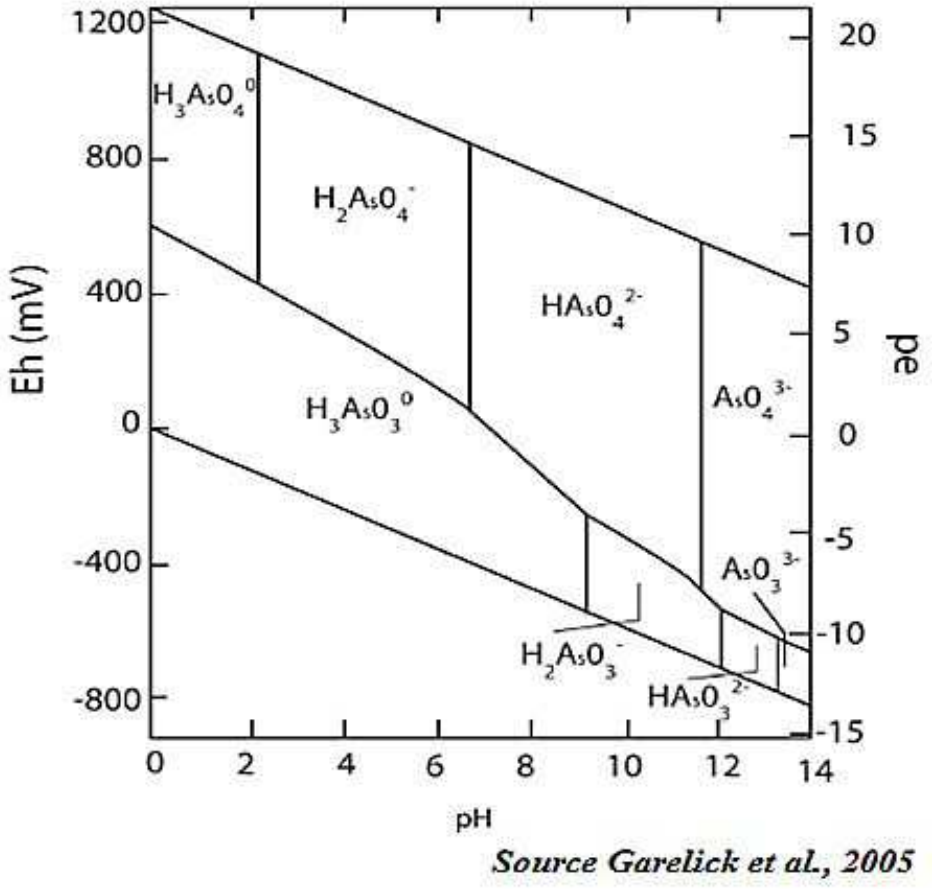

Fig. 2.1: pe Vs pH diagram of arsenic

2.3 EFFECT ON HUMAN HEALTH

Humans are exposed to arsenic contamination mainly through inhalation, skin adsorption or ingestion; however, ingestion, among these is the most prominent form of arsenic intake. Exposure to large arsenic doses can result in severe toxic complications like gastrointestinal disorder (e.g. vomiting, diarrhea and poor appetite etc.), some disturbance in the cardiovascular system and nervous system activities (like heart disease, muscle cramps etc.) and sometime death (National Research Council 2000; Quamruzzaman et al., 2003 ;Abernathy and Morgan 2001).

The rise of arsenic concentration in water has become a serious health concern. The carcinogenic effects of arsenic were not known in early times, harmful health effects arising from arsenic containing compounds were observed as early since 1556 (Peter

Rietkerk, 2007), e.g.it was found that arsenic cobalt "ate away" the skin of worker's hands (Smith et al., 1992). Ingestion of arsenic contaminated drinking water result in large scale harmful health effects (WHO, 2004). In Taiwan, arsenic poisoning caused "Blackfoot Disease," a type of gangrene (Morales et al., 2000). Arsenic in drinking water has been linked to different types of skin cancer, lesions (on the extremities and torso), various neurological disorders, diabetes and hyperkeratosis (smith et al., 2000).

The toxicity of arsenic is mainly dependent on the form in which it is present. The trivalent inorganic arsenic compounds are found to be more toxic than the pentavalant form. Organic arsenic forms (typical in sea food) are not as much toxic as the inorganic ones (present in drinking water). Trivalent arsenic is about 70 times more toxic than oxidized pentavalent state. Inorganic arsenic compounds are about 100 times more toxic than organic arsenic compounds (Jain et al., 2000). A few compounds of arsenic along with their toxicity are listed in Table.2.1 (Chappell et al., 1999). Generally toxicity is measured in mg/kg i.e. milligram of the toxicant per kilogram of the target body weight, that will cause death in half of the individuals who ingest it in a single dose, within a few days. This lethal concentration of that toxicant is known as Lethal dosage 50 (LD50). The following table shows LD50 value for a few arsenic compounds. It must be noted that the lower is the LD50 value, more toxic is the compound.

Table 2.1: Acute toxicity value for different arsenic compounds

Arsenic Form	Oral LD50 (mg/Kg of body weight)
Sodium Arsenite	15- 40
Arsenic Trioxide	34
Calcium arsenate	20-800
Arsenobetane	>10,000

**Source: Chappel et al., 1999*

Exposure of an individual to such high degree of arsenic toxicity is not possible. However, continuous use of drinking water contaminated with lower arsenic concentration for a longer time period can result in serious health hazard (National Research Council 2000; UN 2001; WHO 2001; UNICEF 2006).

The first visible symptoms resulting from exposure to low arsenic concentrations in drinking water are *melanosis* (abnormal black-brown skin pigmentation) and *keratosis* (hardening of palms and soles). Continuous intake of arsenic contaminated water cause de-pigmentation of skin, resulting in white dots which appear in the form of raindrops (this condition is medically termed as as*leukomelanosis*). Further thickening of soles and palms occur resulting in the formation of painful cracks. Medically these symptoms are known as hyperkeratosis which leads to skin cancer (WHO 2001).

Internal body organs may also get attacked by arsenic causing no visible symptoms, thus making it hard to recognize arsenic poisoning. High concentration of arsenic in blood, urine, nails and hairs can act as an indicator of arsenic poisoning in human before the appearance of external visible symptoms (Rasmussen and Andersen 2002).

The carcinogenic effect of inorganic arsenic to humans has been determined by the International Agency for Research on Cancer (IARC, 1980). It has also been classified as a human carcinogen by the United State Environmental Protection Agency (USEPA, 1988). It is classified as a Class I human carcinogen by the International Agency for Research on Cancer (Akif et al., 2010).

According to US-EPA, arsenic in drinking water is suspected to be caused or provoked by the following diseases;

- Cancer of skin, kidney, liver, lungs, bladder and prostate
- Still births
- Post neonatal mortality
- Heart attack
- Diabetes mellitus
- Chronic inflammation of kidneys (Nephritis)
- Degenerative kidney diseases (Nephrosis)
- Hypertension, hypersensitive heart diseases
- Emphysema, bronchitis
- Chronic airway obstruction

- Tumors in the lymph (Lymphoma)
- Black foot disease and development deficit

2.4 GUIDELINE AND STANDARDS

Due to the widespread negative health effects of arsenic on humans, in 1993 WHO lowered the permissible limit of arsenic in drinking water from 50 μg/L (0.05 mg/L) to 10 μg/L (0.01 mg/L, this provisional guideline level is retained by WHO in the latest edition of its standards (WHO, 1993; WHO, 2004). This WHO permissible limit of 10 μg /L for arsenic in drinking water has been adopted by most of the countries including Jordan, Japan, USA, Mongolia, and Syria and by the European Union (EU).

This new MCL of 10μg/L is currently not possible for some countries badly affected by arsenic contamination, including India and Bangladesh; they have retained the MCL of 50μg/L limit. Many other countries like Bahrain, China, Egypt, Oman, Philippines, Saudi Arabia, Sri Lanka, and Zimbabwe, have also retained the older WHO guideline of 50μg/L for arsenic (UN 2001). Canada has adopted a standard of 25μg/L. The toughest standard for MCL of arsenic in drinking water is adopted by Australia, which is 7μg/L.

2.5 ARSENIC PROBLEM IN PAKISTAN

Considering the harmful human health effects due to inorganic arsenic, different investigations have been done in Pakistan. In 2000 Pakistan Council for Research in Water Resources (PCRWR) and UNICEF jointly initiated the first investigation on groundwater arsenic in Attock and Rawalpindi Districts of Pakistan. A second investigation (a detailed one) was carried out through the National Water Quality Monitoring Program by PCRWR. These investigations proved the presence of high amount of arsenic in the groundwater of many cities in the Punjab province including Bahawalpur, Gujranwala, Kasur, Lahore, Multan and Sheikhupura,. Some of the Sindh province cities like Khairpur and Dadu had also high concentration of arsenic in its water.

A recent water study carried out in Punjab (11 cities) by PCRWR shows a high fluoride and arsenic concentrations in the water supply systems of six cities; Bahawalpur, Gujranwala, Kasur, Multan, Lahore and Shaikhupura (PCRWR 2004). Moreover, in these six cities about 2 million people are drinking unhealthy water, some contaminated with a high concentration of arsenic. 20% of Punjab and 36% of Sindh population is exposed to arsenic contamination over 10 ppb in drinking water, similarly 3% of Punjab and 16% of Sindh population is exposed to over 50ppb of arsenic in drinking water (Ahmad et al., 2004). The most alarming situation exists in Kalanwala village (East Punjab) where the arsenic concentration in groundwater is as high as 1900µg/L (Farooqi, A. et al., 2006).

2.6 ARSENIC REMOVAL TECHNOLOGIES

2.6.1 Coagulation/Flocculation

Coagulation is the process of neutralization of charges followed by formation of a gelatinous mass that trap the particles thus forming settleable mass. Flocculation is the gentle agitation that encourages the particles formed to agglomerate into large settleable mass.

Coagulation is the most commonly used treatment process used for arsenic removal in USA (Buswell, 1943). Commonly used chemicals in coagulation/flocculation technique are ferric salts, aluminum salts, ammonium sulphate, copper sulphate, manganese sulphate, etc (Mondal et al., 2006). The metals are removed through the following three main processes during coagulation and flocculation (McNeill, 1994):

- Precipitation: in this process insoluble compound like Al (AsO_4) or Fe (AsO_4) are formed.
- Co-precipitation: in this step the soluble arsenic species are incorporated into a growing metal hydroxide phase.
- Adsorption: in this step the soluble arsenic electrostatically binds to the external surface of the insoluble metal hydroxide.

After coagulation and flocculation, the hydrous aluminum oxide and hydrous Ferrous oxide along with the sorbed arsenic can be removed through filtration (Ashutosh, 2005).

The main disadvantage of the process is the direct addition of coagulants to the water, resulting in an increase in the level of iron or aluminum. The permissible limit of Fe and Al in drinking water according to EU drinking water directive (EC, Council Directive, 1998) is 200ppb. Moreover, being a pH sensitive process, some appropriate reagents are often added to maintain an optimum pH (Adrian Oehmen, 2011) which increases the risk of secondary contamination by these reagents.

2.6.2 Ion Exchange Resins

An ion exchange is a physio-chemical process involving the switching of ions between a solution and a solid resin phase. Synthetic ion exchange resins, due to their greater removal efficiency and regeneration ability are commonly employed for water treatment processes (MWH, 2005). Anion exchange resins, both strong base anion (SBA) and weak base anion (WBA) are used for arsenic removal (Wang et al., 2000). SBA is a better option for arsenic removal from drinking water (Wang et al., 2000).Just like adsorption process, ion exchange process also have preferential tendencies for various ions. The arsenic removal efficiency of the ion exchange process greatly depends on pH of the solution and the concentration of other competing ions, like nitrates, sulfates, selenium and fluorides. The type of resin selected is a function of competing ions and the anion concentration (Ashutosh, 2005). The SBA resins have the following order of selectivity for various water constituents (MWH, 2005).

$$SO_4^{2-} > NO_3^- > HAsO_4^{2-} > NO_2^- > Cl^- > H_2AsO_4^- > HCO_3^- >> Si(OH)_4 , H_3AsO_4$$

Ion exchange is usually recommended for use where there are low sulfates, low TDS and low nitrates (Ashutosh, 2005). Competing ions greatly affect the regeneration frequency, which in turn affect both operational and maintenance cost of the process.

2.6.3 Reverse Osmosis

Reverse osmosis (RO) can also be used for arsenic removal from aqueous solution with efficiency reaching 100% (Ng et al., 2004). The big advantage of RO over adsorption is that removal efficiencies are less affected in the former case than the later by the interfering ions and pH of the water (Sato et al., 2002). However, the As(III) and As(V) removal efficiency has been reported to increase by 20%, by rising pH from 7-10 and from 3-5, necessitating the use of optimum pH value even for RO (Ng et al., 2004). In RO also the removal efficiency is high for As(V) than for As(III), necessitating the pre-oxidation of As(III) to As(V) before treatment (Ng et al., 2004). However, use of oxidizing reagents like chlorine can damage the membrane material (Kartinen and Martin 1995), so the membrane used should be carefully selected.

The main disadvantage of RO is the higher cost due the membrane used. Operation cost, requiring high pressure further increase the cost, and finally, membrane fouling is the main drawback of this process.

2.6.4 Adsorption Processes

Adsorption is a process in which a solid surface is used for removal of either gaseous or liquid contaminants. Adsorption is one of the most widely used methods for arsenic removal. Many adsorption techniques are used for the removal of arsenic from water. The removal or more correctly the adsorption capacity of an adsorbent is the extent of arsenic removed by a standard weight or volume of the media (usually measured in mg As/L of solution or μg As/g of dry media). Various materials have been used as adsorbent. Some of the materials used as adsorbent for arsenic removal are described below.

2.6.4.1 Activated Carbon

Activated carbon is one of the most commonly used materials for arsenic removal (Huang, C.P. and Fu, P.L.K., 1984; Gimbel, R. and Hobby R., 2000). Activated carbons impregnated with various metal ions greatly improve their arsenic adsorption capacity. Activated carbon pretreated with Cu^{2+} or Ag^{+} ions enhances its

As(III) adsorption capacity but reduces the As(V) adsorption (Rajakovic, 1992). Impregnating carbon with tartaric acid or ferric hydroxide also improves its arsenic adsorption ability (Evdokimov et al., 1973). Activated carbon pretreated with Cu(II) or with high ash content has high affinity for As(V) than As(III) (Lorenzen et al., 1995).

2.6.4.2 Other Natural Products

Pollard et al., (1992) and Baily et al., (1999) have reviewed the preparation of several low cost adsorbents: Agricultural byproducts like coconut husk (Manju et al., 1998), rice husk (Khalid et al., 1998; Lee et al., 1999), carbonized wood powder (Pulido et al., 1998), orange juice residue (Ghimire et al., 2002), coconut coir (Baes et al., 1997), sawdust (Raji et al., 1999) and pretreated waste tea fungal biomass (Murugesan et al., 2006).

2.6.4.3 Activated Alumina (Al2O3)

Activated alumina (AA) is a porous granular, amber colored media formed by the dehydration of aluminum hydroxide at elevated temperature. Two aluminum based technologies, *Alcon AAFS-50* and *BUET* Activated Alumina have been evaluated for arsenic removal from ground water in Bangladesh (Sutherland et al., 2001). The adsorption efficiency of AA is very much pH dependent, the optimum pH range being 6-8 (Bissen and Frimmel, 2003). By lowering the pH below neutral, the removal capacity of AA increases (Khandaker et al., 2006). Among the two dominant species, AA favors arsenate over arsenite (Jang et al., 2006). The arsenic removal efficiency of AA is affected in the presence of competing ions like, chloride, phosphates, fluorides and sulfate (Pal, 2001) but not to the same extent as ion exchange resins. AA adsorption has the following order of selectivity for various competing ions (Ashutosh, 2005).

$$OH^- > H_2AsO_4^- > Si(OH)_3O^- > F^- > HSeO_3^- > TOC > SO_4^{2-} > H_3AsO_3$$

The selectivity of AA for arsenite is poor as compared to arsenate, so pre- oxidation of arsenite to arsenate is essential.

The AA adsorption media is one of the most costly media available on the market, but as far as raw material is concerned, it is considered as one of the inexpensive treatment choice available.

2.6.4.4 Zeolites

Zeolites occur as a crystalline, hydrated aluminosilicate mineral of alkali and alkaline earth metal ions (Mampton, 1997) but can also be synthesized (Nery et al., 2003). Zeolites are one of the important components in wastewater treatment (Kesraoui-Ouki et al., 1994). About 30 different natural zeolites are known, however, only seven of these are available in sufficient amount and purity to be exploited (Mohan et al., 2007). Zeolites were used for drinking water treatment as the first ion exchangers (Gonzalez et al., 2001; Smit & Krishna 2003). Some new zeolites have shown As(V) removal efficiency equivalent to activated alumina (Xu et al., 2002). Elizalde-Gonz´alez et al (2001), reported arsenic adsorption by Clinoptilolite containing rock. Competing ions, like nitrate, chromate, chloride, sulfate and acetate ions have little effect on arsenic adsorption while phosphate greatly influence arsenic adsorption by zeolites.

2.6.4.5 Iron Oxide

Iron oxides are also one of the most widely used sorbents for water contaminants, especially hazardous wastes. Arsenic from ground water has been removed by passing it through sand and zero-valent iron (Leupin and Hu, 2005). Arsenic sorption occurred on the hydrous ferric oxides (HFO) resulted from the iron oxidation. Other similar compounds have also been used, like amorphous ferric hydroxide (Matis et al., 1987; Driehaus et al., 1998; Quan et al., 2001) and iron hydroxide (Pierce and Moore, 1982), ferrihydrite, iron (III) oxide containing silica (Zeng, 2003), iron oxide coated sand (Thirunavakkarasu et al., 2003), Ce(IV)- doped iron oxide (Zhang, 2003), ferric chloride (Meng et al., 2000) and polymeric materials coated with iron oxide (Katsoyiannis and Zouboulis, 2002) are also used for arsenic removal. Granular ferric hydroxide (GFH) possesses a high adsorption potential for arsenic removal (Thomas et al., 2007). Like other adsorbent GFH also has more

affinity towards arsenate, thus requiring pre-oxidation step if arsenite is present (Carollo engineers, 2006). GFh adsorption is pH sensitive, with arsenic adsorption declining with raising the pH (Driehaus et al., 1998). Asrenic speciation has an effect on its adsorption (Bissen and Frimmel, 2003). Arsenate adsorption occurred faster at lower pH but at elevated pH adsorption of both arsenate and arsenite occurred at comparable rates (Bissen and Frimmel, 2003). At influent pH below neutral, GFH adsorption efficiency is slightly affected in the presence of sulfate (Driehaus et al., 1998). Increase in phosphate concentration greatly reduces arsenic removal potential (Driehaus et al., 1998).

2.6.4.6 Other Metal Oxide Based Adsorbent

Other metal oxide based adsorbents used for arsenic removal include manganese oxide (Chen et al., 1998; Chiu and Hering, 2000), alumina (Kazuo and Toshio, 1998; Osamu et al., 2000) and zirconium oxide (Suzuki et al., 1997; Suzuki et al., 2000). Manganese oxide readily oxidizes and adsorbs arsenic (Moore et al., 1990; Manning et al., 2000). Oxidation of As(III) is coupled with reductive dissolution of MnO_2 resulting in the release of both Mn(II) and As(V) into the solution at low pH (Moore et al., 1990; Nesbitt et al., 1998).

The main drawback of adsorption process is the disposal of wastewater resulting from column regeneration and the spent media. As after a few reuses, it becomes necessary to replace the media due to irreversible fouling and excessive attrition, so the disposal of this exhausted adsorbent containing high concentration of adsorbed metals presents a major concern due to its hazardous nature.

2.7 Need for Cost Effective and Point-of-Use Method of Arsenic Removal

In the last few years, a great deal of research has been directed to find novel technologies for the removal of arsenic from water, specially low-tech, low cost and point-of-use systems that can be applied anywhere. Many of these technologies depend on oxidation of As(III) to As(V), then filtration through a porous material, where arsenic is removed mainly by adsorption and co-precipitation. Adsorption

processes are the best choice for small water treatment facilities. Adsorption technologies have the following advantages over others;

- They have high arsenic removal efficiency over a wide range of pH.
- Competing ions (chlorides, fluoride, sulfate, nitrate etc) have less effect on the removal efficiency.
- Have low operation cost.
- Can be regenerated easily, does not require high skill labor.
- Does not pose hazardous if used on throwaway basis.

2.8 Titanium Dioxide (TiO2)

Titanium dioxide (TiO2) due to its usefulness in various technologies has been the subject of considerable interest. In the metal oxide surface science, Titanium dioxide stands out as the most thoroughly investigated single crystalline system due to its high photocatalytic activity, non-toxicity, chemical inertness and its different polymorphs that it forms under different chemical conditions, pressure and temperature.

There are three main polymorphic forms of titania namely Rutile, Anatase and Brookite. Rutile and anatase have tetragonal geometry, containing 2 and 4 formula units, respectively and brookite has orthorhombic. However, only anatase and rutile forms have the main role in TiO2 applications. The unit cells of both are shown in Fig.2.2. In both the structures, each Titanium atom is coordinated to six oxygen atoms and each of the O atoms in turn is coordinated to three Ti atoms. In each structure, the TiO_6 octahedron is a little distorted with the four Ti-O bonds slightly shorter than the other two and some deviation in O-Ti-O bond angles from 90^o (Akurati, 2008). On the other side, brookite possesses a more complex structure having eight formula units in the orthorhombic cell and also has six different Ti-O bond lengths (1.87 – 2.04 Å). The structure of these three polymorphs can be compared as well in terms of (TiO_2^{6-}) octahedral (Akurati, 2008). The common characteristic of all these three phases is that the deformed oxygen octahedra contain Ti atoms inside. The different crystalline phase is because the deformed oxygen octahedra shares different number of edges.

Rutile, brookite and anatase shares 2, 3 and 4 octahedra edges respectively (pauling, 1929). Brookite can be considered to be formed from octahedra connected by both their edges and vertices, in rutile, only the edges are connected, and in anatase only the vertices are connected (Akurati, 2008). From photoctalytic point of view, the most important phases of TiO_2 are rutile and anatase.

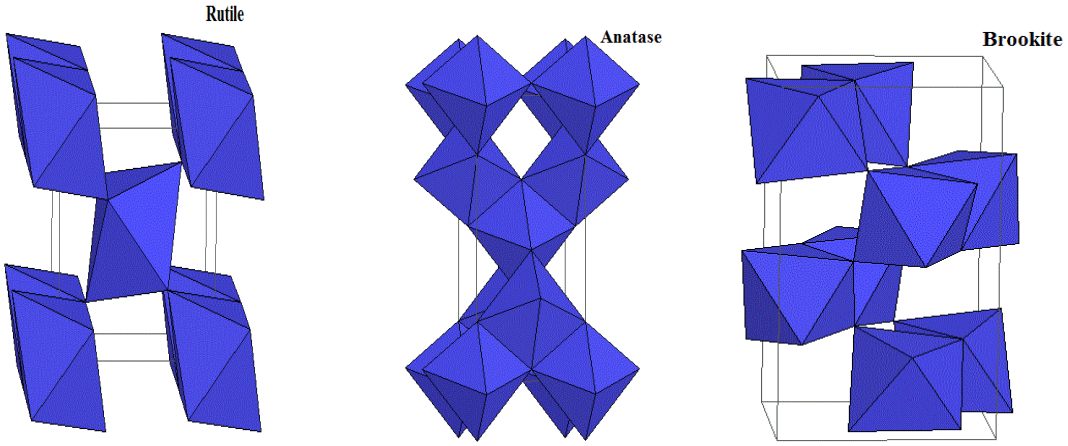

Fig. 2.2: Polymorphic forms of Titanium dioxide (TiO_2)

2.8.1 Photocatalytic activity of Pure and Metal Doped TiO2

Titanium dioxide (TiO_2), a white powder with titanium in IV oxidation state (Ti^{+4}). It therefore has no d electrons (d^o). Its two important polymorphs are anatase, with a band gap of 3.2 eV and rutile, with a band gap of 3.02 eV. Being a semiconductor, its HOMO is called *Valance band* and its LUMO is called *Conducting band.* Light absorption results in the transfer of electrons from oxygen to the vacant d-orbital of Ti. In both anatase (3.2 eV) and rutile (3.02 eV) this transition occurs in the UVA region, giving a sharp absorption band at 390-400 nm. After UV light absorption, promotion of electron from valance to the conducting band occurs, forming a “hole” (positive charge) in the valance band and an electron (negative charge) in the conducting band. The hole being powerfully oxidizing wants to retrieve its lost electron back. This can happen either by a radiative or by a non-radiative process. Due to the close energy levels in rutile form (lower band gap) the non-

radiative process is more active and so the recombination is active as compared to anatase form, where the band gap is higher.

Alternate pathways are available for recombination and that is the reason why TiO_2 is used as a photocatalyst. The hole can oxidize water molecule, forming hydroxyl radicals, which themselves are strong oxidizing agents and can oxidize any organic specie in the vicinity to CO_2 and H_2O. The electron in the conduction band on the other hand can oxidize oxygen to form superoxide anion, which subsequently reacts with water molecule forming hydroxyl. The process is given in Table.2.2.

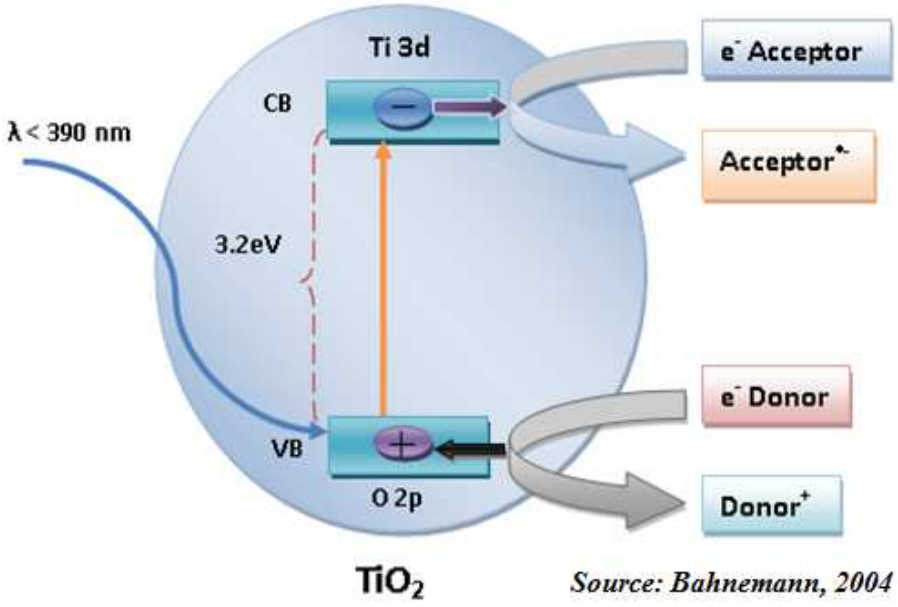

Fig. 2.3: photochemistry of pure Titania (TiO2)

Table 2.2: Photochemical reactions resulting after light absorption by TiO_2

Process	Reaction
Initiation Step	$h\nu + TiO_2 \longrightarrow h_{VB}^{+} + e_{CB}^{-}$
Hydroxyl radical ($^{\bullet}OH$) formation	$H_2O + h_{VB}^{+} \longrightarrow {}^{\bullet}OH$
Hydroxyl radical ($^{\bullet}OH$) formation	$O_2 + e_{CB}^{-} \longrightarrow O_2^{\bullet-} + H_2O \longrightarrow {}^{\bullet}OH$

** Source: Bahnemann, 2004*

The main requirement for photocatalysis is that there should be water near TiO_2 surface for efficient oxidation plus the water must be aerated so that it contains oxygen. Also the pollutant to be degraded must be close to the TiO_2 surface or

adsorbed by it, hence the greater the surface area of TiO_2 photocatalyst, the more pollutant it can adsorb. From here the concept of nanoparticles arrives.

The primary limitation of TiO_2 is that it absorbs UV light only, which is less than 5% of the sunlight. A great deal of research has been carried out to increase the visible light photocatalytic activity of TiO_2. The second limitation is that of recombination, a competitive and efficient process.

2.8.2 Shifting the Absorption Band to Visible Region

The requirement for TiO_2 photocatalytic activity was UV light; Researcher became interested in bringing the absorption band to visible region, so that TiO_2 can be used outdoor as well as indoor (in room light). There are two main processes used to bring the absorption of TiO_2 into visible region.

2.8.2.1 Non-Metal Doping

There are three main approaches available for modification of TiO_2 with non-metal doping and shifting its absorption to visible region. These are as follows,

a) *Band Gap Narrowing:* Asahi et al., (2001) doped TiO_2 with nitrogen to produce yellow TiO_2 (due to yellow color), and shifted the absorption band from 390 nm to 500 nm, well within the visible range. Nitrogen doping results in the introduction of a new occupied (e^- containing) orbital between the valance band (O-2p orbital) and conducting band (Ti-3d orbital). The N-2p orbital act as a step up for the O-2p orbital, which now has to make a much smaller jump for promotion into the conducting band. Once this promotion occurs, the electron in the original valance band moves to the mid-band gap energy level (i.e. N-2p) and leaving a hole in the valance band (Irie et al., 2003; Nakamura et al., 2004).

b) *Impurity Energy Level:* In nitrogen doped TiO_2 above the valance band, nitrogen form isolated impurity energy levels (Irie et al., 2003). UV irradiation

results in the excitation of both the VB and the impurity energy levels, while visible light excites only the electrons of the impurity energy level.

c) *Oxygen Vacancies:* Oxygen deficient sites resulting in the grain boundaries are necessary for visible light absorbance and doping with nitrogen in part of oxygen-deficient sites, as a blocker are very important (Ihara et al., 2003).

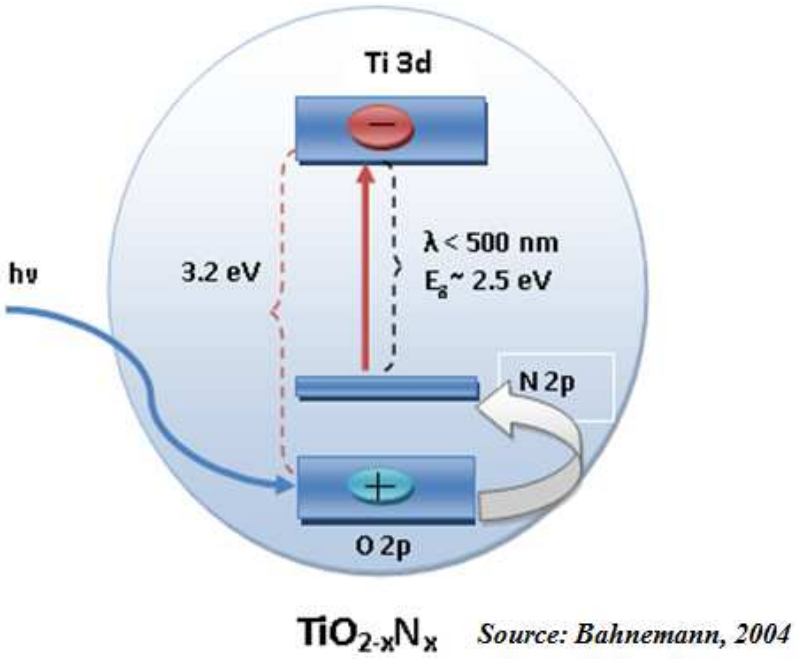

Fig. 2.4: Photochemistry of Nitrogen (non-metal) doped Titania

2.8.2.2 Metal Doping

The second approach of shifting the TiO_2 absorption band into the visible region is by incorporation of metal nanoparticles into the TiO_2 material. Consider the example of TiO_2 doped with a small quantity of silver (1-5%). Silver has an electron accepting region (Fermi level) just below the conduction band in energy. Therefore, when light in visible region is absorbed, charge separation occurs and the electron in the conduction band can be trapped by the silver and the hole can carry out the oxidation of water into hydroxyl radicals, without any danger of recombination.

From research, it is concluded that there is some optimum amount (or Goldilock's zone) of metal doping. Only sufficient amount of metal is required, so that the metal sites are dispersed through the material for rapid electron capture. Too much of the metal may cover the TiO_2 surface and prevent it from light absorption.

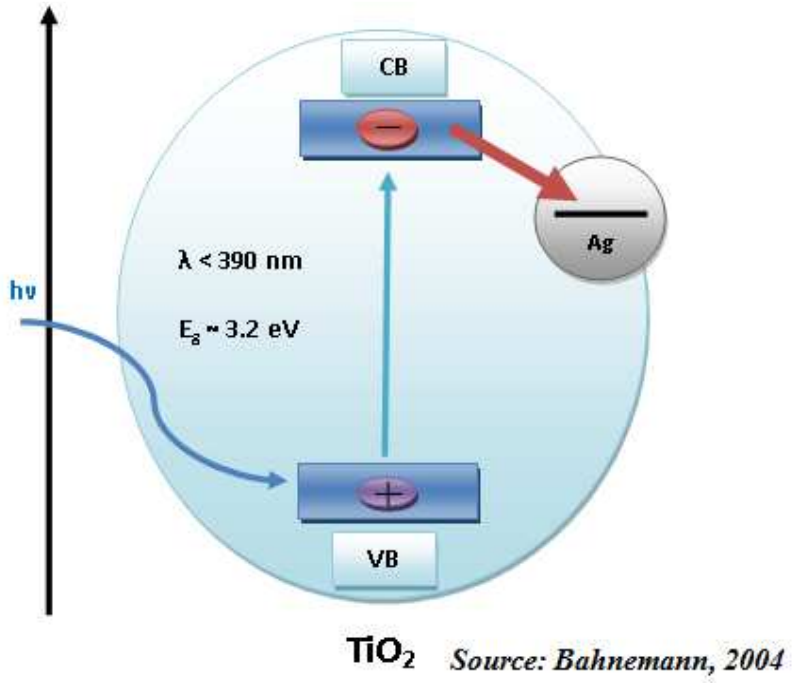

Fig. 2.5: Photochemistry of Silver (metal) doped Titania

2.8.3 Mechanism of Removal of Arsenic by Titanium Dioxide

2.8.3.1 Mechanism of Photocatalytic oxidation of As(III) by TiO_2

The use of Titania nanoparticles for arsenic removal is new advancement. Titania due to its physical and chemical stability, low-toxicity, lower cost and the resistance to corrosion nature possesses high potential for the environmental applications (Hung et al., 2006; Akif et al., 2010). Titania nanoparticles possess good porosity and high surface area that enhances its adsorption capacity (Akif et.al. 2010). Deedar et al., (2009) immobilized titania nanoparticles on sand and evaluated its arsenic removal potential. Titania possesses a strong affinity for arsenic. Being an excellent light induced photocatalyst over a wide pH range (2-14) titania shows excellent affinity towards arsenic (Balaji and Matsunaga, 2002). Titania like other

adsorbent, preferentially adsorb As(V) as compared to As(III), So for maximum removal, pre-oxidation of As(III) to As(V) is necessary(Akif et.al. 2010). Titania, not only adsorb both arsenic species but being an excellent photocatalyst photo-oxidizes As(III) to As(V) (Bang et al., 2005; Ferguson et al., 2005).

TiO_2 being a strong photocatalyst is very effective in oxidative degradation of a large number of contaminants both in air and water. It has been demonstrated experimentally that in UV- illuminated TiO_2 suspension, As(III) is oxidized to As(V) (Yang et al., 1999; Lee and Choi, 2002; Bissen et al., 2001). The photocatalytic process starts with the absorption of UV light by TiO_2 and results in the excitation of electron from the valance band into the conductance band, thus giving an electron-hole pair at the TiO_2 surface. These electron-hole pair may react with the adsorbed species such as water and oxygen and generate free radicals such as $^{\bullet}OH$, $HO_2^{\bullet}$ and $O_2^{\bullet -}$ as shown below (Pena et al., 2005).

$$TiO_2 \longrightarrow e^- + h^+$$

$$O_2 + e^- \longrightarrow O_2^{\bullet -}$$

$$H^+ + O_2^{\bullet -} \longrightarrow HO_2^{\bullet}$$

$$2HO_2^{\bullet} \longrightarrow H_2O_2 + O_2$$

$$HO_2^{\bullet} + O_2^{\bullet -} \longrightarrow HO_2^- + O_2$$

$$HO_2^- + h^+ \longrightarrow HO_2^{\bullet}$$

$$2H_2O + h^+ \longrightarrow OH^{\bullet} + H^+$$

$$OH^- + h^+ \longrightarrow OH^{\bullet}$$

These electron-hole pair and radicals formed oxidize As(III) to As(V) through the following possible ways (Pena et al., 2005).

$$h^+ + As(III) \longrightarrow As(IV)$$

$$OH^{\bullet} + As(III) \longrightarrow As(IV)$$

$$O_2^{\bullet-} + As(III) \longrightarrow H_2O_2 + As(IV)$$

$$H_2O_2 + As(III) \longrightarrow 2OH^- + As(IV)$$

$$O_2 + As(IV) \longrightarrow O_2^{\bullet-} + As(V)$$

$$OH^{\bullet} + AsI(V) \longrightarrow As(V)$$

$$O_2^{\bullet-} + As(IV) \longrightarrow As(V)$$

$$O_2 + H^+ + As(IV) \longrightarrow HO_2^{\bullet} + As(V)$$

In the TiO_2/UV system any of the oxidizing agents (i.e. h^+, superoxide ion, hydroxyl radical and hydrogen peroxide) produced may oxidize As(III) to As(IV) as shown in the above reactions. As(IV) thus formed can be oxidized to As(V) through any of the four possible reactions (as shown above). The main dispute is on the fact that which reaction controls the oxidation of As(III). According to some papers As(III) is oxidized by dominantly by superoxide anion (Lee and Choi, 2002; Ferguson et al., 2005) while other shows hydroxyl radical as the main responsible specie for As(III) oxidation (Pena et al., 2005).

2.8.3.2 Mechanism of Arsenic Adsorption on Titania surface

Although the photocatalytic oxidation of As(III) to As(V) by TiO_2 has been controversial for the past 10 years. The adsorption mechanism of the two arsenic species on various TiO_2 – based adsorbents has been clearly defined. Pena et al. (2006) used various techniques to investigate the interaction of As(III) and As(V) at the surface of nanocrystalline TiO_2 . He proved that both As(III) and As(V) form bidentate binuclear surface complexes with TiO_2 and the dominant specie for As(III) was $(TiO)_2\ AsO_2^-$ and for As(V) was $(TiO)_2AsO^-$.

Jagadeesan et al.(2006, 2010) used X-ray absorption near edge structure (XANES) and X-ray absorption fine structure (EXAFS) spectroscopy to find the mechanism of arsenic adsorption on TiO_2. They found that partial oxidation of As(III) to As(V) occurred when As(III) was adsorbed onto amorphous TiO_2, but As(III) remained as

such when adsorbed on commercial crystalline TiO_2. Their data also proved the formation of binuclear bidentate inner-sphere complex of As(III) and As(V) with amorphous TiO_2 at pH 7.

Li et al. (2010) studied the adsorption mechanism of As(III) and As(V) on Ce-Ti bimetallic oxide and proved that an inner-sphere complex is formed on the surface of the adsorbent. Further FTIR analysis showed that hydroxyl groups present on the surface of adsorbent were involved in the adsorption of arsenic and X-ray photoelectron spectroscopy (XPS) also proved that hydroxyl groups are involved in the sorption and formation of mono and bidentate complexes on the surface of the adsorbent.

In the pH range of 6.5-8.5, the complexation between various arsenic species and TiO_2 surface can be illustrated in the following figure (Fig.2.6).

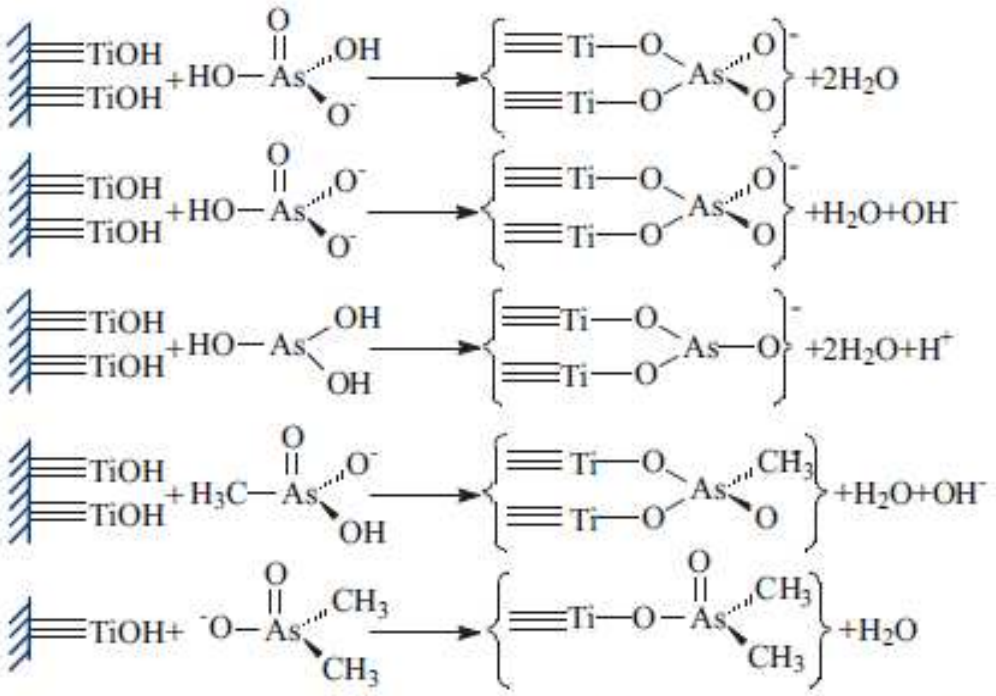

Source: Guan et al., 2012

Fig. 2.6: Scheme of the complexes formed between TiO_2 and different arsenic species

CHAPTER 3

MATERIALS AND METHODS

3.1 MATERIAL AND CHEMICALS

All the solutions were prepared in deionized water (EC < 0.7 μS/cm) obtained from deionization plant (Labconco Waterpro PS). General purpose reagent Titanium (IV) oxide (Riedel-DeHaen) was used as a source of Titania nanoparticles, Nitrate salts of Fe (Merck, Germany), Ag (Merck, Germany) and Cr (Riedel-DeHaen) were used as a precursor for metals. Sodium Arsenate, $Na_2HAsO_4.7H_2O$ (BDH) was used as a source of Arsenite [As(III)]

3.2 ARSENIC STOCK SOLUTION

Arsenic (III) stock solution (100 ppm) was prepared by dissolving 420 mg of Sodium Arsenate in One Liter De-Ionized water. The pH of the solution was adjusted to 7.0 (± 0.1), using 0.1 M Nitric acid. The solution was shaken well and then stored in dark.

3.3 INSTRUMENTATION

The quantitative determination of As(III) was done by Atomic Absorption Spectrophotometer (AAS Vario 6, analytikjena (Germany)) in hydride generation mode. A pH meter (Cyberscan 500) was used to adjust the pH of the As(III) stock solution, with 0.1 M HNO_3 and 0.1 M NaOH.

3.4 EXPERIMENTAL SECTION

3.4.1 Synthesis of Pure and Metal Doped Titania Nanoparticles

Pure and metal doped Titania nanoparticles were prepared using Liquid Impregnation method (Behnajady et al., 2008; Sahoo et al., 2005) as described below:

In 300 ml water in a beaker, placed on a magnetic stirrer, 50 grams of GPR Titania was added slowly and stirred for 24 hours. The Titania suspension was then removed from the stirrer and allowed to stand for 24 hours, dried at 105^{o}C, grinded using mortar and pestle, calcinated at 400^{o}C in furnace for 6 hours and then allowed to cool down at 10^{o}C per minute. The nanoparticles were then transferred to a plastic bottle and placed in dark.

The metal doped nanoparticles were prepared using the same procedure; with 1 % molar ratio of the metal salt being added to the solution before adding Titania.

3.4.2 Glass Beads Etching

Etching of the glass beads was done using three methods.

3.4.2.1 Basic Etching

In this method a 5% NaOH solution was prepared in a plastic bottle and the glass beads were placed in it while the bottle covered. The glass beads were soaked in NaOH solution for 24 hours, after that they were removed from the basic solution and washed with water to remove any traces of NaOH.

3.4.2.2 Acidic Etching

In this method the glass beads were dipped in a 10 % HF solution in a covered plastic bottle for 24 hours, they were then removed from the solution and rinsed with water to remove any traces of HF left.

3.4.2.3 Acidic Cleansing and then Basic Etching

In this process the glass beads were first cleaned with 1 N H_2SO_4. To increase roughness, glass beads were successively soaked for 24 hours in: 37% HCl, 10% H_2CrO_4 and 37% HCl, rinsed with deionized water and dried. The beads were then placed in 5% NaOH solution in a plastic bottle for 24 hours and then rinsed with water.

3.4.3 Glass Beads Coating

Glass beads were coated with nanoparticles using Heat Attachment method; 5g of Titania nanoparticles were dissolved in 100-200 ml water in a 250 ml titration flask and placed on a shaker at 150 rpm for 15 minutes, 200 grams of etched glass beads were weighed and transferred to the Titania suspension, this was kept on shaking for 1 hour. The glass beads were then transferred to a petri dish and were dipped in the Titania suspension. The petri dishes were placed in an oven at 105 ^{o}C till drying. The nanoparticles get dry on the surface of the glass beads, the glass beads were then carefully removed from the petri dish, transferred to a china dish and placed in furnace at 600 ^{o}C for about 2 hours. The coated glass beads were then cooled washed with distilled water till none of the nanoparticles attached to the surface gets detached with water. These beads were then dried in oven at 105^{o}C, transferred to a plastic bottle and kept in dark.

The metal doped Titania nanoparticles were also coated on the glass beads using the same procedure.

3.4.4 Characterization

The nanoparticles synthesized were characterized using the following techniques.

3.4.4.1 X-Ray Fluorescence (XRF)

XRF Spectra were obtained with Energy Dispersive X-Ray Fluorescence Spectrometer (JEOL, Model JSX-3202 M). The applied tube voltage and current were 30 kV and 1 mA, respectively. The scan range was 0 to 41 keV and the collimator was of 4 mm diameter.

3.4.4.2 Scanning Electron Microscope (SEM)

Scanning Electron Microscope (SEM) is a powerful instrument that uses focused beams of electrons to obtain largely magnified image.

The high-resolution, three-dimensional images produced by SEMs provide information like,

- **Topography :** Its appearance; limit of detection is a few nanometers.
- **Morphology:** The form, size and order of the constituent particles from which that object is made, that are present on the sample surface or exposed by etching or grinding; limit of detection is a few nanometers.
- **Chemistry:** The elemental composition of the sample and the relative ratio of each element present, in areas ~ 1 µm in diameter.
- **Crystallography:** The degree of order and arrangement of different atoms present in that specimen. This is useful in case of particles composed of single crystalline form > 20 µm.
- **Orientation of grains**
- **In-situ experiments:**
    - Reactions with atmosphere
    - Effects of temperature

These applications make SEM invaluable in a variety of science and industry applications.

The SEM uses a beam of energetic electrons that are focused on a stage, where a solid sample is placed. When the incident electrons strike the sample, they release energetic electrons from the sample surface. The pattern of scattered electrons released by the sample surface gives information about its shape, size, texture and composition. Elemental and mineral information can be obtained from the x-rays emitted by the beneath of the sample.

SEM images were obtained from JEOL JSM-6460 scanning electron microscope, which was operated at an acceleration voltage of 5, 10 and 15 kV and filament current of 60 mA.

3.4.4.3 Energy Dispersive X-Ray Spectroscopy (EDS)

Energy dispersive X-ray spectroscopy (EDS) is a simple but very powerful analytical technique used to know elemental composition of very small samples (up to μm^3). This instrument is attached to SEM and allows gathering information about the elemental composition of the specimen under observation.

Its principal is based on the rule that every element emits x-rays characteristic of that element. When the sample is hit with energetic electron beam they produce x-rays (to discharge the excess energy) characteristic of the elemental composition of the sample. EDS works on detecting these x-rays and form peaks in the spectrum. An individual element can produce more than a single characteristic peak and few peaks arising from different elements may overlap to some degree.

The EDS spectra, due to precise control on the electron beam can be collected from any particular point or any individual particle of the sample, giving complete analysis of very small part of the material. Moreover, the beam of electrons can sweep over a specific chosen area of the sample to determine its elemental composition in that region. EDS system embedded with JEOL JSM-6460 was used in this study for the characterization of synthesized nanoparticles by assessing the elemental composition.

3.4.4.4 X-Ray Diffraction (XRD)

X-ray powder diffraction is a very rapid nondestructive analytical technique primarily used for phase identification of a crystalline material. It can provide information on unit cell dimensions. The material to be analyzed is finely ground, homogenized, and average bulk composition is determined.

XRD can determine,

- The average spacing between rows and layers of atoms.

- Orientation of a single atom or grain.
- The crystal structure of unknown material.
- Internal stress and size and shape of small crystalline region.

The average grain size is determined using Scherer formula (Liu et al., 2009)

$$L = \frac{0.94\lambda}{\beta_{1/2}\cos\theta} \qquad \mathbf{1}$$

Where,

λ = 1.54 A^o, CuKα1 wavelength

$\beta_{1/2}$ = Full width of a diffraction line at one half of maximum intensity (FWHM) in radian

XRD studies of pure and metal doped TiO2 were carried out using JEOL JDX-II, X-ray diffractometer using CuKα radiation. The applied voltage and current were 40 kV and 30 mA respectively. Scanning was done from 10^o to 80^o at a scan rate of 6^o per minute.

3.4.4.5 Band Gap analysis

To find the wavelength of light needed for the excitation of TiO_2 photocatalyst, it is very important to find the Band gap (Gaya, 2011). The TiO_2 samples were analyzed in the diffused reflectance mood of Perkin Elmer, Lambda 35 UV/Vis spectrophotometer.

When photons having energy greater than or equal to the band gap is absorbed by a semiconductor, an electron from the valance band jumps to the conduction band, and depending on the band gap energy there occur a rise in the absorbency of the semiconductor. The relation between the absorption coefficient (α) and the energy of the incidental photon depends on the type of electronic transition (Valencia et al., 2010). There are two types of transition,

- Direct transition – when the electron momentum is conserved.
- Indirect transition – when the momentum of electron is not conserved.

The electronic properties of the synthesized pure and metal doped TiO_2 were analyzed using the remission function of Kubelka-Munk, F (R_∞) (Tandon and Gupta, 1970; Valencia et al., 2010).

$$F(R_\infty) = \frac{(1 - R_\infty)}{2R_\infty} = \frac{\alpha}{S} \qquad \mathbf{2}$$

Where, R_∞ is the diffuse reflectance (of a given wavelength), of a dense layer of non-transparent infinite material and is given by,

$$R_\infty = \frac{(R_{sample})}{R_{s\tan dard}} \qquad \mathbf{3}$$

α and S are the absorption coefficient (cm^{-1}) and dispersion factor respectively. For particle larger than 5μm, S is independent of the wavelength. α is related to the energy of incident proton by the following equation (Valencia et al., 2010).

$$\alpha = A(E - E_g)^\gamma \qquad \mathbf{4}$$

Where: A is a constant and depends on material properties, E is energy of photon, E_g the band gap and □ is a constant, depending on the type of electronic transition it can take different values as (López et al., 2003; Valencia et al., 2010).

- □ = 1/2 – permitted direct transition.
- □ = 2 – permitted indirect transition.
- □ = 3/2 – prohibited direct transition.
- □ = 3 – prohibited indirect transition.

Therefore:

$$F(R_\infty) = \frac{\alpha}{S} = A\frac{(E - E_g)^\gamma}{S} \qquad \textbf{5}$$

And

$$E(eV) = \frac{hc}{\lambda(nm)} = \frac{1236}{\lambda(nm)} \qquad \textbf{6}$$

Where h is plank's constant and C is speed of light. In case of direct transition the equation is:

$$F(R_\infty)^2 = \left(\frac{A}{S}\right)^2 = (E - E_g) \qquad \textbf{7}$$

While for an indirect transition the equation takes the following form.

$$F(R_\infty)^{\frac{1}{2}} = \left(\frac{A}{S}\right)^{\frac{1}{2}} = (E - E_g) \qquad \textbf{8}$$

The plot of F (R_∞)$^{1/2}$ Vs E (eV) gives the indirect transition while the direct transitions are obtained by plotting F (R_∞)^2 Vs E (eV).

3.5 BATCH EXPERIMENTS

3.5.1 Removal Efficiency

The removal efficiencies of pure and metal doped Titania were calculated using the following formula.

$$E = \frac{C_o - C_f}{C_o} \times 100\% \qquad \textbf{9}$$

Where C_o is the initial and C_f is the final equilibrium concentration of As (lll) (mg/L) in the solution.

For each sample 100 ml of 0.5 mg/L of As(III) solution was prepared from the stock and transferred into a 250ml volumetric flask, 0.75 g of the respective pure and metal doped Titania nanoparticles were added to it and the flask were placed on an orbital shaker at 145 rpm for 90 minutes for the equilibrium to reach. After shaking the solution were centrifuged at 4000 rpm for 25 minutes to separate the nanoparticles. The supernatant was analyzed using Atomic Absorption Spectrophotometer (AAS Vario 6, analytikjena (Germany)) in hydride generation mode.

3.5.2 Effect of pH on Removal Efficiency

The process was done at different pH (4, 7, 10) and removal efficiency at each pH was calculated.

3.5.3 Batch Adsorption Studies

For adsorption studies 100 ml of As (lll) solution of different concentrations (0.1, 0.2, 0.4, 0.8, 1.5, 3 and 6 ppm) were taken in a 250 ml volumetric flasks. 0.35 g of the concerned nanoparticles was added to it and was placed on an orbital shaker at 145 rpm for 90 minutes. The solutions were then centrifuged at 4000 rpm for 25 minutes and then preserved by adding 2 ml of nitric acid. They were then analyzed with AAS (AAS Vario 6, analytikjena (Germany)).

3.5.4 Batch Kinetic Studies

The kinetic studies were performed using 250 ml volumetric flasks. 100 ml of 0.5 ppm As(III) was taken in ten volumetric flask each, 0.35 g of pure Titania nanoparticles was added to each flask and then placed on an orbital shaker at 145 rpm, one volumetric flask was removed from the shaker at time (5 , 10, 20, 30, 40, 50, 60, 70, 80 and 90) minutes and centrifuged at 5000 rpm for 25 minutes. The solution left after was analyzed using AAS (AAS Vario 6, analytikjena (Germany)). The same process was repeated for the doped Titania nanoparticles as well.

The amount of As(III) adsorbed (q_t) was calculated using the following formula.

$$q_t = \frac{(C_o - C_t)V}{m} \qquad \textbf{10}$$

Where C_o and C_t are the initial As(III) (mg/L) concentration and the As(III)concentration after the time interval t, respectively V is the volume of As(III) (L) and m is the mass (g) of the Nanoparticles.

3.5.5 Column Studies

Ordinary 100 ml Burette was used for the preparation of columns, with a diameter of 1.5cm and height of 2 feet. The bottoms of the columns were plugged in with folded aluminum foil just to make a support for the glass beads. Cotton wool or glass wool was not used due to possibility of clogging by the nanoparticles. The columns were packed with the desired nanoparticles coated glass beads to the height needed by weighing the glass beads and then packing them in the columns. The column was then operated in such manner that a calculated amount of arsenic stock solution was constantly added to it through a graduated cylinder and allowing it to flow along gravity with a constant rate. The rate of flow was constantly checked by measuring the amount flowing per minute after every ten minutes. Once the process started, samples were collected at regular interval using plastic bottles. This process was continued till column exhaustion. The amount of arsenic in different samples was analyzed using AAS (AAS Vario 6, analytikjena (Germany)). From these results "Breakthrough curves" were drawn. Yoon-Nelson and Thomas model were used to determine the breakthrough curves and to find the different characteristic column parameters which are useful for the process design.

3.5.6 Column Regeneration

When the column was fully exhausted after long column runs, it was revived using NaOH (10% w/v) solution. Sufficient amount of the regenerant (10 bed volumes) was passed through the column at a very slow flow rate (0.5 ml/min). The column was then rinsed thoroughly with mild warm deionized water at 2 ml/min for about 10 bed volumes.

CHAPTER 4

RESULTS AND DISCUSSION

4.1 CHARACTERIZATION

4.1.1 X-Ray Fluorescence (XRF)

The XRF spectra of pure and metal doped TiO_2 nanoparticles were obtained using Energy dispersive X-ray fluorescence spectrometer (JEOL, Model JSX-3202 M). The XRF patterns are given in the Fig.4.1 - 4.4. From the figures it is clear that all the metal doped Titania are composed of about 99% TiO_2 and 1% of the dopant metal, which was in accordance with the amount of metal aimed. The elemental composition obtained is given in the Table.4.1.

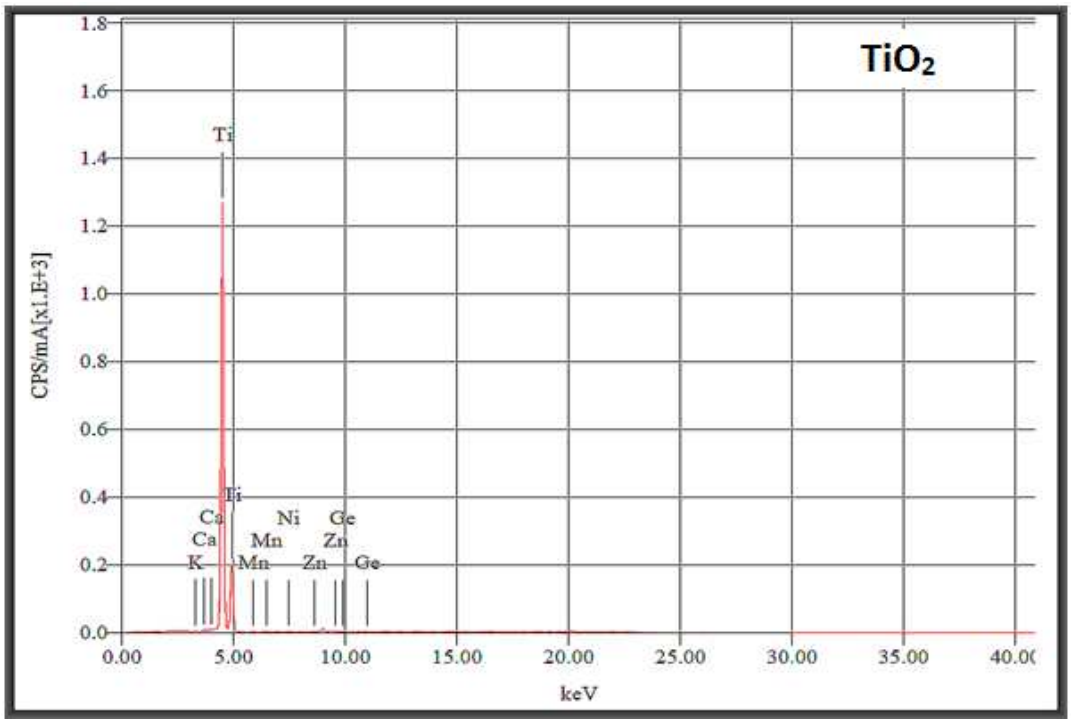

Fig. 4.1: XRF pattern of pure Titania nanoparticles

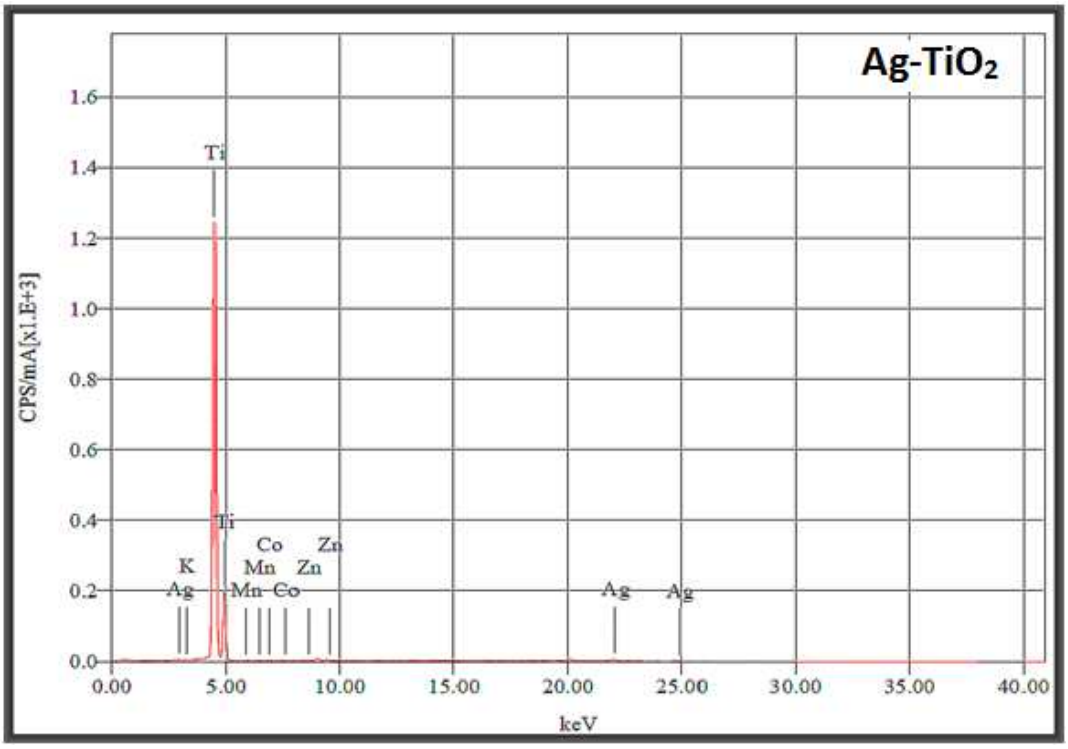

Fig. 4.2: XRF pattern of Silver doped Titania nanoparticles

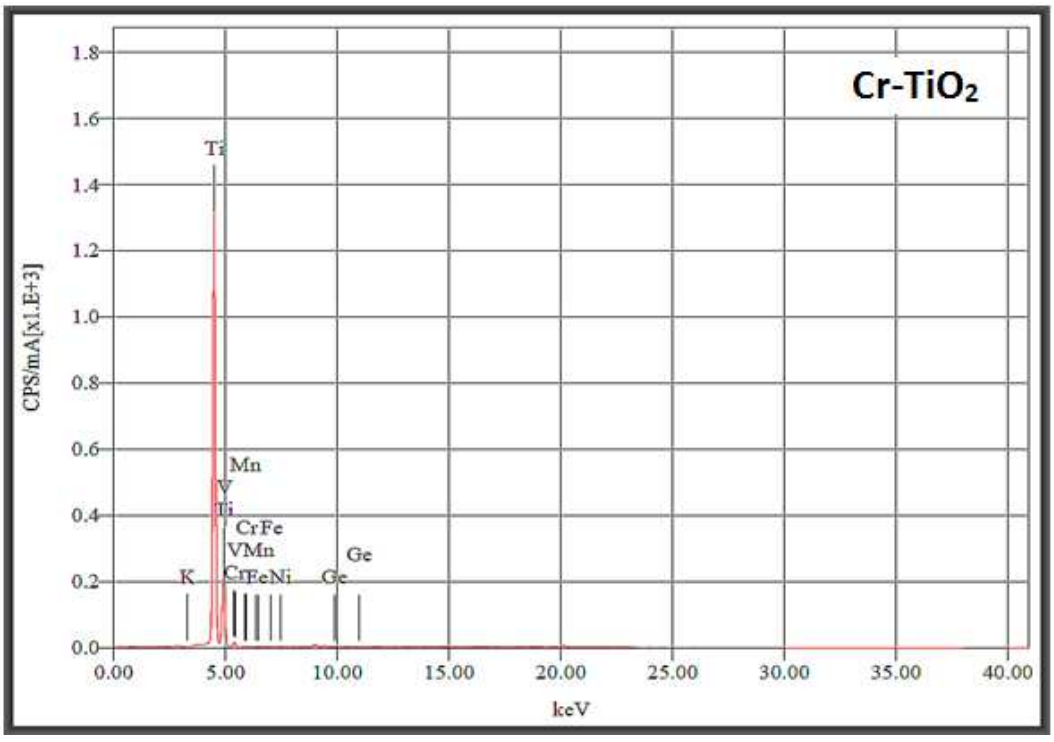

Fig. 4.3: XRF pattern of Chromium doped Titania nanoparticles

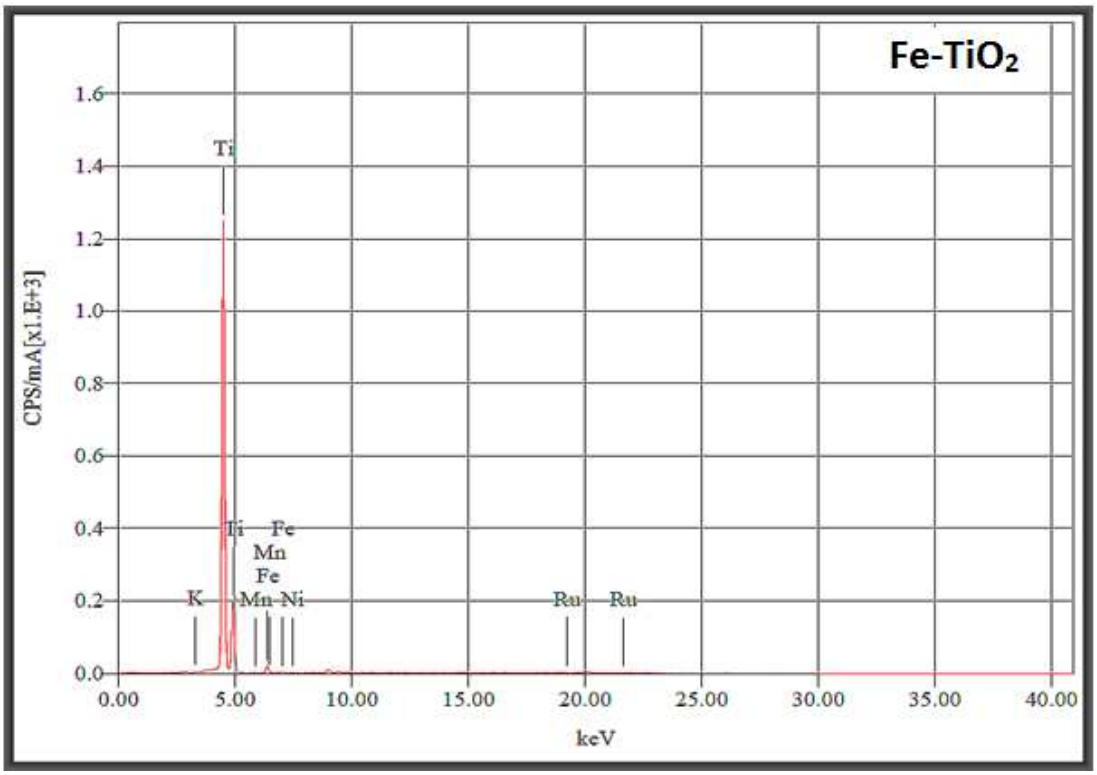

Fig. 4.4: XRF patterns of Iron doped Titania nanoparticles

Table 4.1: XRF composition of pure and metal doped Titania

Nanoparticles	TiO_2 (%)	Dopant metal (%)
TiO_2	100	-----
Ag- TiO_2	99.0	1
Cr- TiO_2	98.82	1.18
Fe- TiO_2	98.7	1.3

4.1.2 Scanning Electron Microscope (SEM)

The SEM image of pure and metal doped (Ag, Fe, and Cr) Titania nanoparticles, as shown in Fig.4.5–4.8, were obtained from JEOL JSM-6460 at 10,000 magnifications. It is clear from the SEM images that all the samples were made of fine particles but differed in surface morphology. It is clear from the figure that the nanoparticles are spherical and of almost uniform shape. From the image it can be

seen that the distribution of dopant metal is almost uniform on the TiO_2 surface, and at very few points there is excess of metal which has resulted in some irregularity in shape due to the aggregation of tiny metal crystals. In the dispersion the TiO_2 nanoparticles agglomeration tendency is difficult to determine due to sample preparation, however, it is assumed that agglomerates are present as can be seen in the SEM image.

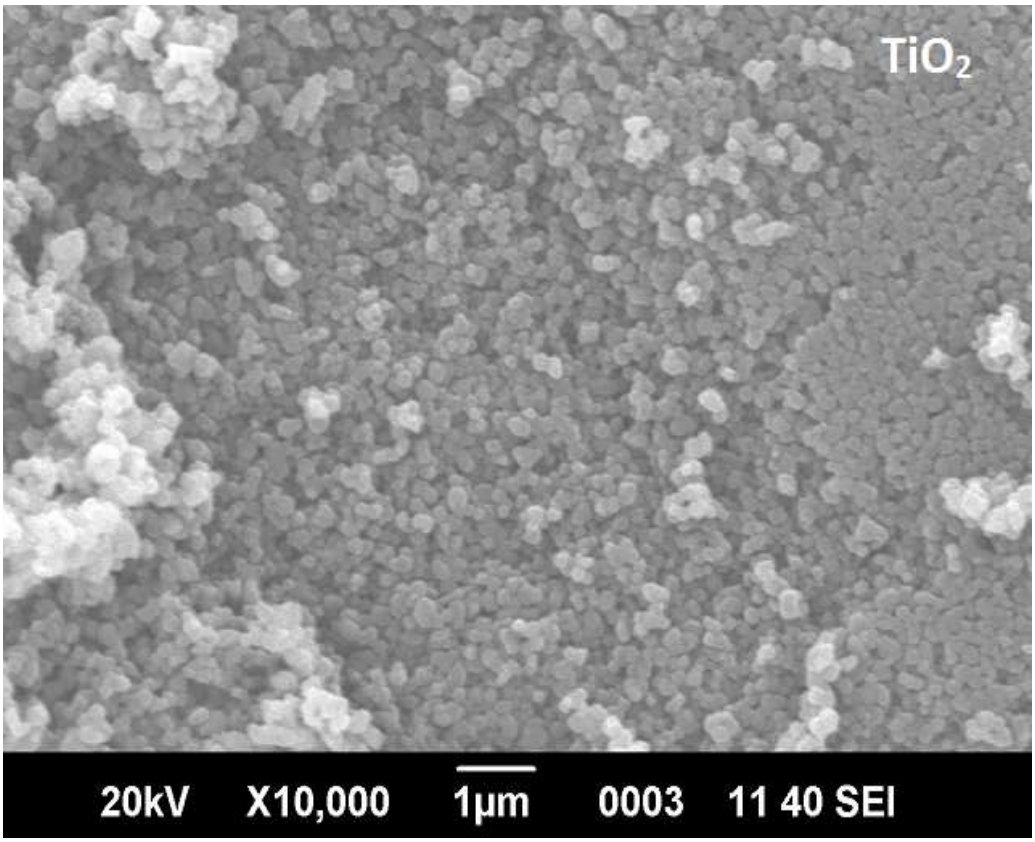

Fig. 4.5: SEM images of pure Titania nanoparticles

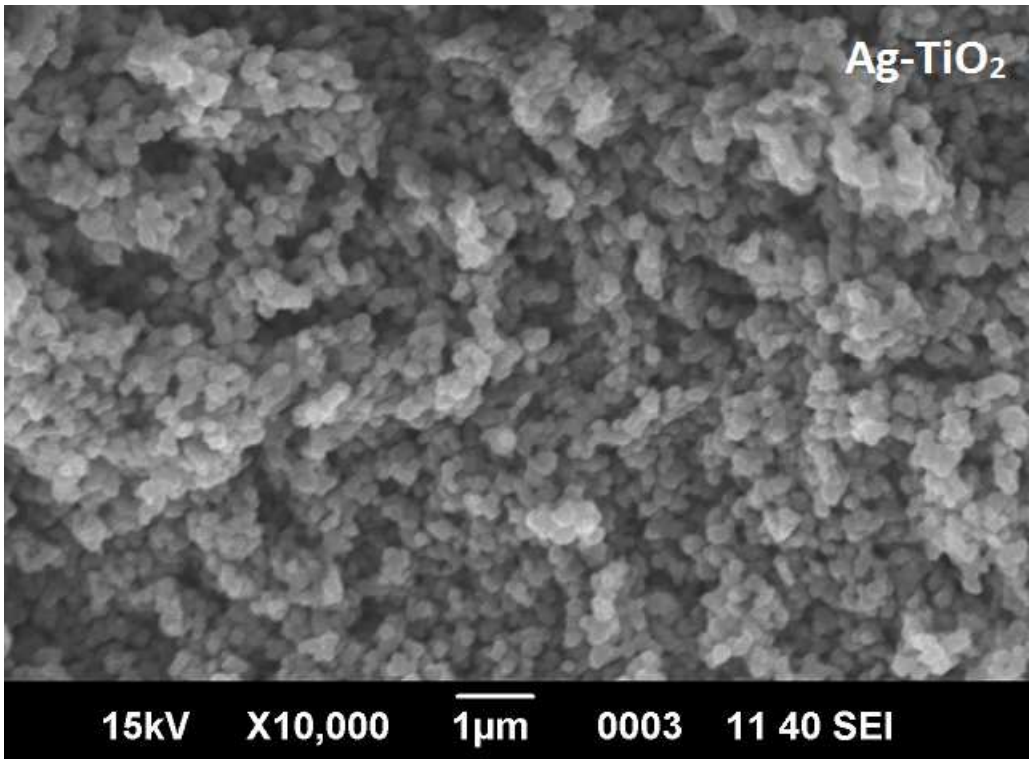

Fig. 4.6: SEM image of Silver doped Titania nanoparticles

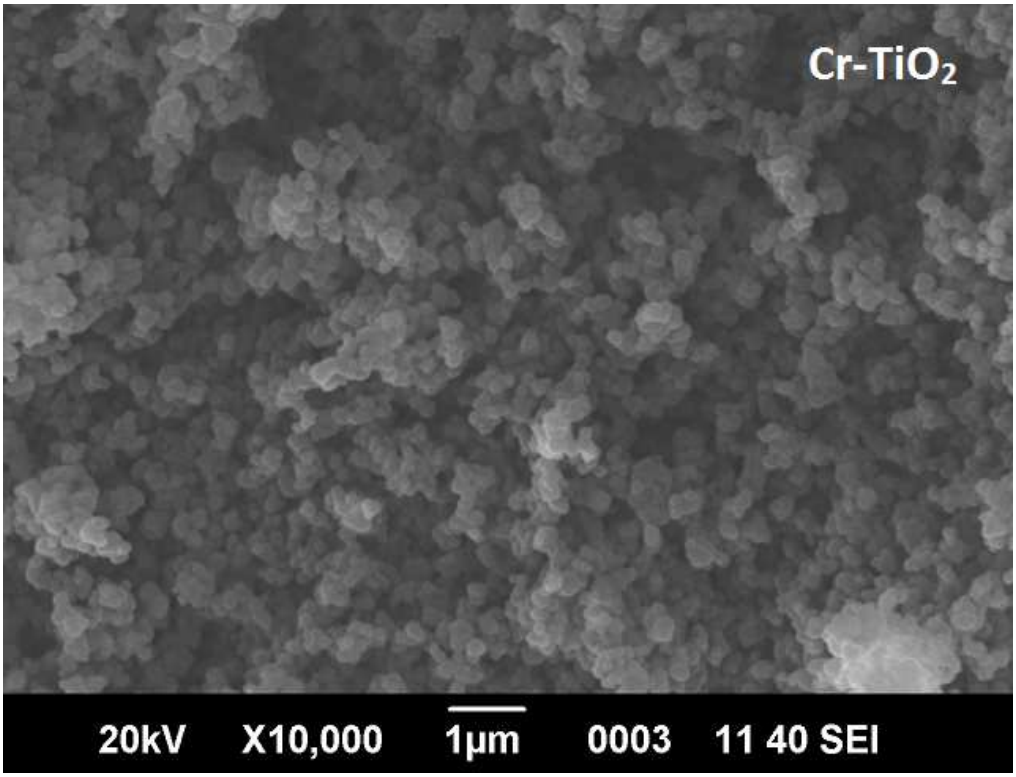

Fig. 4.7: SEM image of Chromium doped Titania nanoparticles

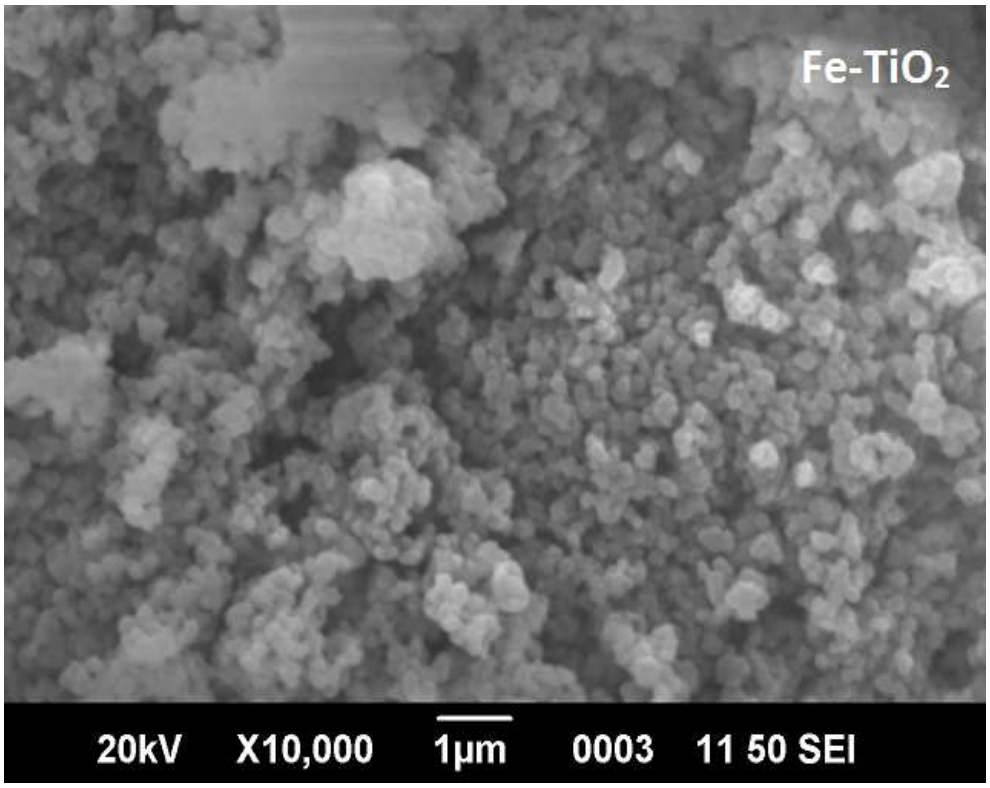

Fig. 4.8: SEM image of Iron doped Titania nanoparticles

The SEM images of unetched and etched glass beads are obtained at 5000 magnification. The surface image shows that the unetched glass beads surface does not have the roughness to hold the nanoparticles, while the glass beads etched by all the ways have resulted in the appearance of pits in the surface of the glass beads making it easy for nanoparticles to be coated on it. Among the glass beads etched by three ways the one etched with HF shows a rougher surface and an even more surface area for the nanoparticles to attach. The SEM images of the various etched glass beads are shown in Fig. 4.9-4.12. Due to the availability of greater surface area and more roughened surface, the glass beads etched with HF were selected for coating with the prepared nanoparticles to conduct column studies.

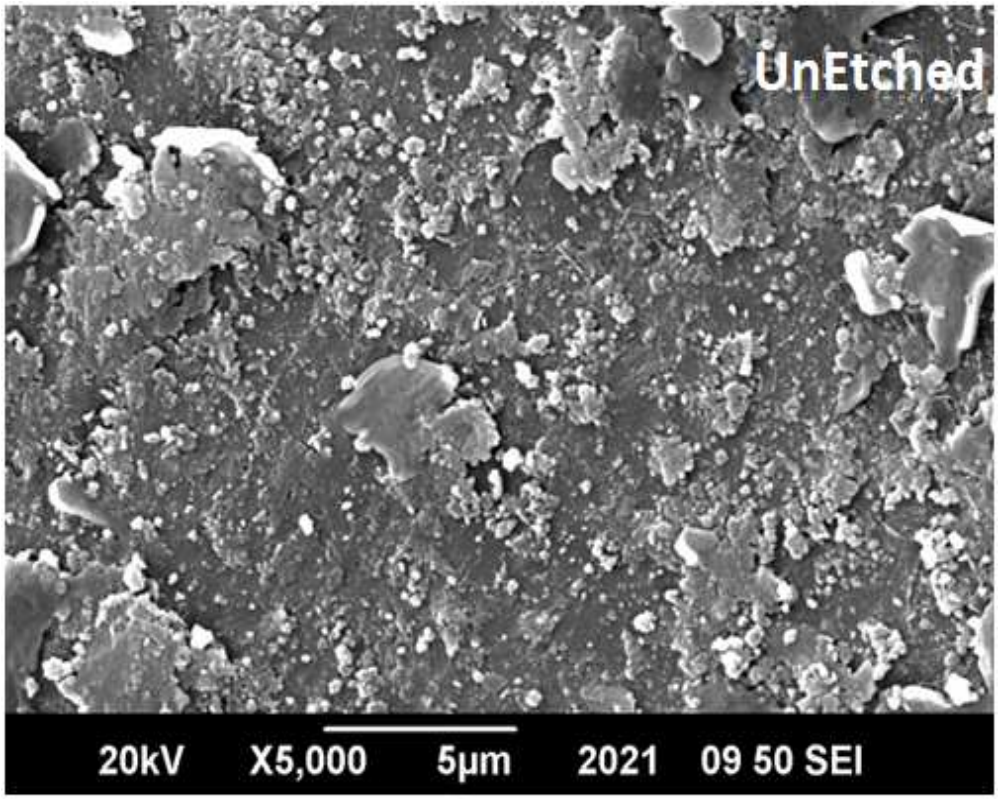

Fig. 4.9: SEM image of Unetched glass bead

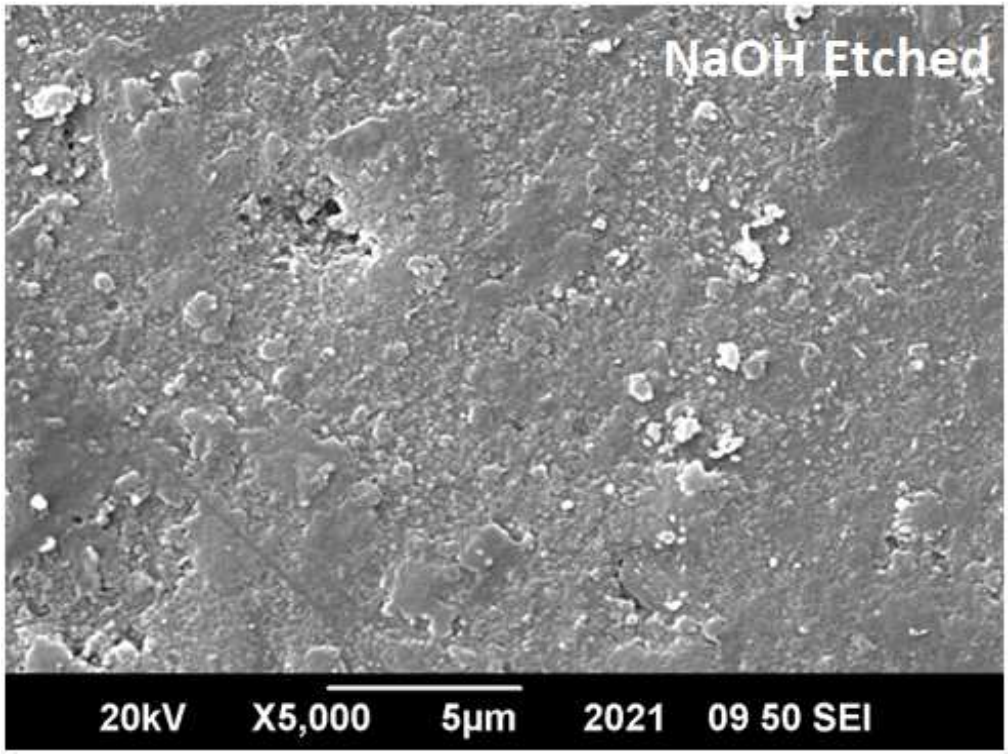

Fig. 4.10: SEM image of NaOH Etched glass bead

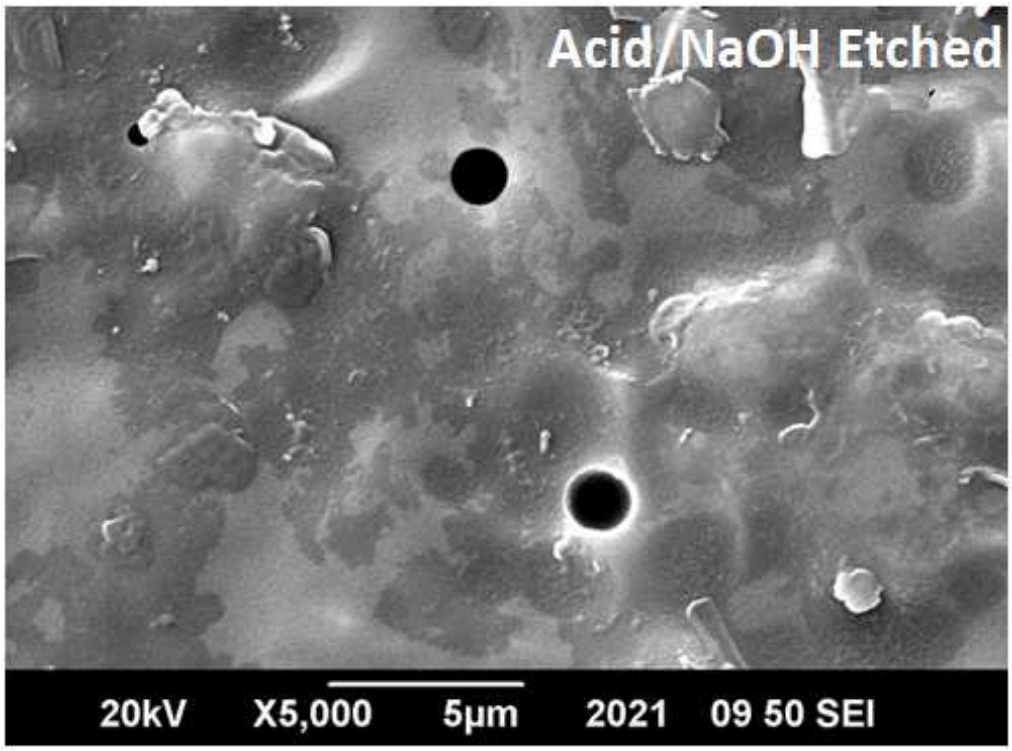

Fig. 4.11: SEM image of Acid Cleansed and NaOH Etched glass bead

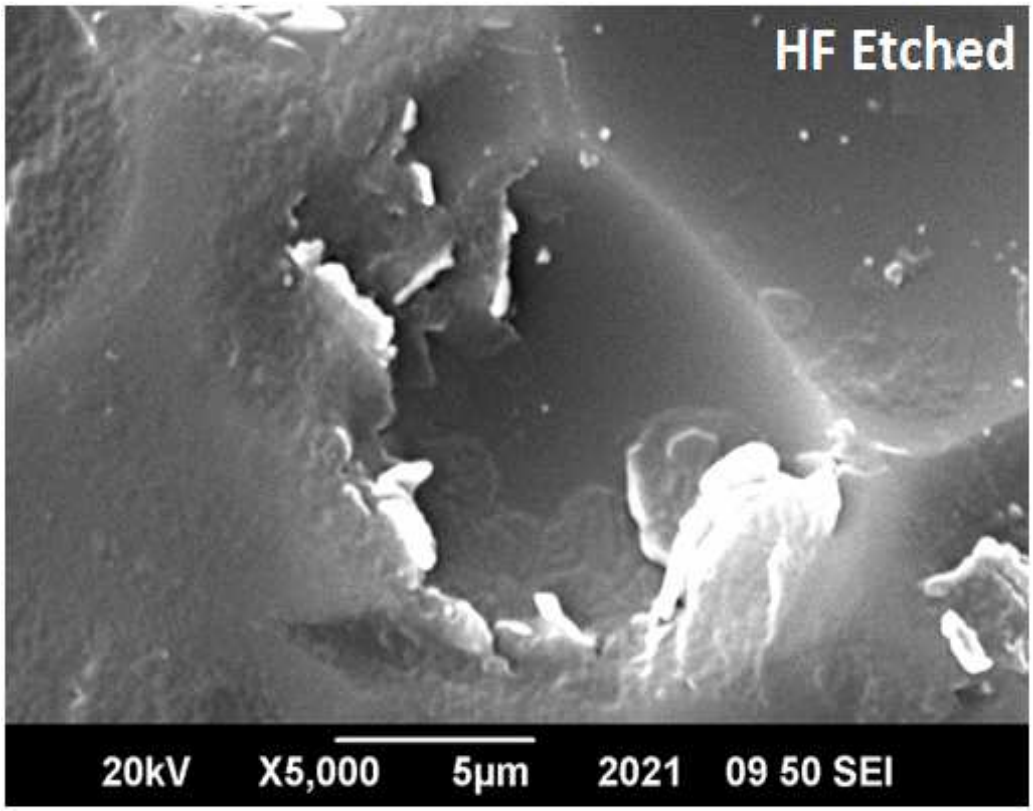

Fig. 4.12: SEM image of HF Etched glass bead

The SEM images of the glass beads coated with the different types of nanoparticles (TiO_2, Ag-doped TiO_2 and Fe-doped TiO_2) were also taken at 10,000 magnifications. It is clear from the SEM images that the nanoparticles after being coated on the glass beads have porous structure and macropores are clearly visible. The nanoparticles have the same spherical and uniform shape. The SEM images of the coated glass beads are given in Fig.4.13-4.15, below.

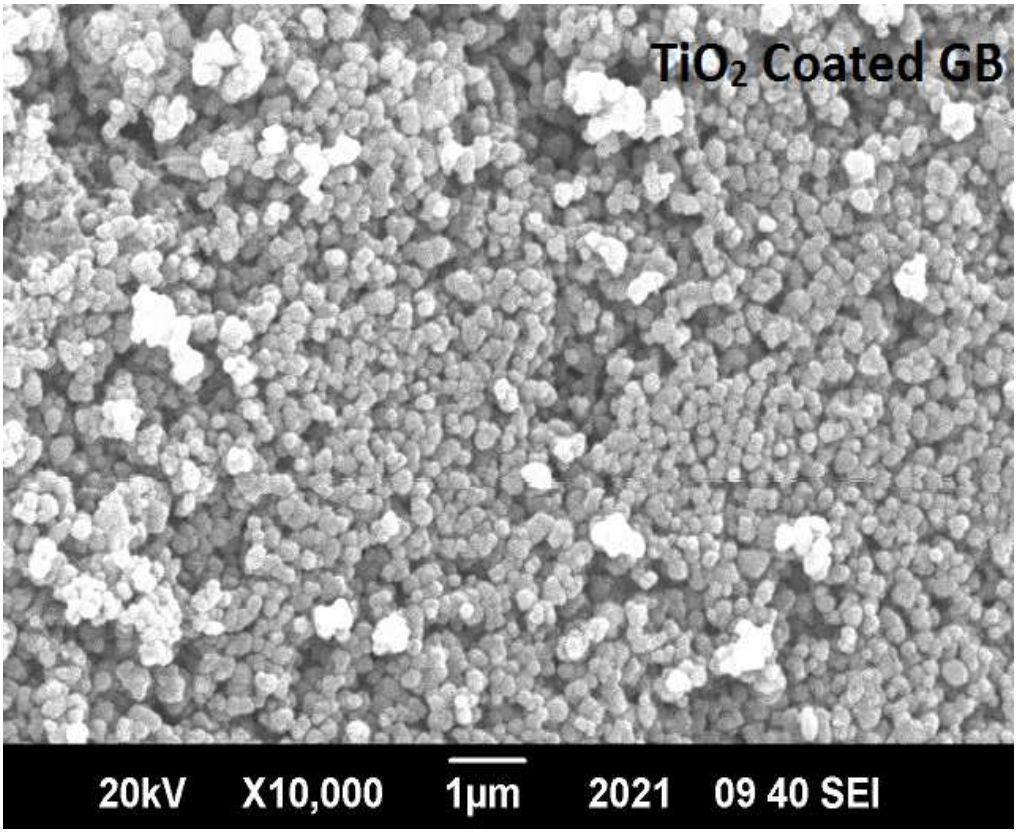

Fig. 4.13: SEM image of TiO_2 coated on glass bead

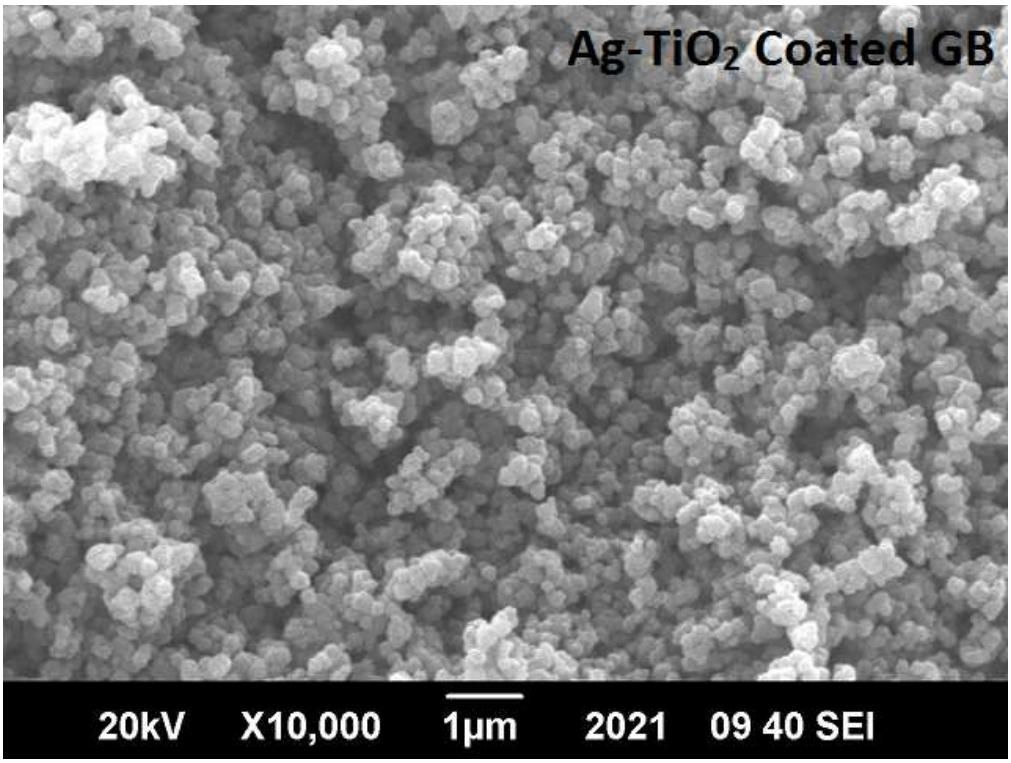

Fig. 4.14: SEM image of Ag-TiO_2 coated on glass bead

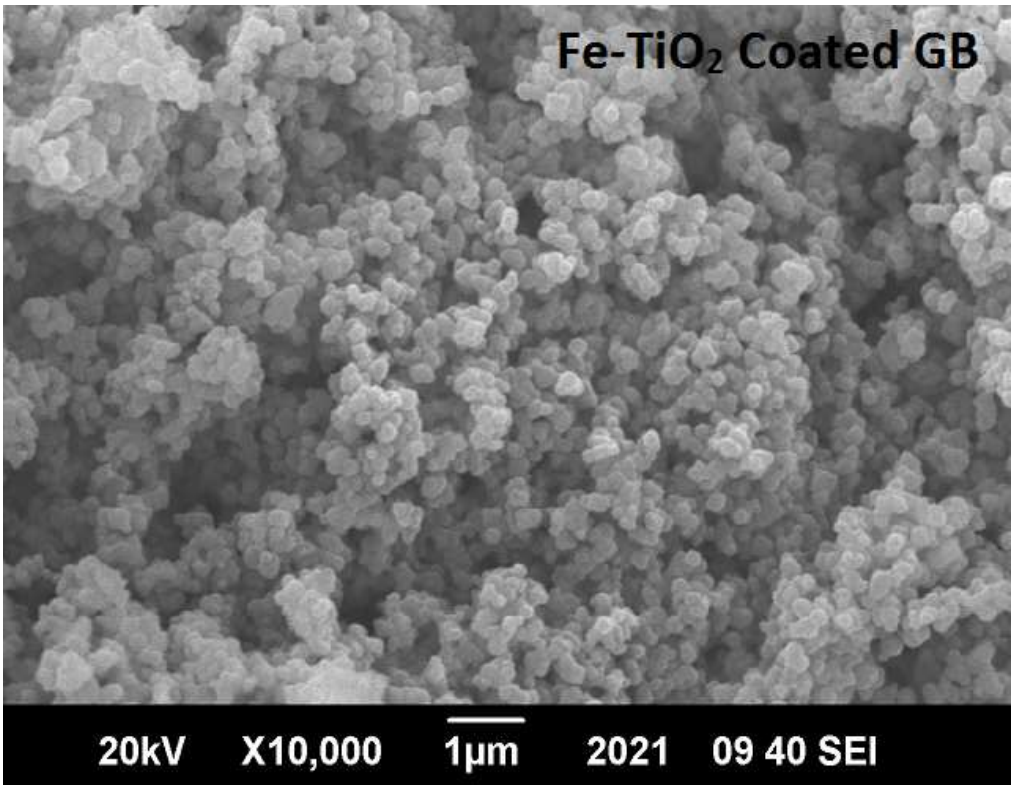

Fig. 4.15: SEM image of Fe-TiO_2 coated on glass bead

4.1.3 Energy Dispersive X-Ray Spectroscopy (EDS)

The chemical composition of the nanoparticles synthesized was analyzed by EDS analysis. The spectrums obtained are given in Fig.4.16-4.19. It is clear from the spectrum that the sample contains only Ti, O and doped element (Ag, Cr or Fe) and no impurity is present. The composition of the elements was uniform throughout showing uniform doping thus confirming SEM and XRD results. The metal composition obtained in the EDS elemental analysis was lower than the actual amount of metal added during synthesis. The elemental composition is given in Table.4.2.

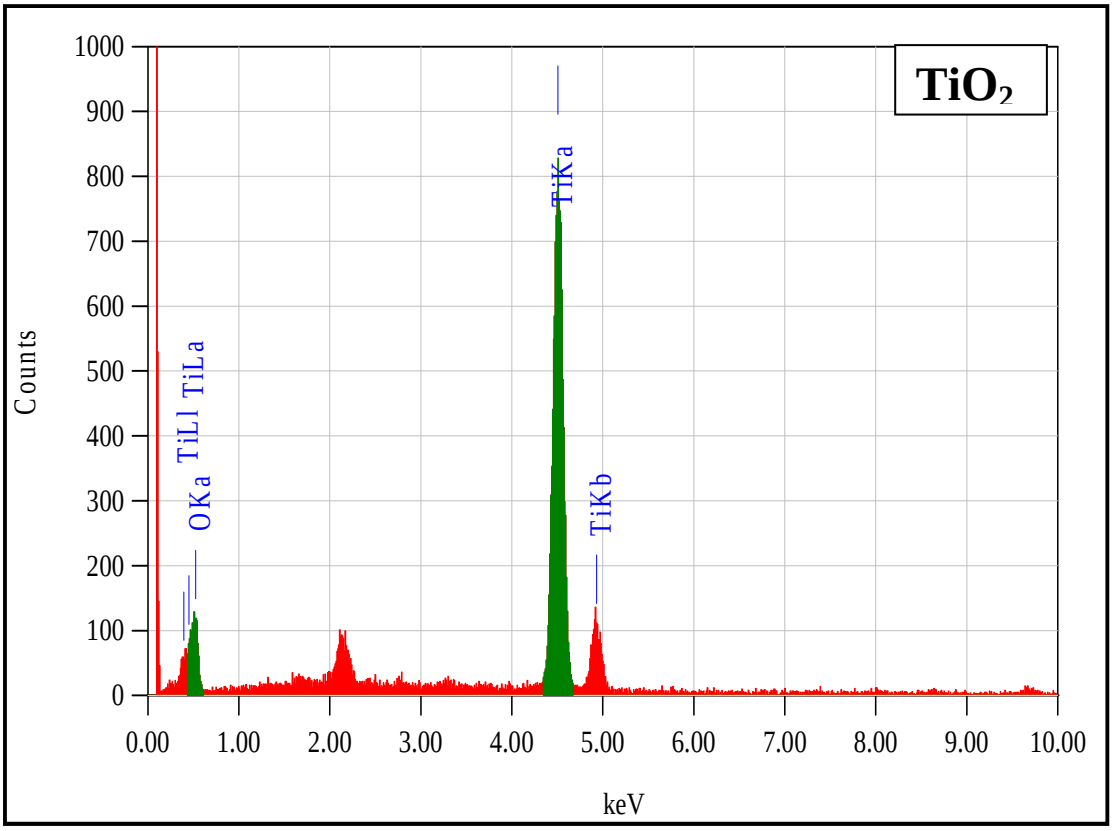

Fig. 4.16: EDS spectra of pure Titania nanoparticles

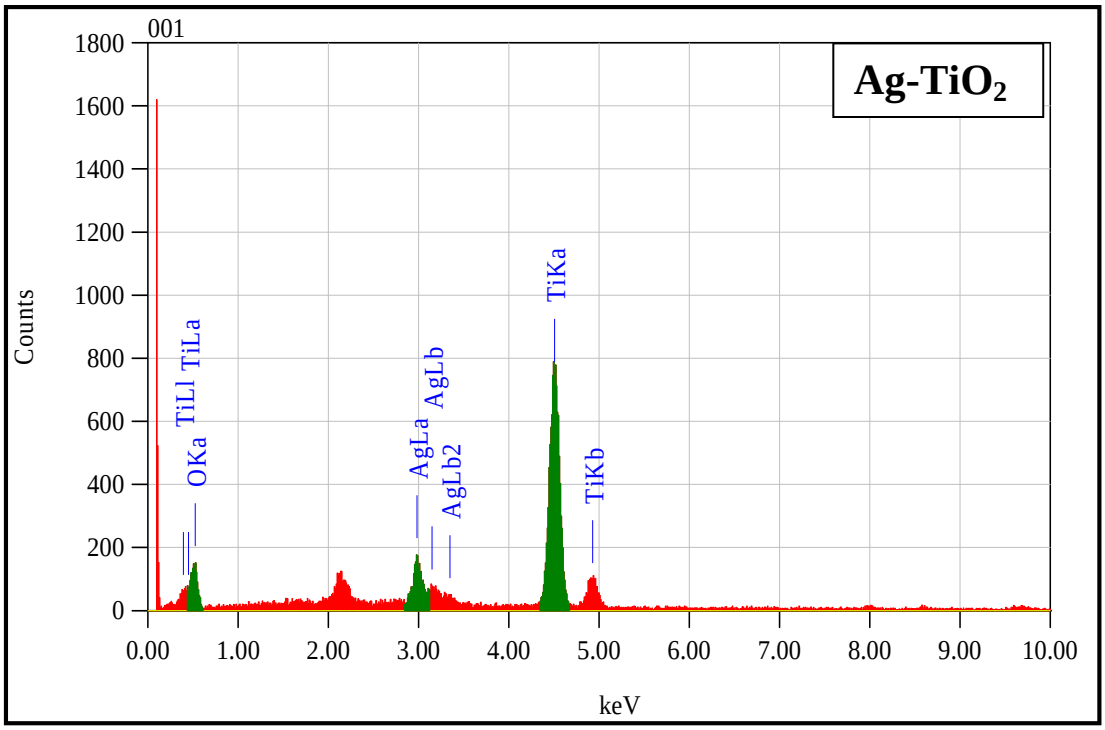

Fig. 4.17: EDS spectra of Silver doped Titania nanoparticles

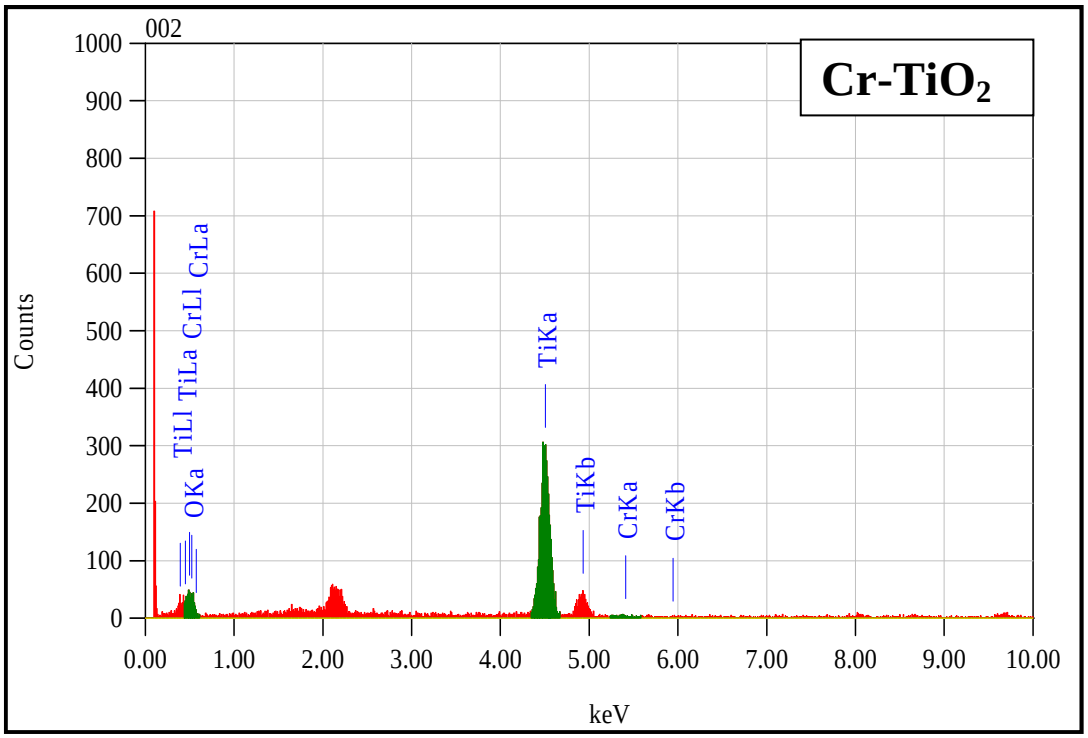

Fig. 4.18 : EDS spectra of Chromium doped Titania nanoparticles

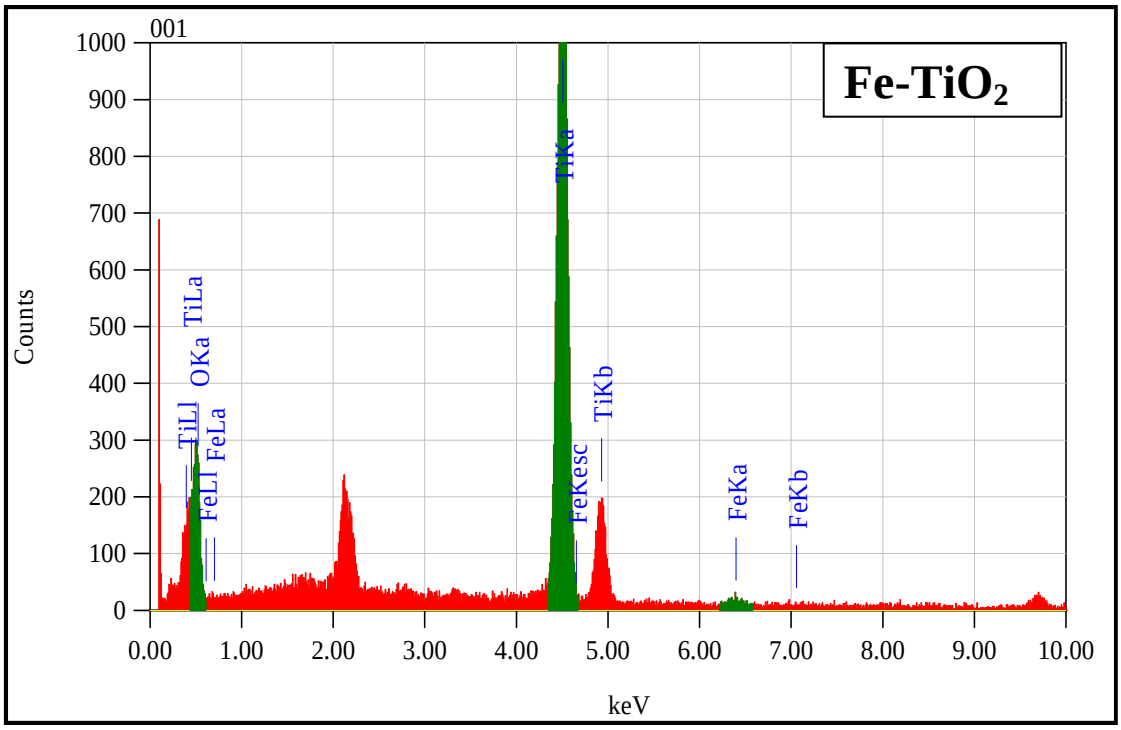

Fig. 4.19: EDS spectra of Iron doped Titania nanoparticles

Table 4.2: EDS composition of pure and metal doped Titania

Nanoparticles	TiO_2 (%)	Dopant metal (%)
TiO_2	100	-----
Ag- TiO_2	99.15	0.85
Cr- TiO_2	99.05	0.95
Fe- TiO_2	99.08	0.92

4.1.4 X-Ray Diffraction (XRD)

The nanoparticles synthesized were analyzed by XRD, JEOL JDX-II, X-ray diffractometer, to find their crystal phase composition and crystallite size. The XRD pattern are shown in Fig.4.20-4.23. The pure and metal doped TiO_2 nanoparticles syntesized showed crystalline nature and the 2θ peaks arising at 25.27 (101), 36.88 (103), 37.7 (004), 38.51 (112), 47.98 (200), 53.76 (105), 54.99 (211), 62.57 (204), 68.6 (116), 70.2 (220) and 74.9 (215). The anatase give main peak in XRD at

2θ=25.25 corresponding to 101 plane, while main peaks of brookite and rutile form appears at 2θ=30.8 (121) and 2θ=27.4 (110) respectively. It is clear from the XRD peaks that nanoparticles are in pure anatase phase (JCPDS 01-089-4921) and no rutile and brookite impurity was found. No characteristic peaks of the metals (Ag,Fe and Cr) were found in the XRD patterns implying either the metals were incorporated in the crystalline of TiO_2, or the metals were in very small quantity and highly dispersed. The average sizes of the synthesized nanoparticles were in the range of 30-40 nm as given in Table.4.3 found from the strongest XRD peak (i.e. at 2θ=25.25) using Scherrer's formula.

Table 4.3: Crystalline sizes of pure and metal doped Titania, from scherrer formula

Nanoparticles	**TiO_2**	**Ag- TiO_2**	**Cr- TiO_2**	**Fe- TiO_2**
Size (nm)	33.83	34.28	37.5	37.02

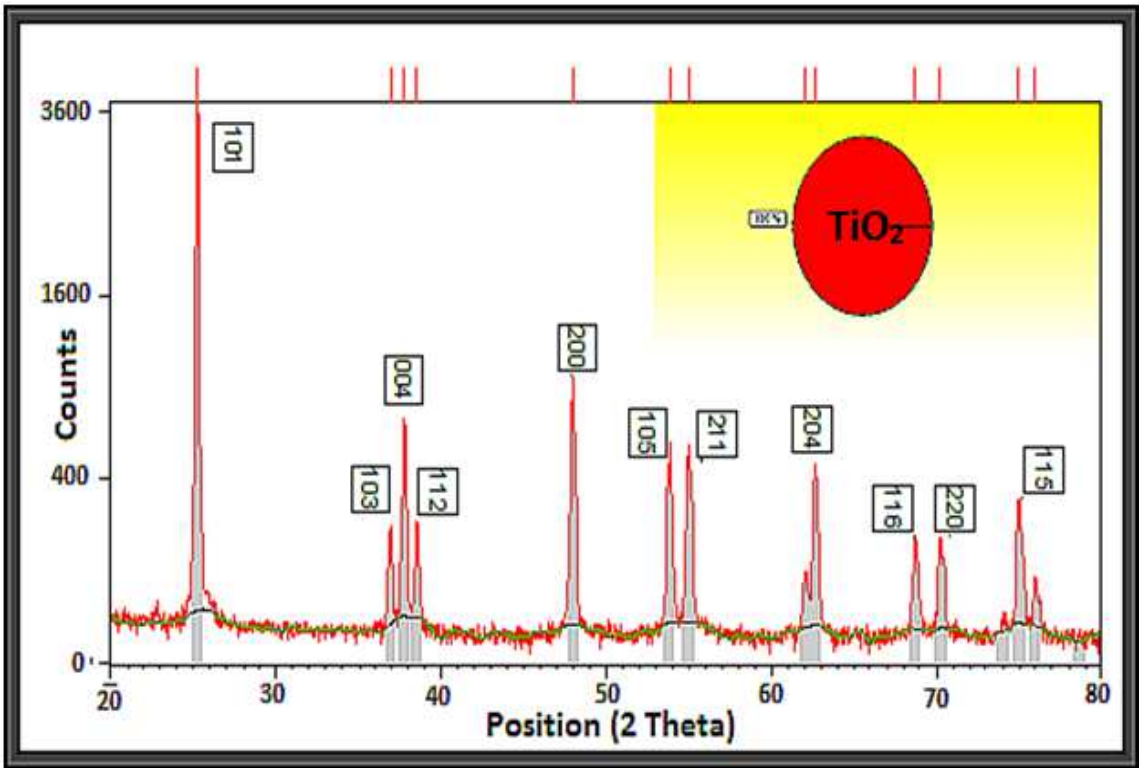

Fig. 4.20: XRD pattern of pure Titania nanoparticles

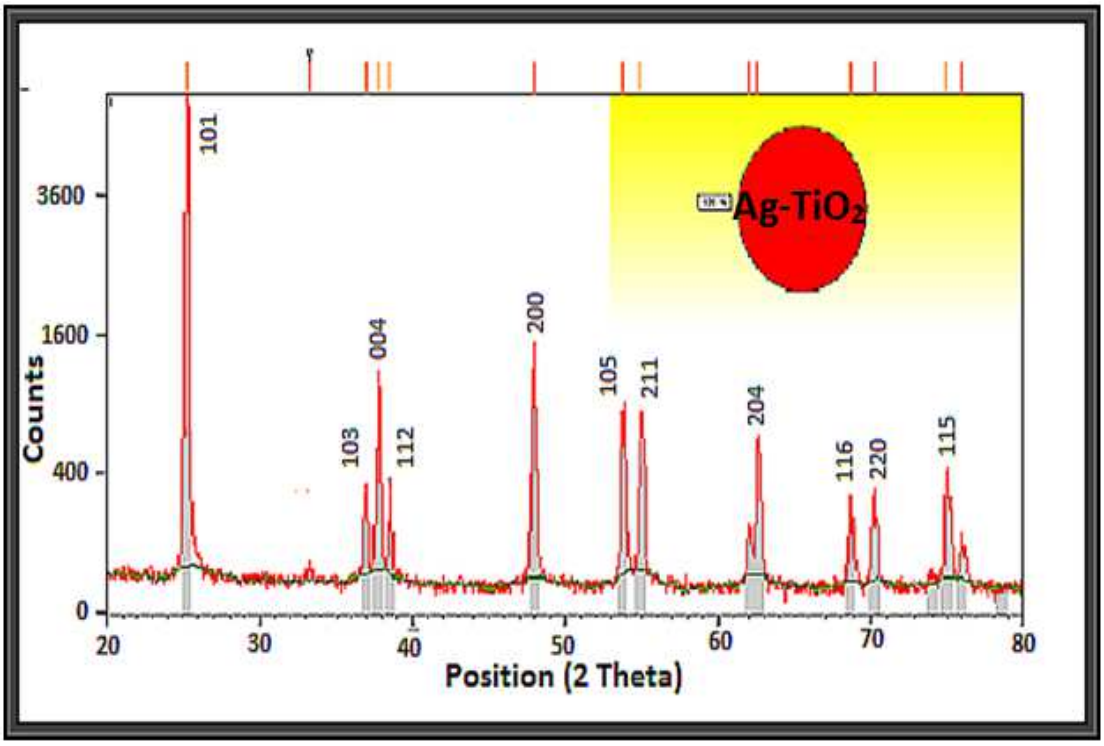

Fig. 4.21: XRD pattern of Silver doped Titania nanoparticles

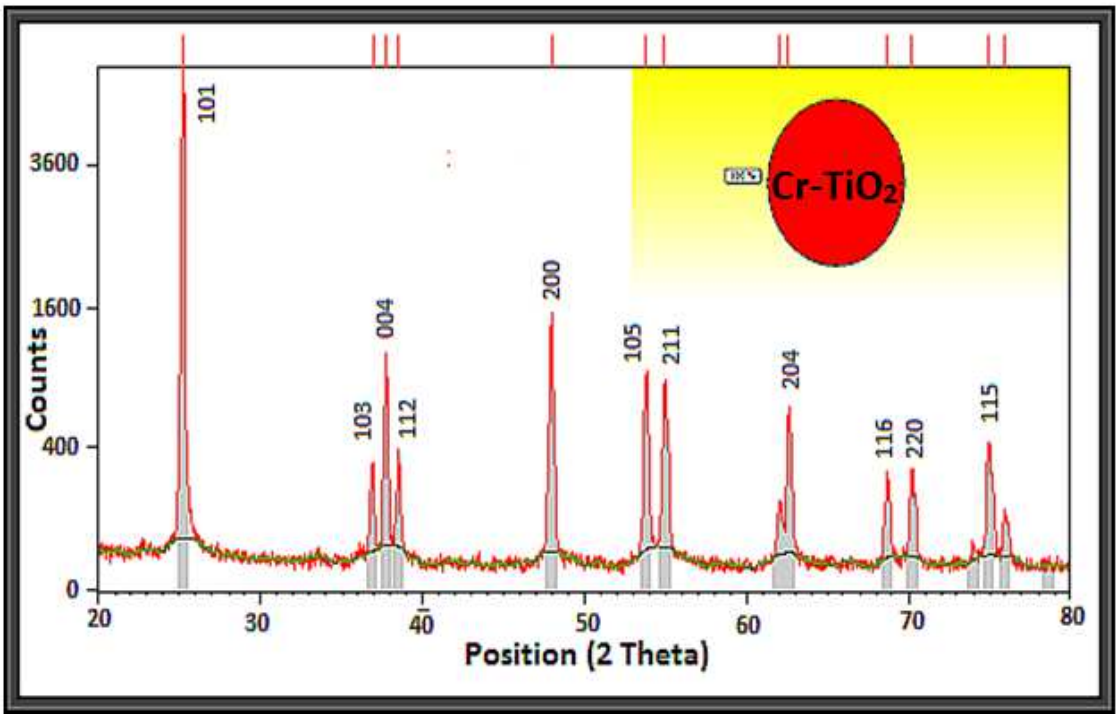

Fig. 4.22: XRD pattern of Chromium doped Titania nanoparticles

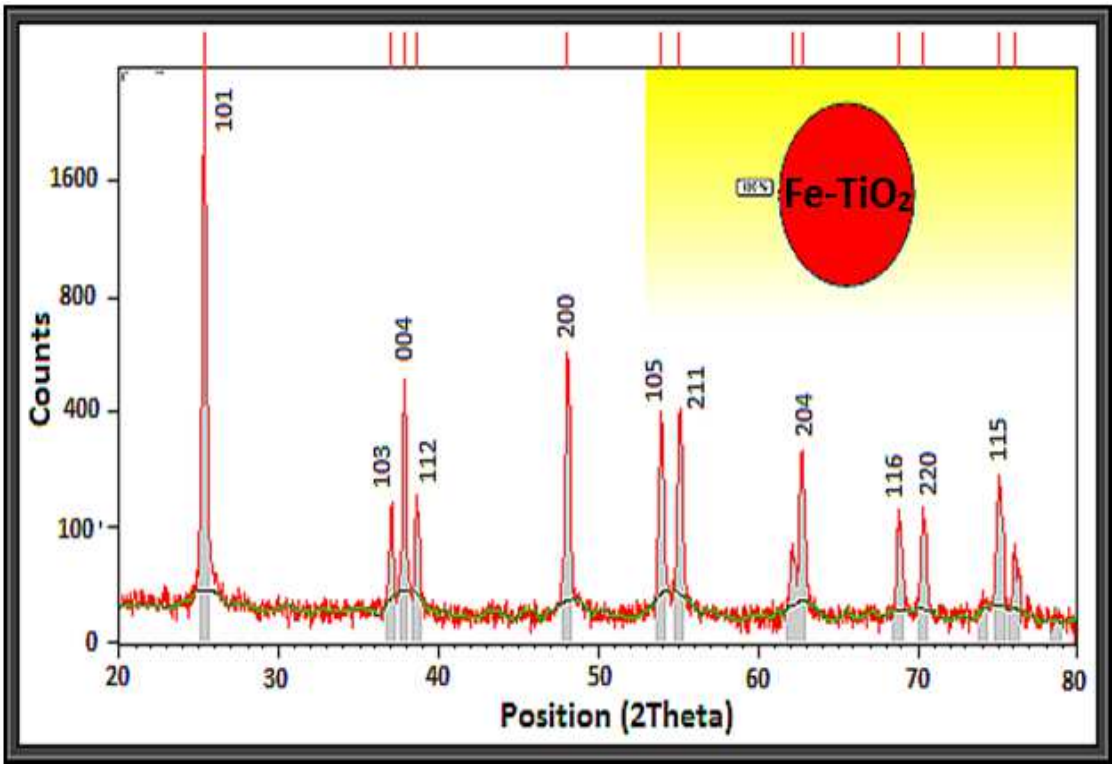

Fig. 4.23: XRD pattern of Iron doped Titania nanoparticles

4.1.5 Band Gap Analysis

The band gaps for pure and metal doped Titania nanoparticles were determined by using the equation 7 for direct transitions, given as under.

$$F(R_\infty)^2 = \left(\frac{A}{S}\right)^2 = (E - E_g)$$

While for an indirect transition equation 8 is used, this is as follows.

$$F(R_\infty)^{\frac{1}{2}} = \left(\frac{A}{S}\right)^{\frac{1}{2}} = (E - E_g)$$

The plot of $F(R_\infty)^{1/2}$ Vs E *(eV)* gives the indirect transitions for the pure and metal doped Titania. The plots are given in Fig.4.24-4.27. By extrapolating the linear part of the graphs the band gap (E_g) is obtained, as shown in the figures.

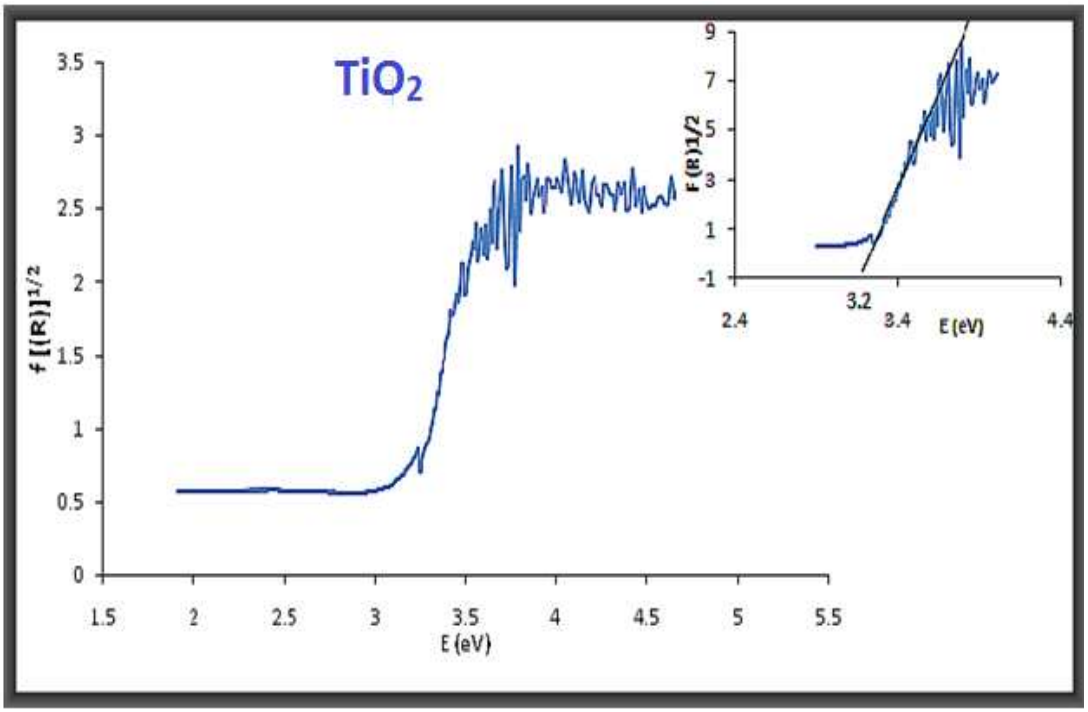

Fig. 4.24: Diffused reflectance spectra for indirect transition of pure Titania nanoparticles

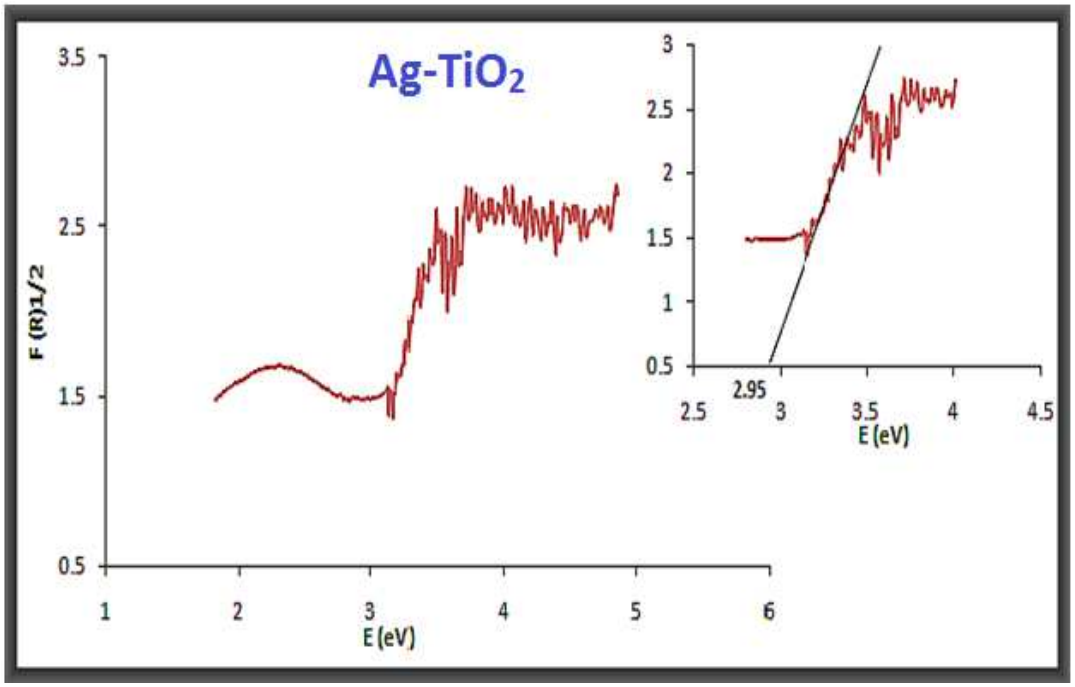

Fig. 4.25: Diffused reflectance spectra for indirect transition of Silver doped Titania nanoparticles

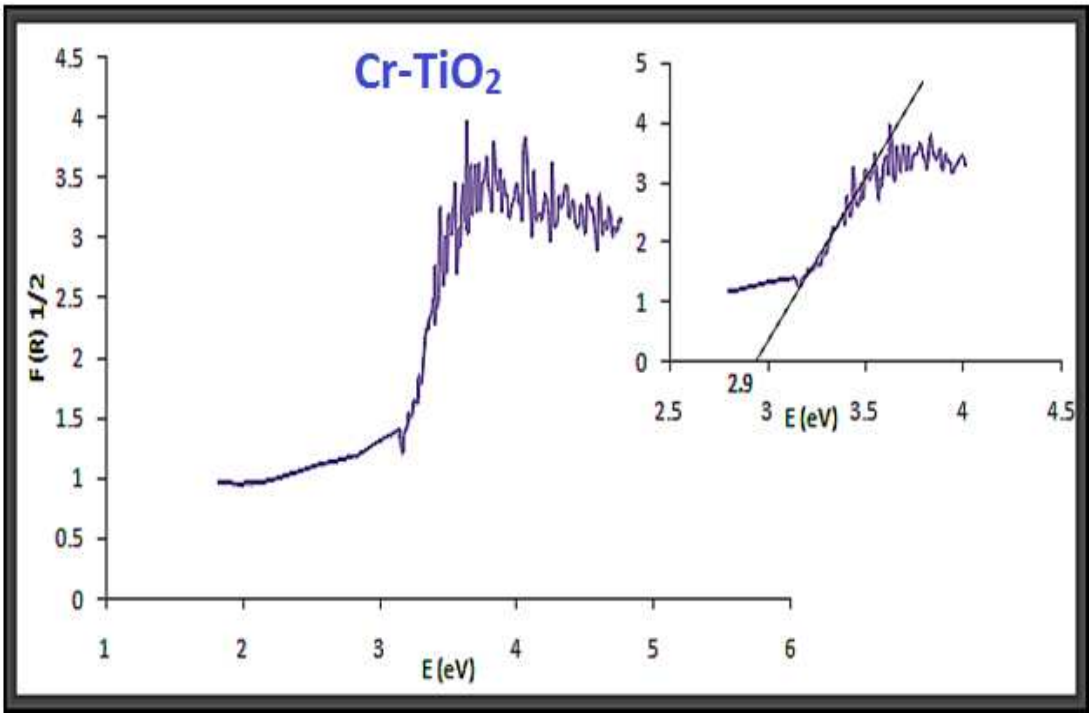

Fig. 4.26: Diffused reflectance spectra for indirect transition of Chromium doped Titania nanoparticles

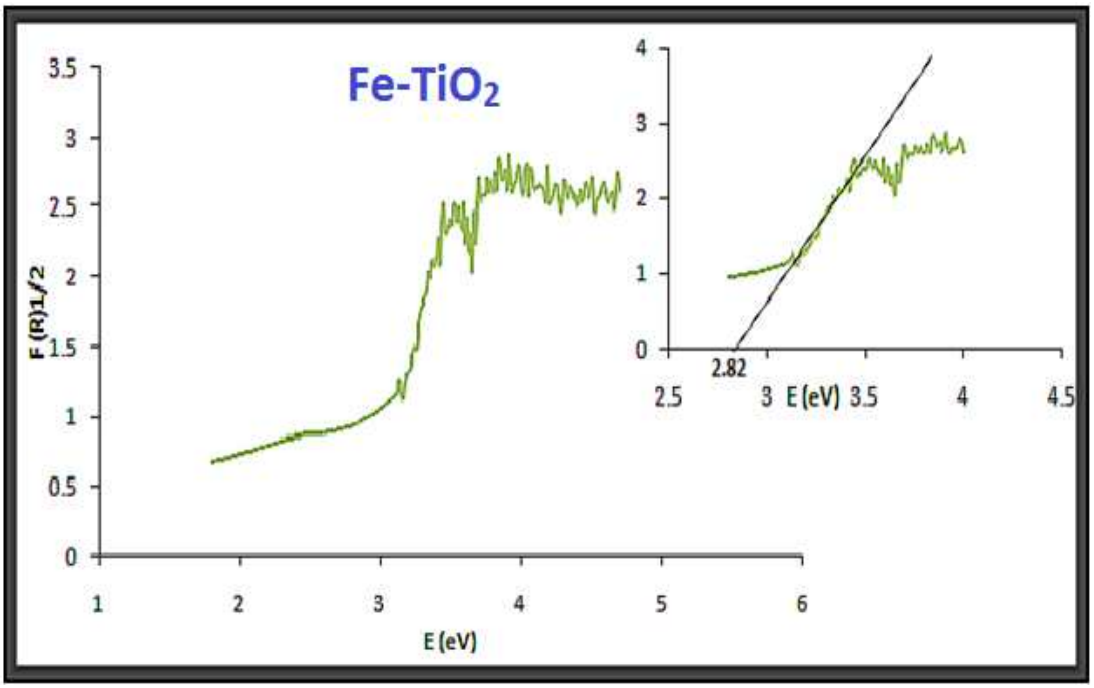

Fig. 4.27: Diffused reflectance spectra for indirect transition of Iron doped Titania nanoparticles

The direct transitions are obtained by plotting $F(R_\infty)^2$ Vs E *(eV)* as shown in Fig.4.28-4.31. The band gap (E_g) in this case is also found by extrapolating the linear part of the graphs as shown in the respective figure.

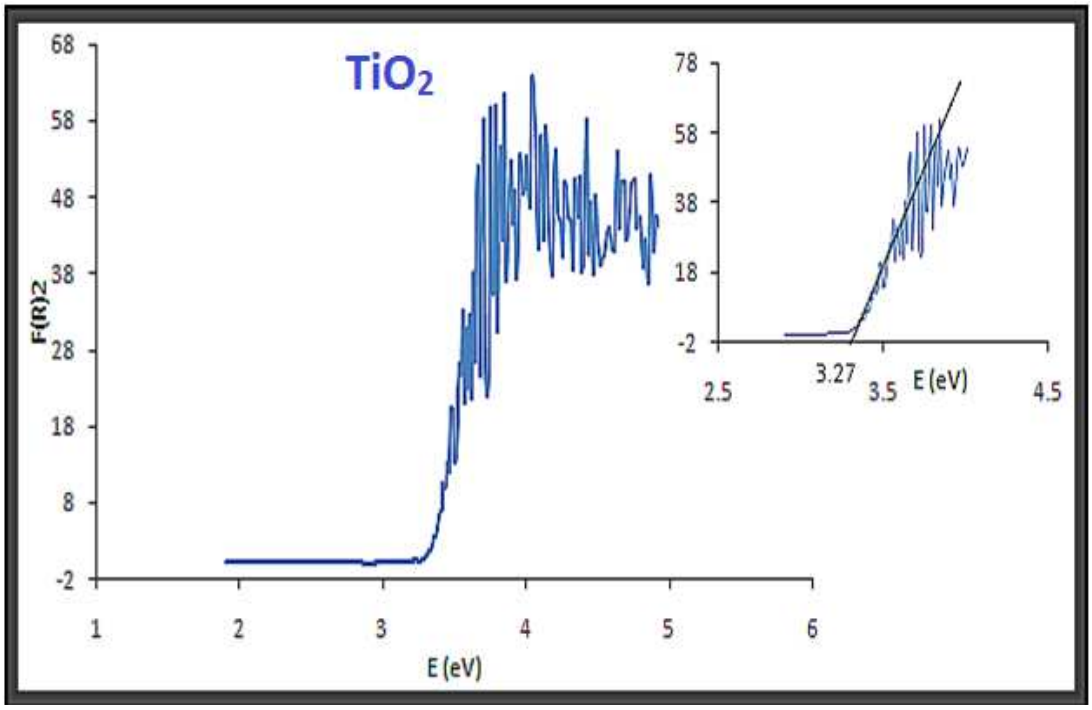

Fig. 4.28: Diffused reflectance spectra for direct transition of pure Titania nanoparticles

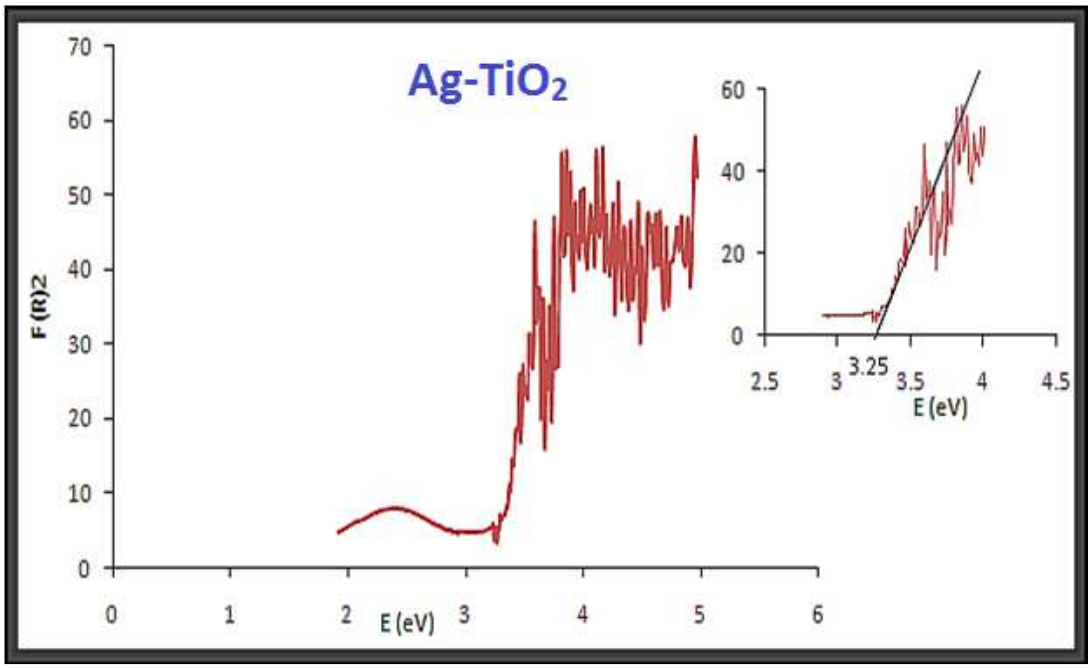

Fig. 4.29: Diffused reflectance spectra for direct transition of Silver doped Titania nanoparticles

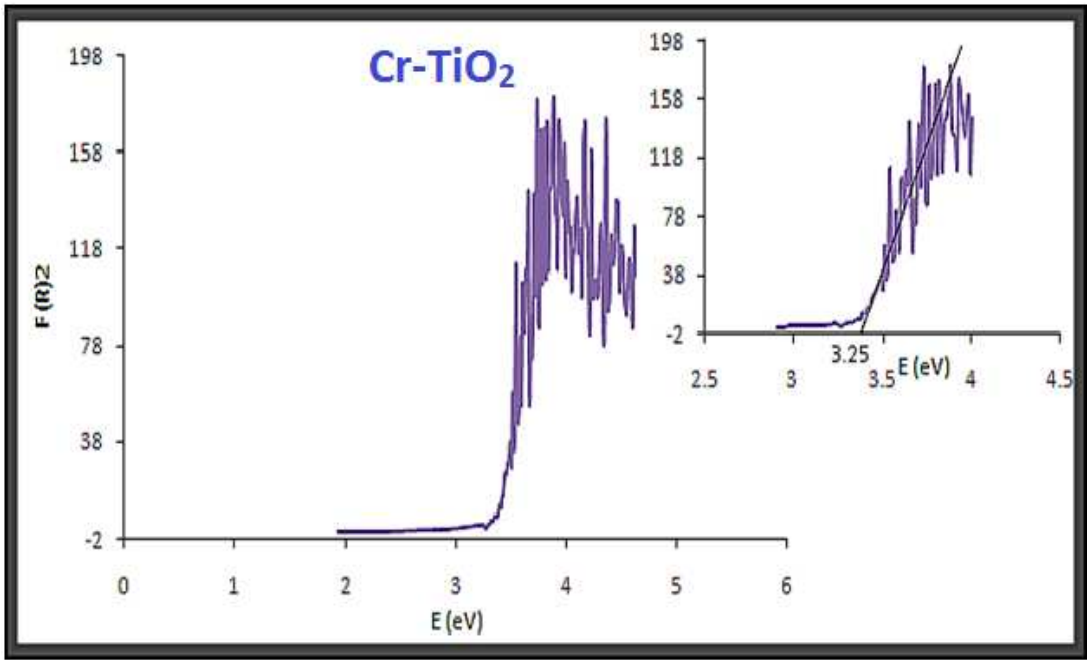

Fig. 4.30: Diffused reflectance spectra for direct transition of Chromium doped Titania nanoparticles

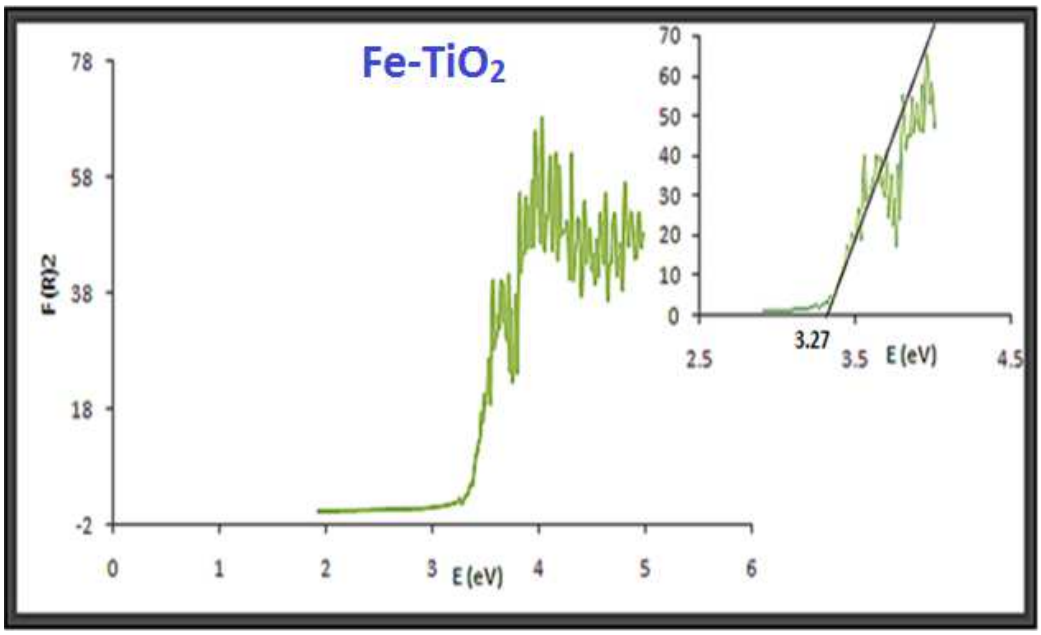

Fig. 4.31: Diffused reflectance spectra for direct transition of Iron doped Titania nanoparticles

Table 4.4: Direct and Indirect bad gap values of pure and metal doped Titania nanoparticles

Nanoparticles	Band Gap	
	Direct	Indirect
TiO_2	3.27	3.2
Ag-TiO_2	3.25	2.95
Cr- TiO_2	3.25	2.9
Fe- TiO_2	3.27	2.82

The band gap of TiO_2 reported in literature is 3.2 eV, which corresponds to a wavelength of 385nm. For the synthesized pure Titania nanoparticles, the direct transition (Fig.13) shows unrealistic value of band gap above 3.27, which for anatase phase are not expected. Similarly some unexpected band gap values were obtained for the metal doped Titania nanoparticles as well (as shown in Table.4.4). The indirect transitions (Fig.12) shows the band gap values of 3.2 eV, 2.95 eV, 2.9 eV and 2.82 eV for pure TiO_2, Ag-TiO_2, Cr-TiO_2 and Fe-TiO_2 nanoparticles respectively, and corresponds to wavelengths of 385 nm, 420 nm, 428 nm and 440 nm respectively. Therefore the synthesized pure and metal doped Titania nanoparticles follow indirect type transitions (Valencia et al., 2010).

4.2 REMOVAL EFFICIENCY

The removal efficiencies of pure and metal doped Titania nanoparticles was calculated by taking 100ml of 0.5 ppm arsenic solution and adsorbent dose of 0.5g at pH 7. The results found after the adsorption are shown in the Table.4.5. It is clear from the table that due to metal doping the removal efficiency of Titania increased enormously. This is due to the fact that due to metal doping the absorption band of Titania is shifted from UV region into the visible region of the spectrum, so it can more readily oxidize As(III) to As(V) and the later can be adsorb more efficiently by Titania.

Table 4.5: Removal efficiencies of different nanoparticles used

Nanoparticles	**TiO_2**	**Ag-TiO_2**	**Cr-TiO2**	**Fe-TiO_2**
Removal efficiency (%)	65	90	95	96

4.3 EFFECT OF PH

The removal efficiencies were measured at three different pH values of 4, 7 and 10, using the adsorbent dose at 0.5 g in 100 ml of 0.5ppm As(III) solutions. The results obtained are as shown in the Fig.4.32.

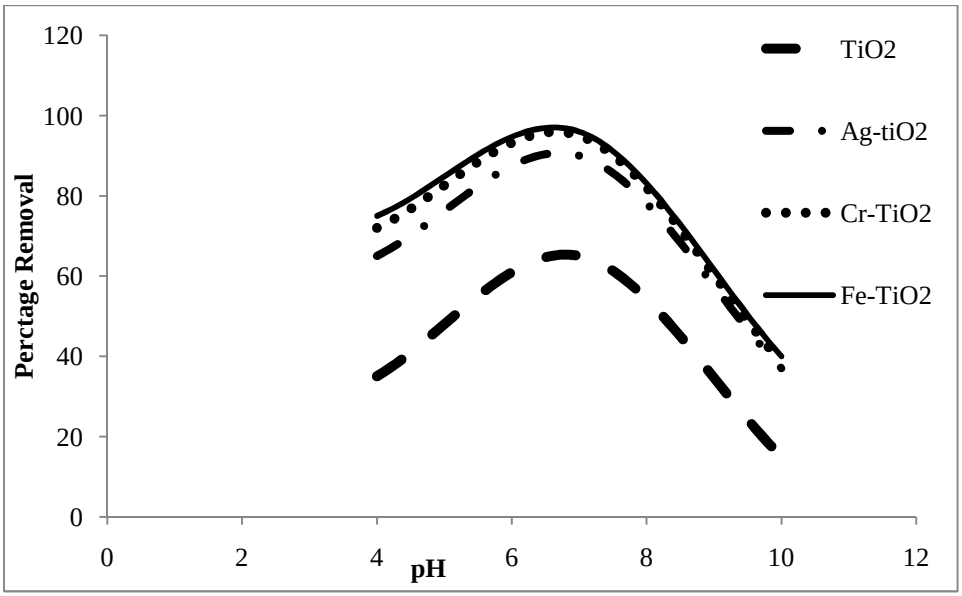

Fig. 4.32: Effect of pH on Removal efficiency

It is clear from the figure that as we approach the neutral pH the removal efficiency increases. The removal efficiency decreases on moving both to acidic and basic pH. The decrease in removal efficiency is more in Basic region than the acidic. Thus from this point forward all the reactions are carried out at Neutral pH i.e pH 7 ± 0.1.

4.4 ADSORPTION ISOTHERMS

Adsorption studies were carried out to determine the suitable conditions for maximum arsenic removal by the nanoparticles. Different As (III) concentration (0.1, 0.2, 0.4, 0.8, 1.5, 3 and 6 ppm) were used. The pH of the solutions was adjusted at 7. Langmuir, Freundlich models were applied for adsorption studies.

The Langmuir isotherm assumes monolayer adsorption at the adsorbent surface. The linear form of Langmuir adsorption isotherm equation is as below (Deniz and Karaman, 2011).

$$\frac{C_e}{q_e} = \frac{C_e}{q_m} + \frac{1}{q_m b} \qquad \textbf{11}$$

Where q_m is the quantity of As (III) adsorbed per unit weight of nanoparticles (mg/g) at equilibrium, Ce is the equilibrium As (III) concentration in the solution after adsorption. q_m and b are Langmuir constants corresponding to maximum adsorption at monolayer coverage (mg/g) and energy of adsorption respectively. The values of q_m and b can be obtained from the slope and intercept of the curves (Fig.4.33-4.36).

The value of b can be represented by another dimensionless quantity R_L given by the following equation (Islam and Patel, 2007).

$$R_L = \frac{1}{1+(bC_o)} \qquad \textbf{12}$$

Where C_o is the initial arsenic concentration, the value of R_L gives knowledge about the isotherm to be Irreversible (R_L =0), favorable (0< R_L < 1), linear (R_L =1) or unfavorable (R_L > 1) (Deniz, Karaman, 2011). The values of all the different

constants obtained are given in Table.4.6. These values clearly suggests that Langmuir isotherm give a good fit to the experimental results, more over the value of constant b for the different nanoparticles also show great affinity of the binding sites and chemical interaction between the adsorbent and adsorbate. The value of R_L for all the four nanoparticles lies between 0 and 1 suggesting favorable adsorption of As (III) by pure and metal doped Titania.

Table 4.6: Langmuir isotherm parameters of As (III) adsorption for pure and metal doped Titania

Nanoparticles	**q_m (mg/g)**	**b**	**R_L***	**R^2**
TiO_2	1.6	0.377	0.84	0.978
Ag-TiO_2	1.71	0.94	0.68	0.988
Cr-TiO2	2.8	2	0.88	0.962
Fe-TiO_2	3.08	2.305	0.46	0.985

* For C_o = 0.5 ppm

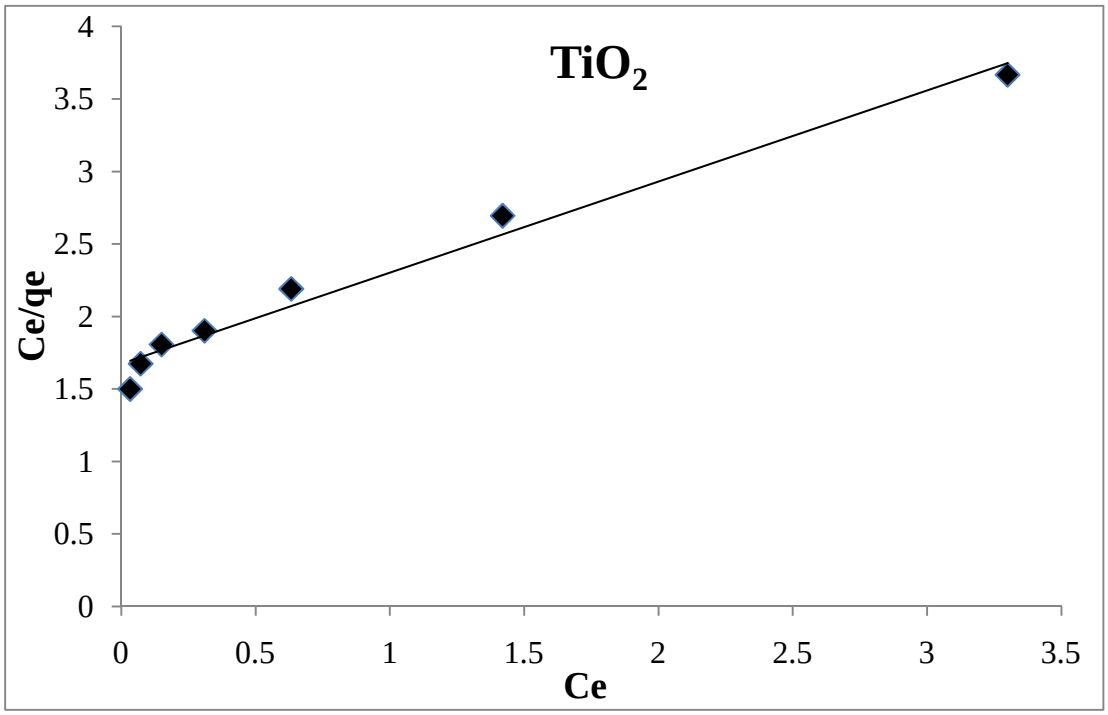

Fig. 4.33: Langmuir adsorption isotherm of pure Titania nanoparticles

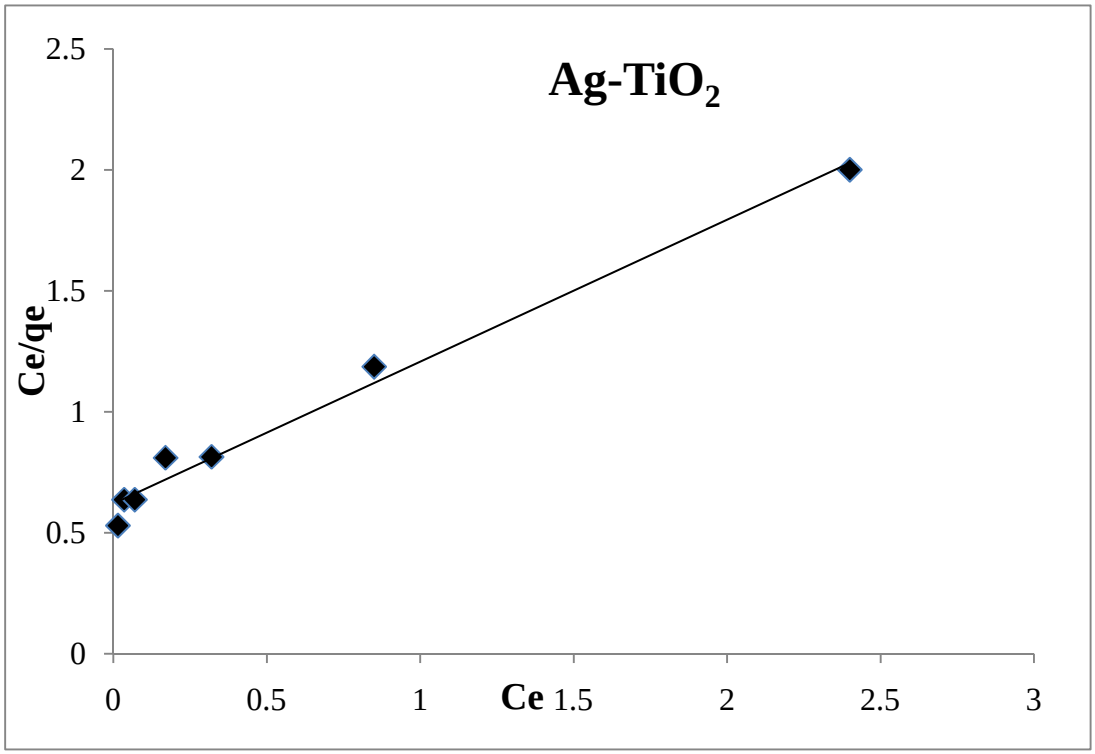

Fig. 4.34: Langmuir adsorption isotherm of Silver doped Titania nanoparticles

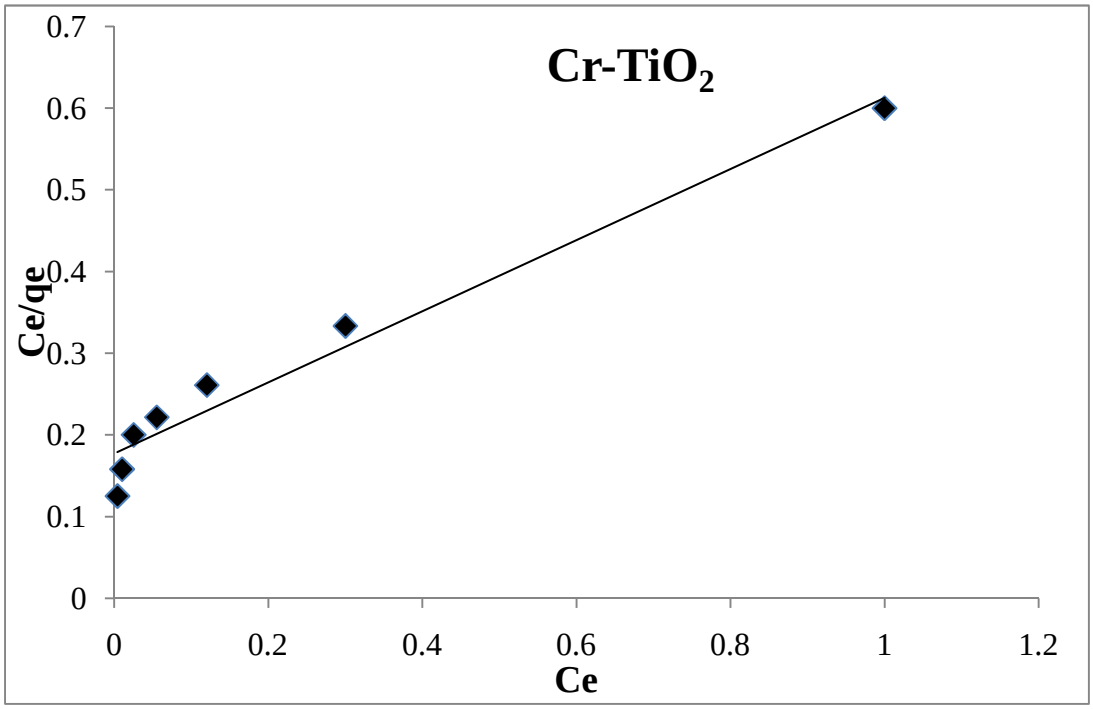

Fig. 4.35: Langmuir adsorption isotherm of Chromium doped Titania nanoparticles

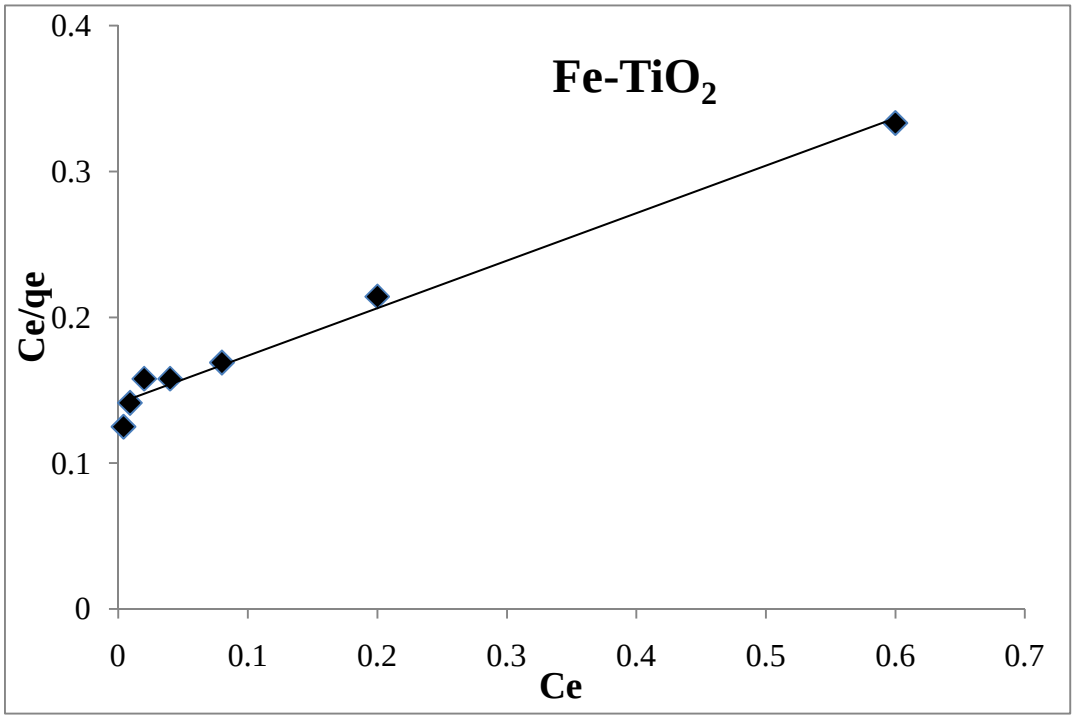

Fig. 4.36: Langmuir adsorption isotherm of Iron doped Titania

The Freundlich isotherm equation is generally given by (Chowdhury and Yanful, 2010; Maiti et al., 2007)

$$q_e = K_F \times C_e^{1/n} \qquad \textbf{13}$$

Where C_e is the amount of As (III) left in the solution after adsorption and q_e is the amount of As (III) in per unit weight of the adsorbent (mg/g). K_F and n are Freundlich constants. The linear form of Freundlich equation in logarithmic form is given as under.

$$\ln q_e = \ln K_F + n \ln C_e \qquad \textbf{14}$$

The plot of ln C_e Vs ln q_e drawn at various initial concentration of As (III) (0.1, 0.2, 0.4, 0.8, 1.5, 3 and 6 ppm) , each gave a straight line with slope equal to n and intercept equal to ln K_F (Fig.4.37-4.40). The values of different parameters obtained from the plots are given in Table 4.7.

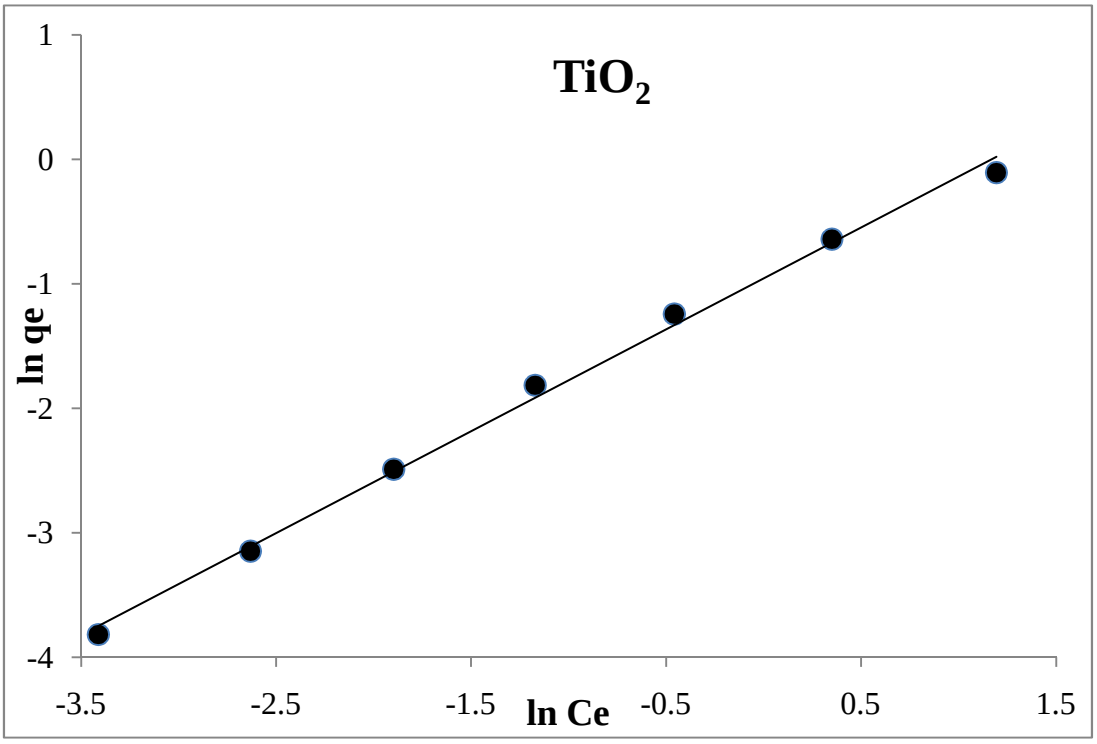

Fig. 4.37: Freundlich adsorption isotherm of pure Titania nanoparticles

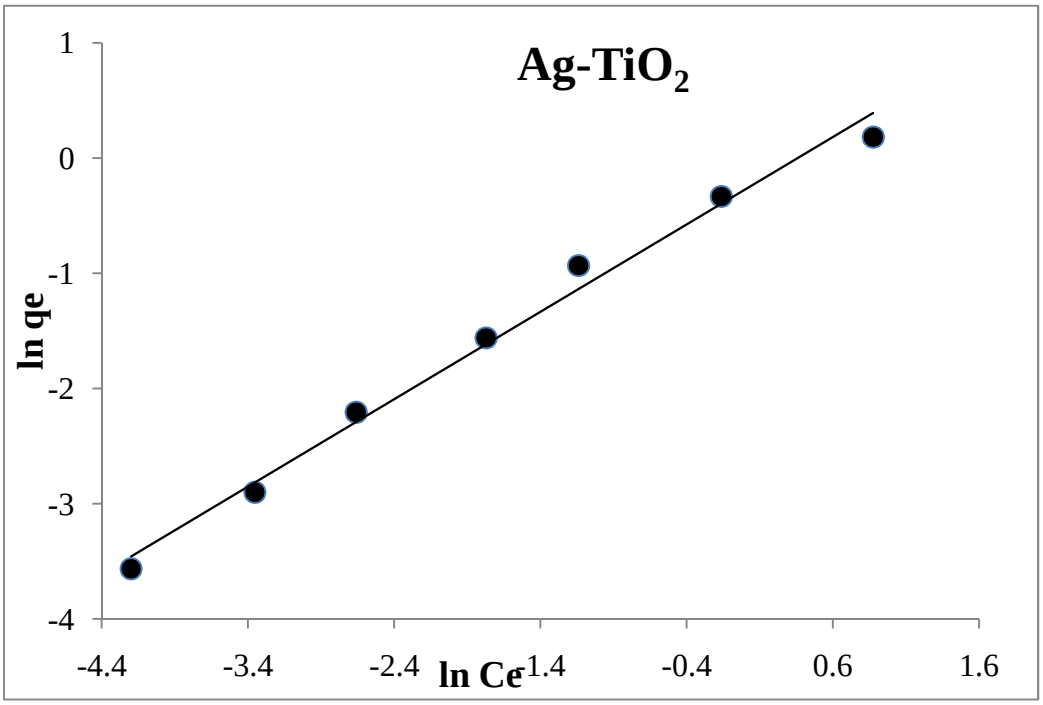

Fig. 4.38: Freundlich adsorption isotherm of Silver doped Titania nanoparticles

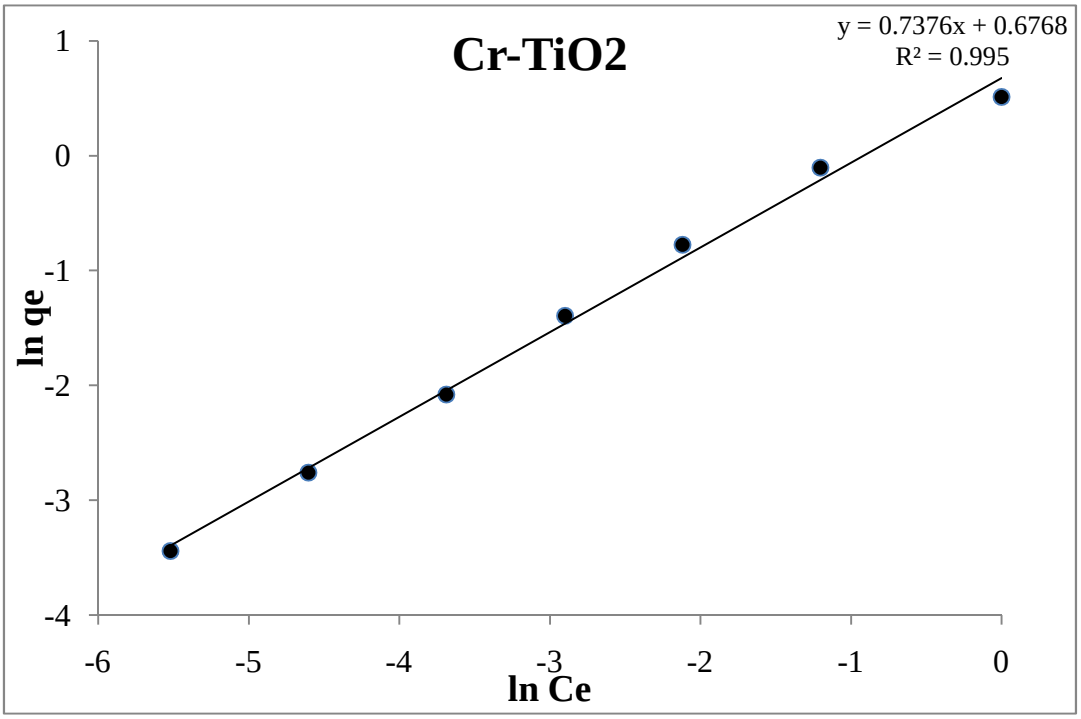

Fig. 4.39: Freundlich adsorption isotherm of Chromium doped Titania nanoparticles

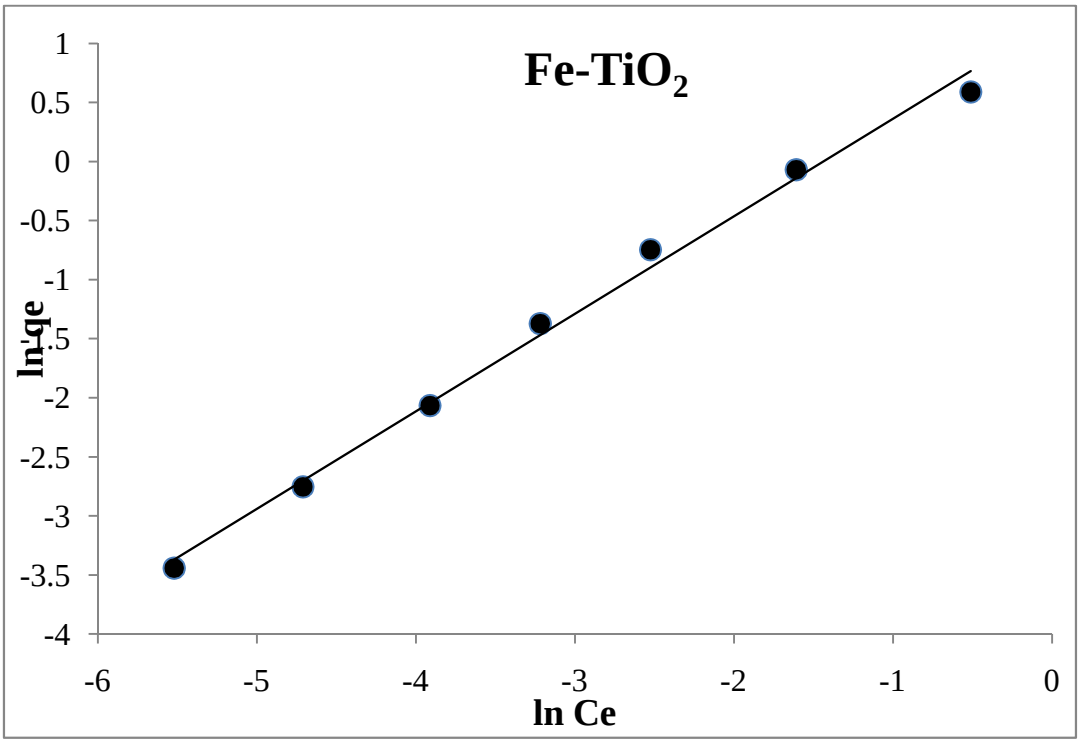

Fig. 4.40: Freundlich adsorption isotherm of Iron doped Titania nanoparticles

Table 4.7: Freundlich isotherm parameters of As (III) adsorption for pure and metal doped Titania

Nanoparticles	n	K_F	R^2
TiO_2	1.22	0.385	0.996
Ag-TiO_2	1.32	0.76	0.990
Cr-TiO2	1.35	2	0.995
Fe-TiO_2	1.21	3.274	0.993

The higher the value of K_F represents higher affinity of the adsorbent for As (III), while the value of n between 1 and 10 shows favorable adsorption. It is clear from the table that the values of n for all the four nanoparticles are above 1, showing that the adsorption process is favorable. From the table it can be seen that the value of K_F for metal doped Titania are higher than pure Titania, moreover the value of K_F for Fe-doped Titania is greater than any other metal doped Titania showing that among the metal doped Titania Fe serves the purpose well. The values of R^2 for all the nanoparticles are also above 0.98, showing strong linear relationship between ln q_e and ln C_e.

4.5 KINETIC ISOTHERM

Several models are available to express the mechanism of adsorption of solute onto the sorbent. To investigate the mechanism of adsorption, characteristic constants of adsorption were determined pseudo-second order equation was used. The pseudo-second order kinetic equation is given as under (Ho and Mckay, 1998).

$$\frac{dq_t}{dt} = k(q_e - q_t)^2 \qquad \textbf{15}$$

Where q_e is equilibrium sorption capacity (mg/g) and q_t is the sorption capacities (mg/g) at time t, respectively, and k is the pseudo-second order rate constant (g mg^{-1}

min^{-1}). At boundary conditions, t = 0 to t and q_t = 0 to q_t, the integrated form of equation (7) is given as (Ho and Ofomaja, 2006).

$$\frac{1}{(q_e - q_t)} = \frac{1}{q_e} + kt \qquad \textbf{16}$$

Rearranging this equation we get

$$q_t = \frac{1}{\frac{1}{kq_e^2} + \frac{t}{q_e}} \qquad \textbf{17}$$

This gets the linear form as

$$\frac{t}{q_t} = \frac{1}{kq_e^2} + \frac{1}{q_e}t \qquad \textbf{18}$$

Where h is the initial adsorption rate as q_t/t, when t approaches to zero, hence:

$$h = k\, q_e^2 \qquad \textbf{19}$$

The equation (10) takes the form as

$$\frac{t}{q_t} = \frac{1}{h} + \frac{1}{q_e}t \qquad \textbf{20}$$

Thus by plotting t/q_t Vs t will give a straight line, as shown in Fig.4.41-4.44. The value of q_e, k and h can be determined from the slope and intercept of the plot. The values of different parameters obtained are given in the Table 4.8.

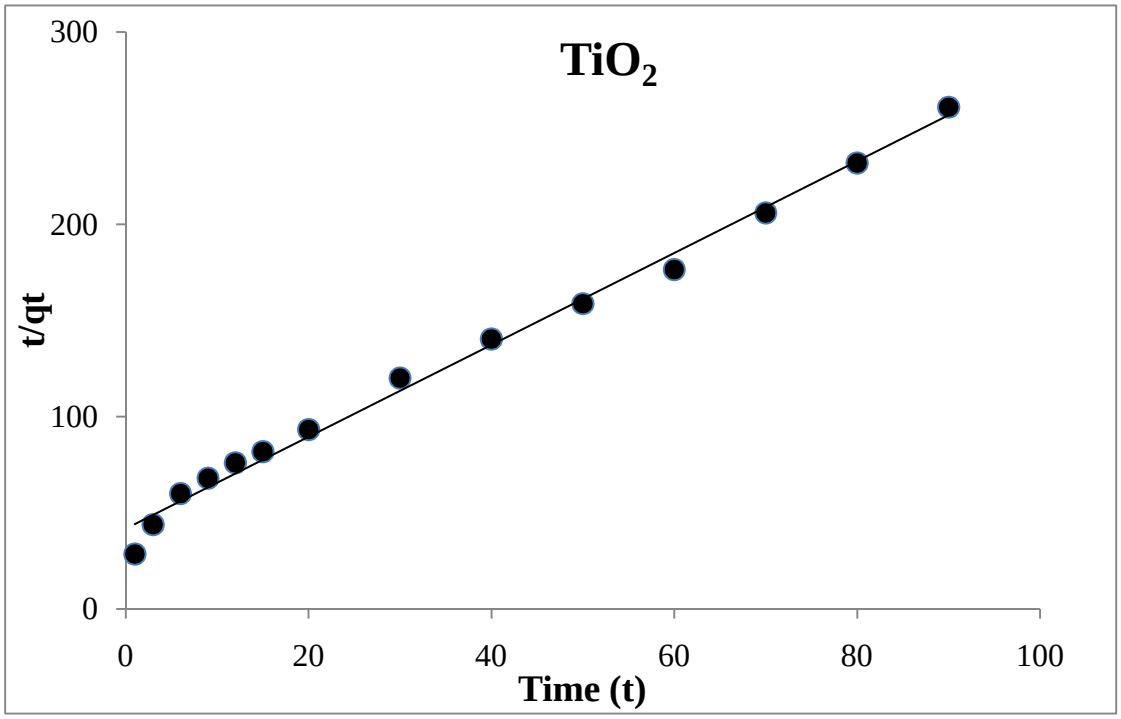

Fig. 4.41: Pseudo-second order kinetics model for pure Titania nanoparticles

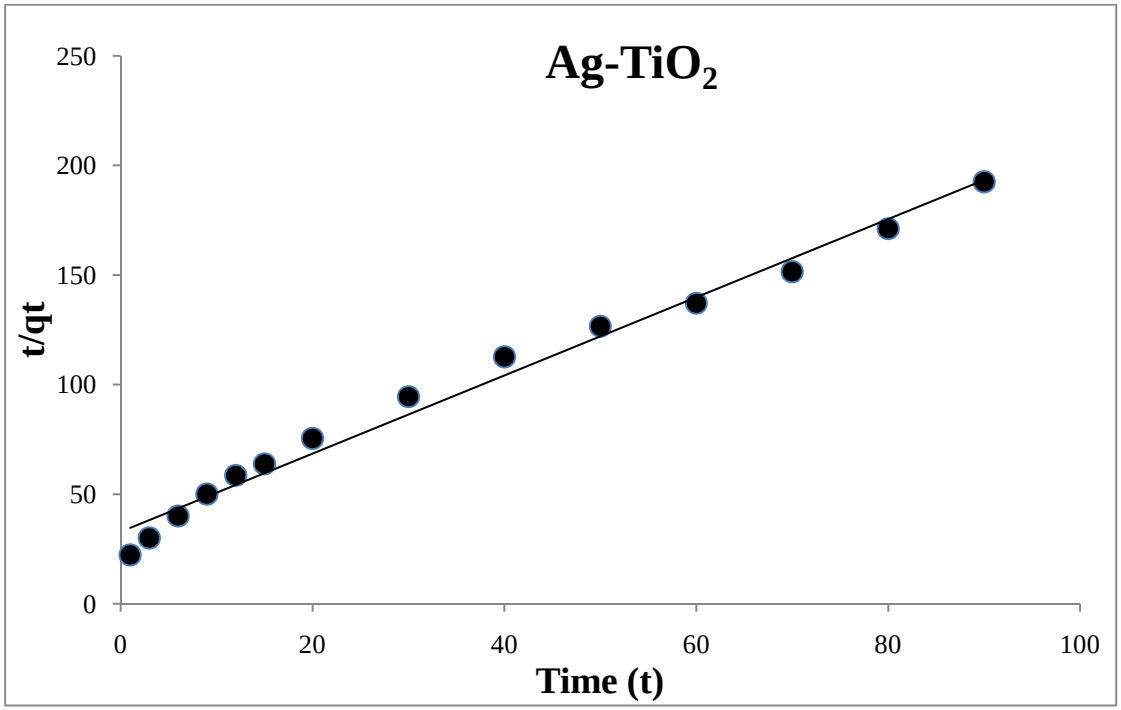

Fig. 4.42: Pseudo-second order kinetics model for Silver doped Titania nanoparticles

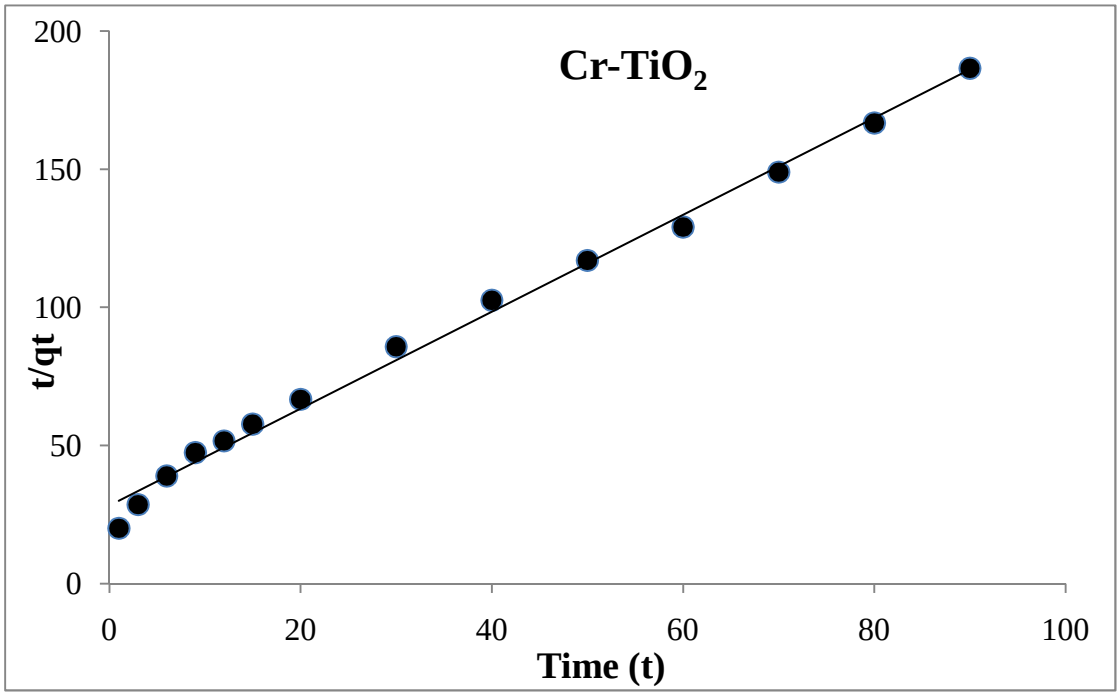

Fig. 4.43: Pseudo-second order kinetics model for Chromium doped Titania nanoparticles

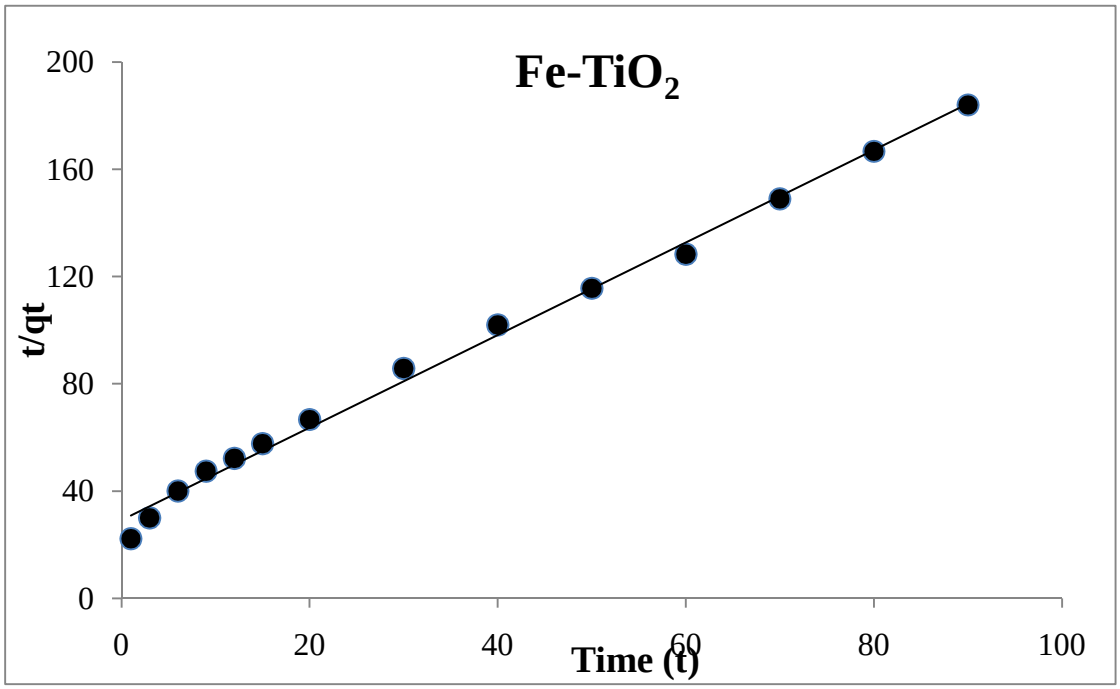

Fig. 4.44: Pseudo-second order kinetics model for Iron doped Titania nanoparticles

Table 4.8: Pseudo-second-order rate parameters for As (III) adsorption on Pure and metal Doped Titania Nanoparticles

Nanoparticles	q_e (mg/g)	k (g/mg min)	h (mg/g min)	R^2
TiO_2	0.42	0.14	0.024	0.992
Ag-TiO_2	0.56	0.097	0.03	0.986
Cr-TiO_2	0.57	0.145	0.047	0.993
Fe-TiO_2	0.59	0.102	0.035	0.995

4.6 COLUMN STUDIES

4.6.1 Adsorption Column Process

In the beginning all the As(III) is adsorbed by the column resulting in zero effluent concentration. As more and more influent is passed through the column, a gradual rise in the effluent concentration was observed. In the down flow mode, when the As(III) bearing water is introduced at the top of the column, most of the As(III) adsorption first occurs in the first few centimeters of the column, called the *adsorption zone.* As the column operation continues, the upper few centimeters of the column became saturated with the influent and the adsorption zone moves down through the column. Finally, the adsorption zone reaches the bottom of the column, and As(III) concentration in the effluent increases. By plotting As(III) concentration (mg/L) in the effluent against time (hrs), a breakthrough curve is obtained. On the breakthrough curve, the point at which the effluent As(III) concentration reaches its maximum permissible limit (0.01mg/L) is called the column breakthrough point and the corresponding time (hrs) as the breakthrough time. The point at which the effluent As(III) concentration reaches 90 % of the influent concentration, is known as column exhaustion point and the corresponding time (hrs) as exhaustion time.

Thomas and Yoon-Nelson models were applied for column design. Effects of different column parameters on the breakthrough and exhaustion time of column were

found. The Titania nanoparticles leaching out of a column of 10 cm height during the adsorption studies was very small, ranging from 0.015 to 0.032 mg/L.

4.6.2 Thomas Model

A successful design of column adsorption procedure needs prediction of the breakthrough curve (i.e. concentration-time profile) for the effluent. Moreover, the maximum adsorption potential of an adsorbent is also required in design. The Thomas model generally serves the purpose well. Thomas model has the following form (Öztürk and Kavak, 2005; Zheng et al., 2008).

$$\frac{C_e}{C_o} = \frac{1}{1 + \exp\left[K_T\left(q_o m - C_o V\right)/\theta\right]} \qquad \textbf{21}$$

Where K_T is the Thomas rate constant (ml/min mg), q_o the maximum solid phase concentration of solute (mg/g), θ the effluent flow rate (L/min), m the adsorbent quantity in the column (g) and V is the effluent volume (L). The linear form of Thomas model is given as;

$$\ln\left(\frac{C_o}{C_e} - 1\right) = \frac{K_T q_o m}{\theta} - \frac{K_T C_o}{\theta} V \qquad \textbf{22}$$

The kinetic coefficient K_T and the adsorption capacity of the column q_o can be determined from a plot of $\ln(C_o/C_e - 1)$ against t at a given flow rate (Fig 4.45-4.47).

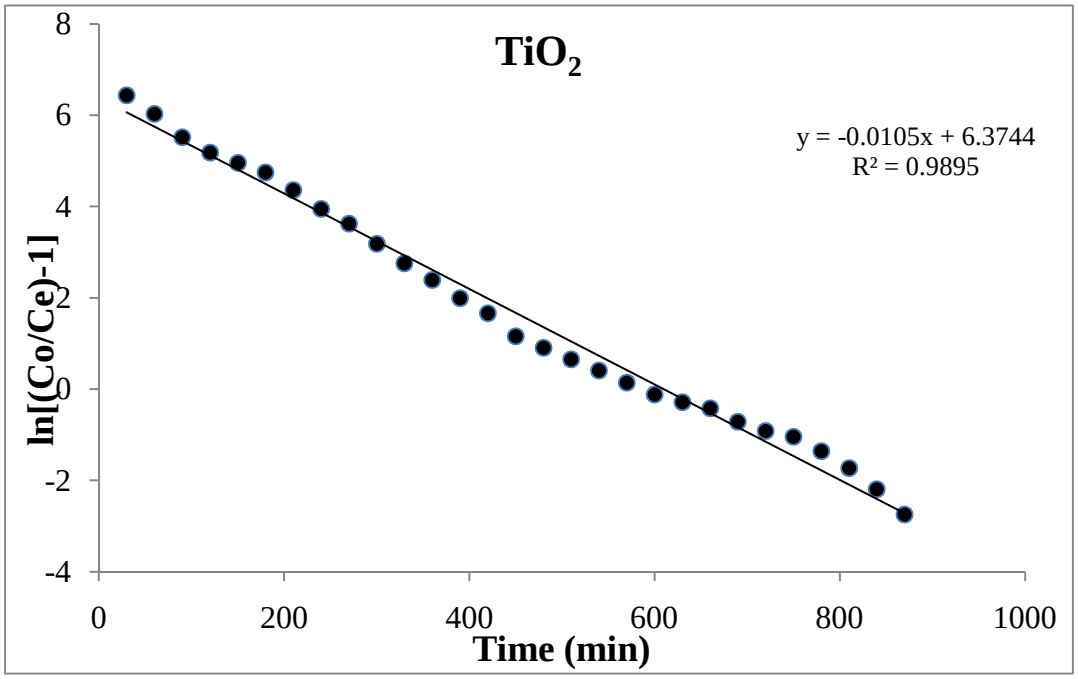

Fig.4.45: Plot of ln (C_0/C_e-1) Vs t for pure Titania coated glass beads

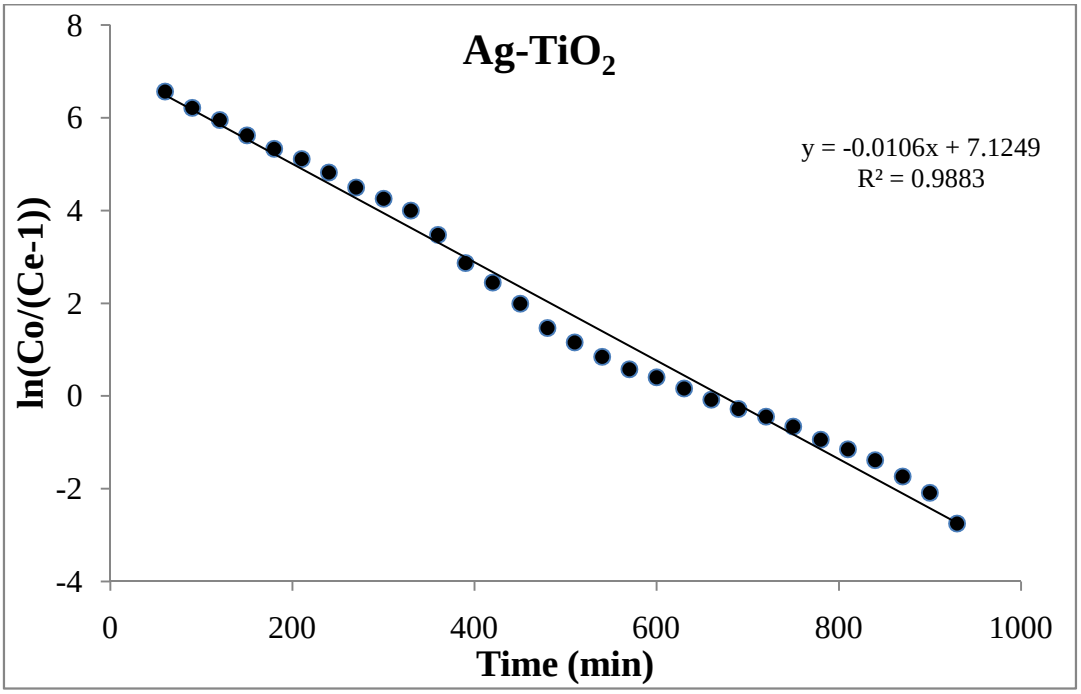

Fig.4.46: Plot of ln (C_0/C_e-1) Vs t for Silver doped Titania coated glass beads

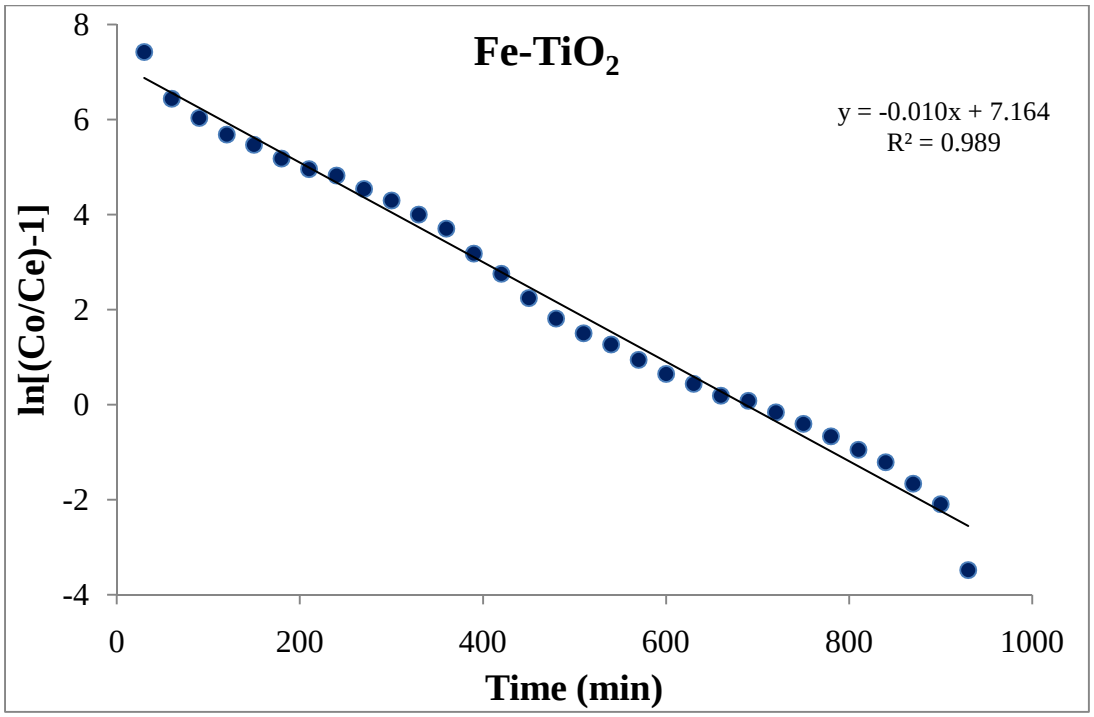

Fig.4.47: Plot of ln (C_0/C_e-1) Vs t for Iron doped Titania coated glass beads

The Thomas equation coefficients, K_T and q_o for As (III) adsorption by pure and metal doped Titania nanoparticles coated glass beadsare given in the Table 4.9. Where q_o is the measure of adsorption capacity at the Nanoparticles for As (III).

Table 4.9: Thomas model parameters for different nanoparticles coated glass beads

Nanoparticles	**TiO_2**	**Ag- TiO_2**	**Fe- TiO_2**
K_T	0.02	0.02	0.02
q_o (mg/g)	0.53	0.6	0.7

The theoretical predictions based on the model parameters are compared in Fig. 4.48-4.50 with the experimental data.

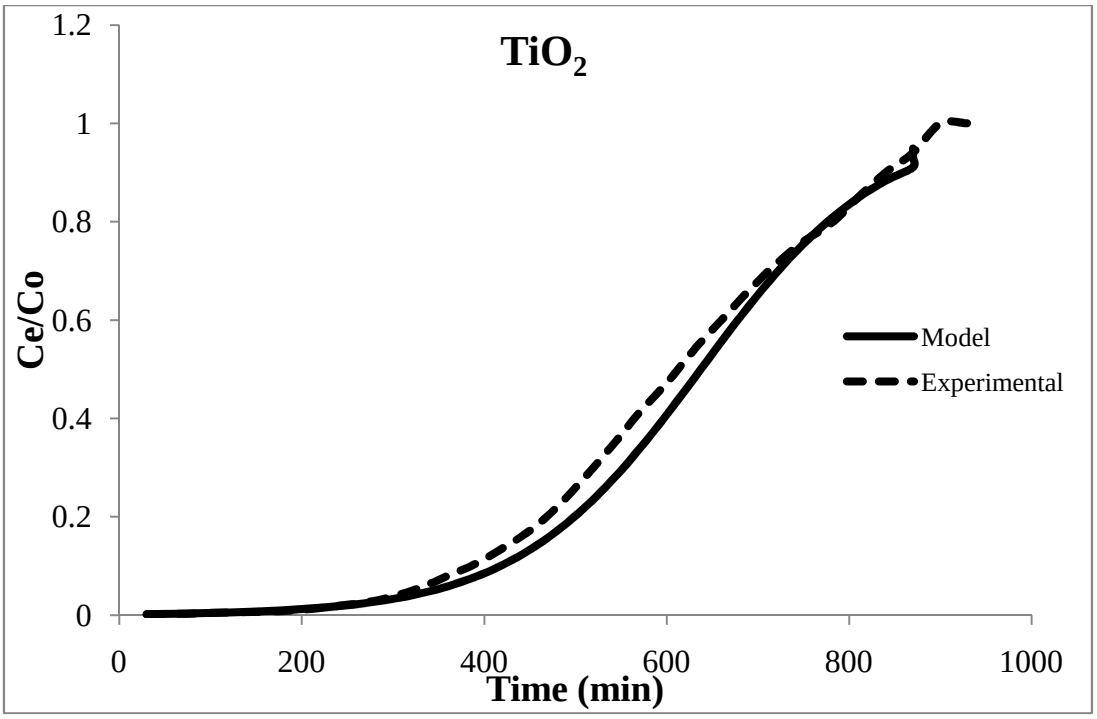

Fig. 4.48: Thomas model, comparison of Experimental and Predicted breakthrough curves for pure Titania coated glass beads (t=25 ◦C, pH=7 and C0 = 0.5 mg/L)

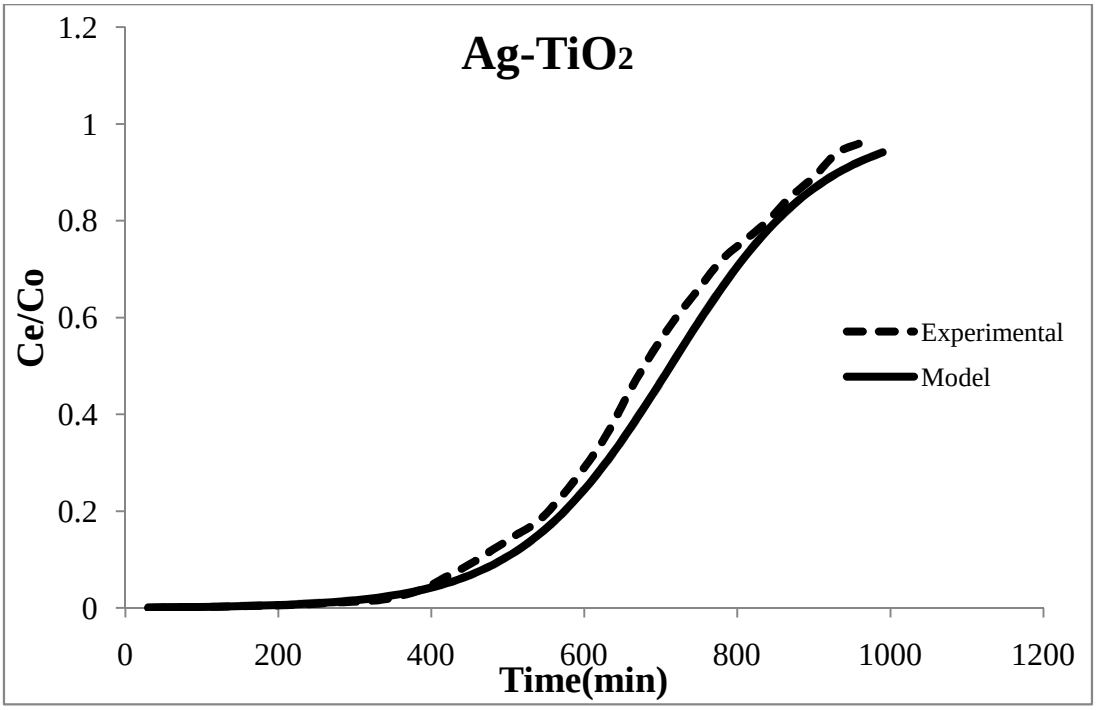

Fig. 4.49: Thomas model, comparison of Experimental and Predicted breakthrough curves for Silver doped Titania coated glass beads (t=25 ◦C, pH=7 and C0 = 0.5 mg/L)

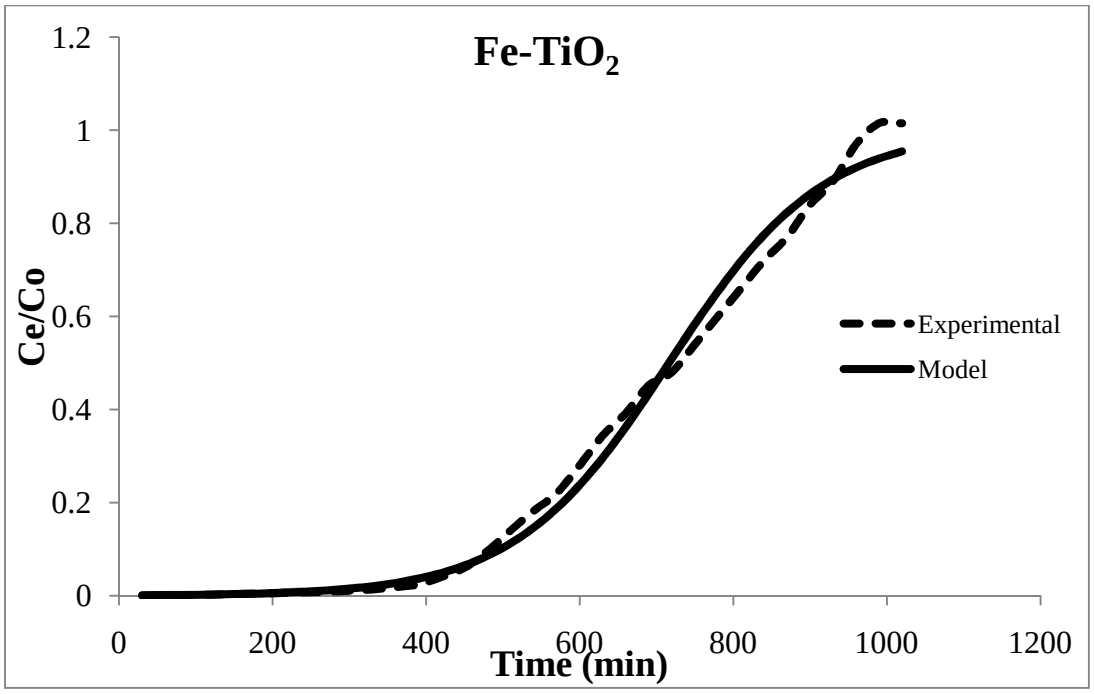

Fig. 4.50: Thomas model, comparison of Experimental and Predicted breakthrough curves for Iron doped Titania coated glass beads (t=25 ◦C, pH=7 and C0 = 0.5 mg/L)

4.6.3 Yoon and Nelson Model

As compared to other models the Yoon and Nelson model is not only less complicated, but also requires no detail related to the characteristics of adsorbate, adsorbent type, and the physical characteristics of the adsorption bed. This model is mainly based on the assumption that for each adsorbate molecule the rate of decrease in the probability of adsorption is proportional to the probability of adsorbate adsorption and the probability of adsorbate breakthrough on the adsorbent (Öztürk and Kavak, 2005). The Yoon-Nelson model equation for a single component system is given as (Aksu and G¨onen, 2004).

$$\frac{C_e}{C_o} = \frac{1}{1+\exp[k_{YN}(\tau - t)]} \qquad \textbf{23}$$

The linear form of the model is as follows:

$$t = \tau + \frac{1}{k_{YN}} \ln \frac{C_e}{C_o - C_e} \qquad \textbf{24}$$

Where k_{YN} is the Yoon and Nelson rate constant (L/min); τ is the time required for 50% adsorbate break through (min) and t is the breakthrough (sampling) time (min). These values can be obtained by plotting $\ln[C_e/(C_0- C_e)]$ against t, Fig. 4.51-4.53.

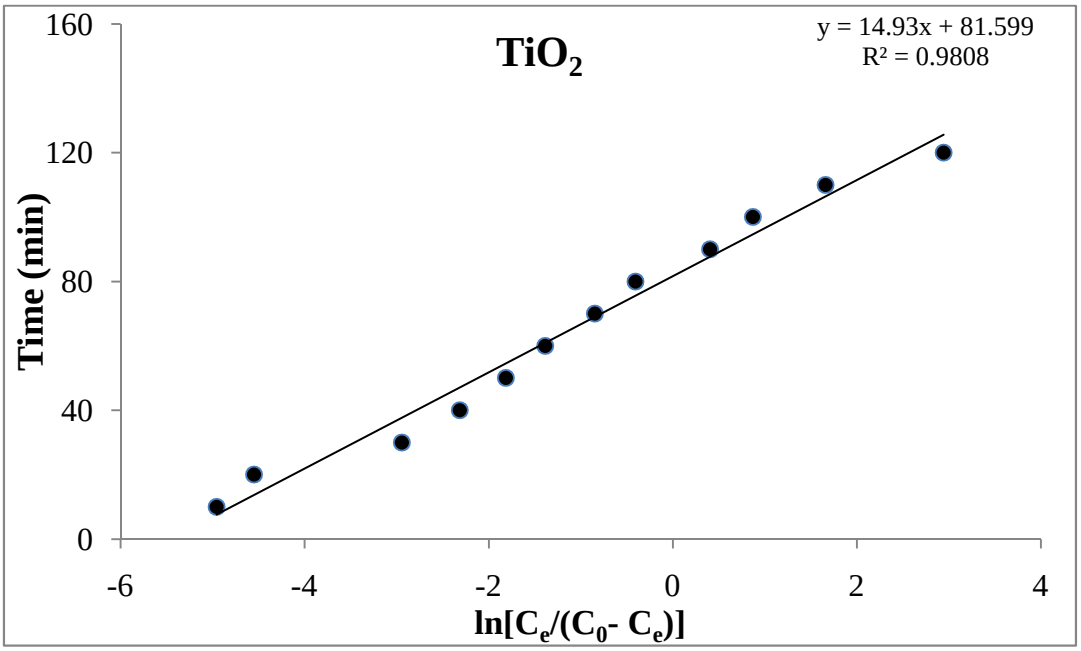

Fig. 4.51: Plot of t Vs $\ln[C_e/(C_o-C_e)]$ for pure Titania nanoparticles

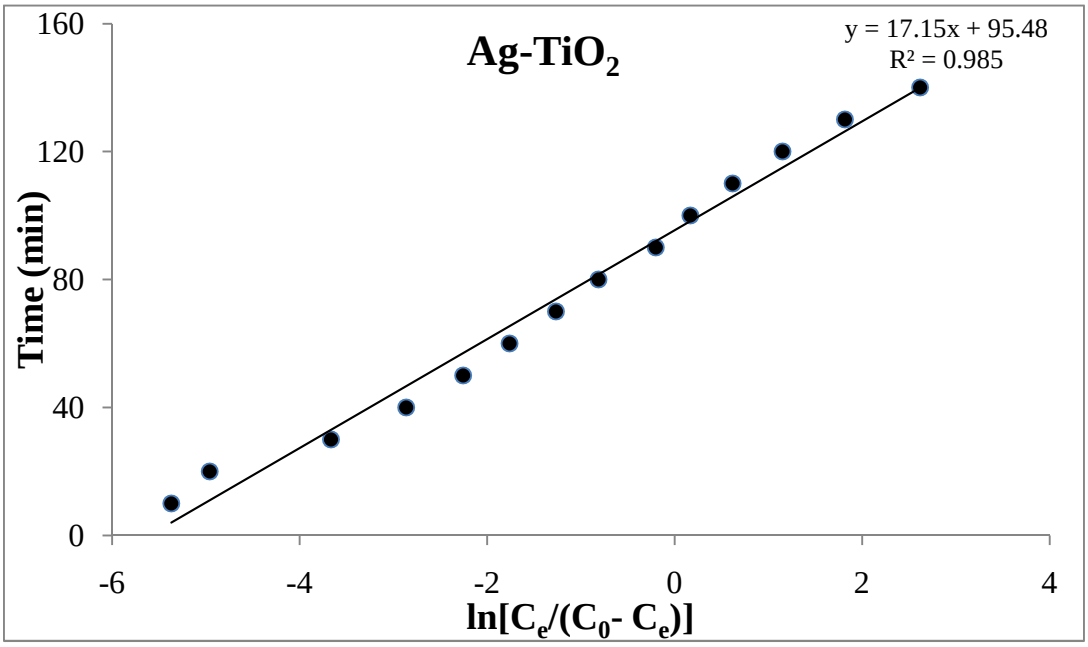

Fig. 4.52: Plot of t Vs $\ln[C_e/(C_o-C_e)]$ for Silver doped Titania nanoparticles

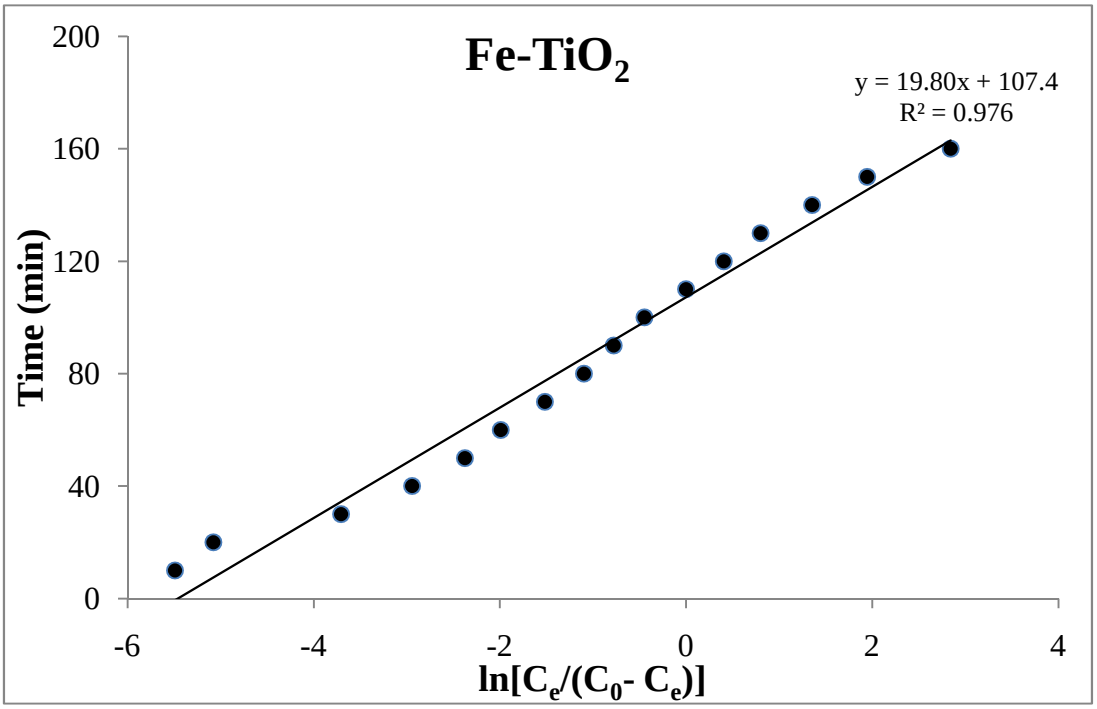

Fig. 4.53: Plot of t Vs $\ln[C_e/(C_o-C_e)]$ for Iron doped Titania

The model parameters obtained for the As(III) adsorption on all the three types of Titania based Nanoparticles coated glass beads are given in the Table 4.10.

Table 4.10: Yoon-Nelson model parameters for different nanoparticles coated glass beads

Nanoparticles	k_{YN} (L/min)	T (min)	q_o (mg/g)
TiO2	0.067	81.59	0.407
Ag-TiO2	0.058	95.48	0.477
Fe-TiO2	0.05	107.4	0.54

Alternatively, when $\ln[C_e/(C_0- C_e)]$ is zero, τ can also be obtained from the adsorption time. This is due to the fact that by definition τ is the adsorption time when C_e is equal to one half of C_o. From these values the breakthrough curves were calculated. The theoretical curves were then compared with the corresponding experimental data in Fig. 4.54-4.56. Derivation of equation (g) was based on the definition that at τ 50% breakthrough of the adsorption occurs. Accordingly, at 2τ the bed should be fully

saturated. Because of the symmetrical breakthrough curve, the As(III) adsorbed by Titania coated glass beads is equal to one half of the As(III) entering the column within 2τ period. This give rise to the following equation (Lin and Wang, 2002):

$$q_o = \frac{1}{2} C_o \theta(2\tau) = C_o \theta \tau \qquad \textbf{25}$$

This equation develops the relation among the adsorption capacity (q_o) of the column, influent concentration (C_o), Flow rate (θ) and the 50% breakthrough time (τ). The value of q_o calculated using Yoon and nelson model for all the three types of column is given in Table 4.10.

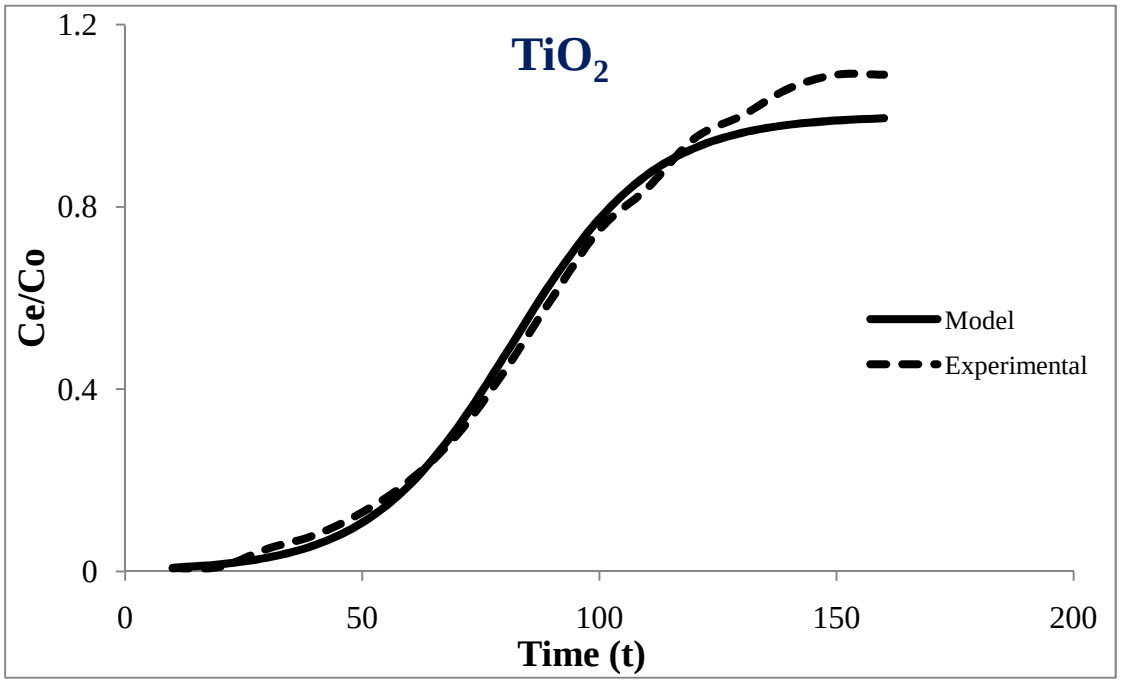

Fig. 4.54: Yoon and Nelson model, comparison of predicted and experimental Curves for TiO_2 coated glass beads

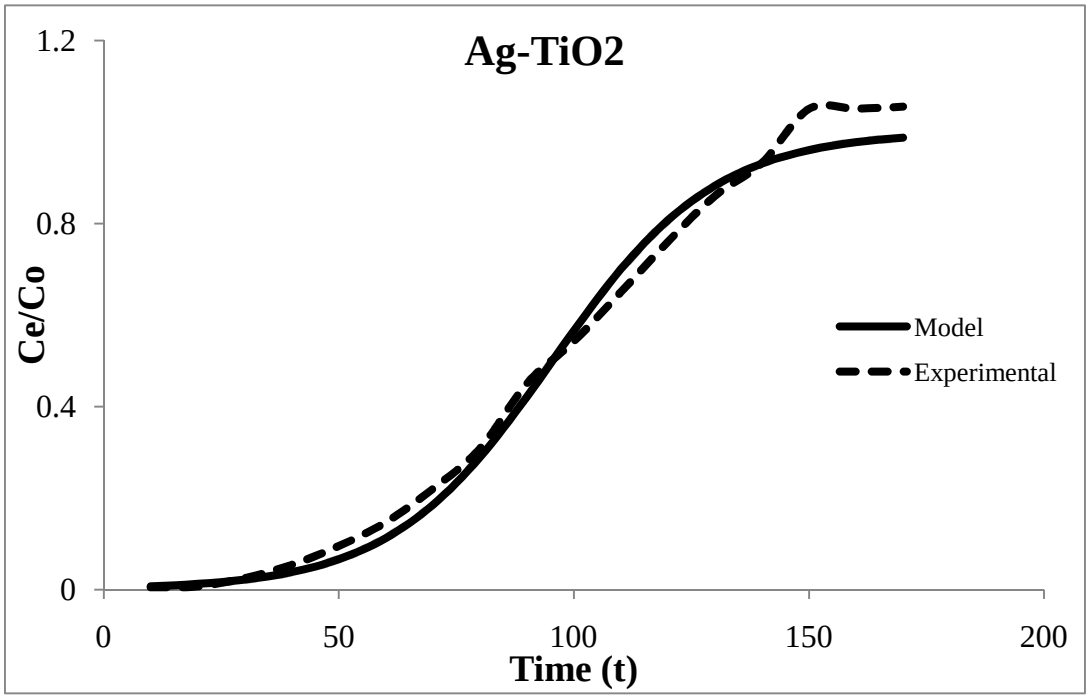

Fig. 4.55: Yoon and Nelson model, comparison of predicted and experimental Curves for Ag-TiO_2 Titania coated glass beads

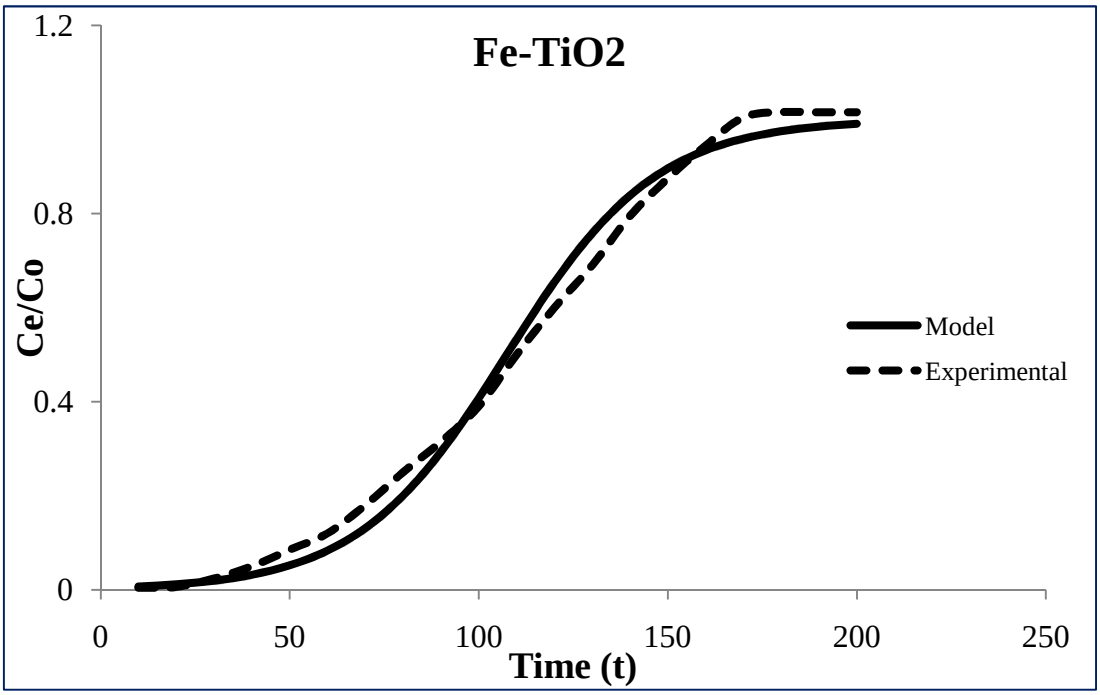

Fig. 4.56: Yoon and Nelson model, comparison of predicted and experimental Curves for Fe-TiO_2 coated glass beads

4.6.4 Effect of Different Operating Conditions on Column Sorption of As (III)

Column operational parameters such as flow rate, Bed height, Arsenic concentration and variation of Nanoparticles are very useful in column design. The influence of these parameters on the adsorption capacity of Nanoparticles were studied for As(III) uptake. The effect of influent pH on adsorption was not studied here, as our previous results showed that maximum As(III) adsorption on our Nanoparticles occurred at pH 7

4.6.4.1 Effect of the Nanoparticles Used

In order to know which nanoparticles packed in the column were having highest arsenic removal efficiency, three columns of the same bed depth and diameter (10 cm and 1.5 cm respectively) each packed with the glass beads coated with different nanoparticles were selected. The same arsenic stock solution of 0.5 ppm was used for all of them and the influent flow rate was kept constant at 5ml/min for each. The column breakthrough times (when the effluent concentration cross 0.1 mg/L) and the column exhaustion times (when effluent concentration reaches 90% of influent concentration), for the three different columns (Fig. 4.57) are shown in the Table. 4.11.

It is clear from figure that the column packed with iron coated glass beads are having high breakthrough and exhaustion time. These results are also shown in the table. Thus it is clear that among the nanoparticles synthesized, iron doped Titania nanoparticles are giving higher removal efficiency both in powder batch experiments as well as in column.

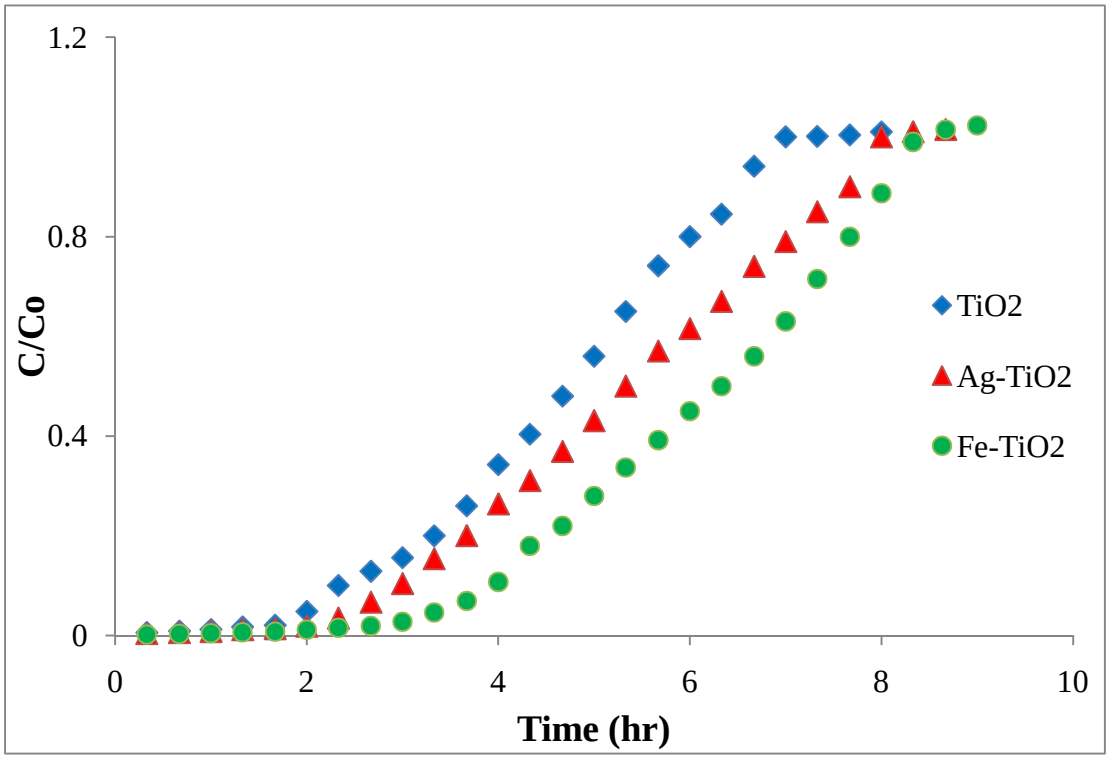

Fig. 4 .57: Effect of nanoparticles used on column parameters

Table 4.11: Effect of nanoparticles used on the column breakthrough and exhaustion

Nanoparticles coated on GB	Breakthrough Time (hr) (WHO / PDWQS.)	Exhaustion Time (hr)
TiO_2	1.67 / 2.33	6.67
Ag doped TiO_2	2.33 /3	7.67
Fe doped TiO_2	3 / 4	8.33

4.6.4.2 Effect of Bed Height

To know how much is the effect of bed height on the arsenic removal efficiency, three columns of bed height 10, 20 and 30 cm of each nanoparticles coated glass beads were taken. Keeping the influent arsenic concentration at 0.5 ppm and it flow rate at 5ml/min. The data obtained is shown in the Table 4.12.

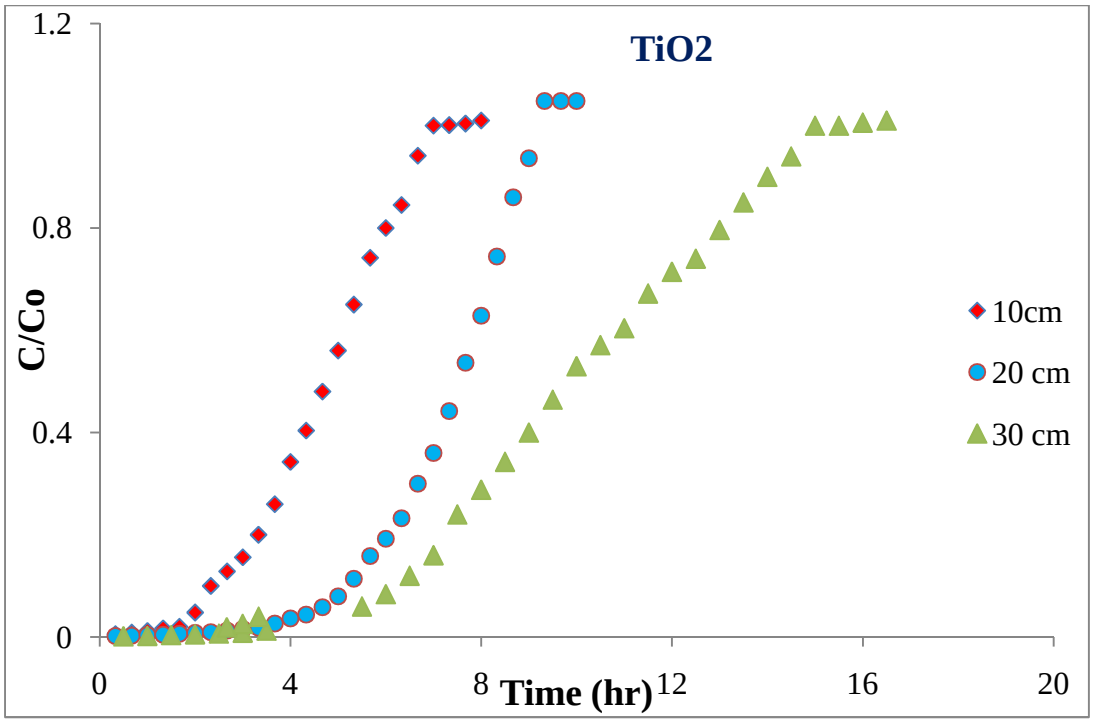

Fig. 4.58: Effect of bed height on the column parameters for TiO_2 coated glass beads

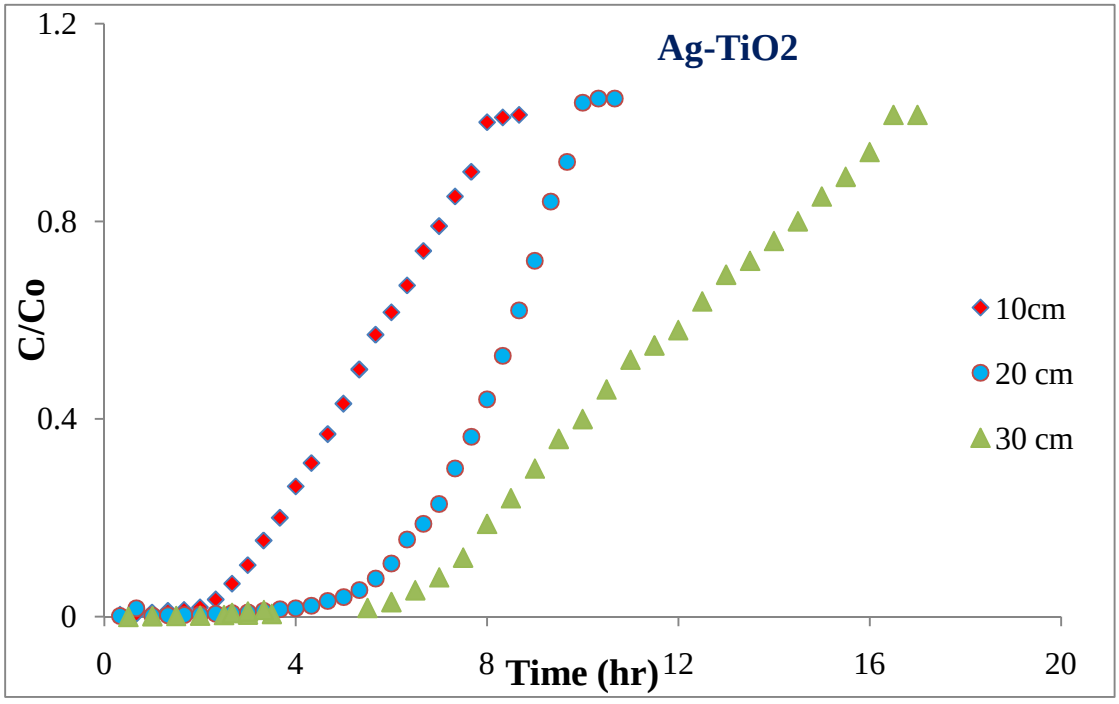

Fig. 4.59: Effect of bed height on the column parameters for Ag-TiO_2 coated glass beads

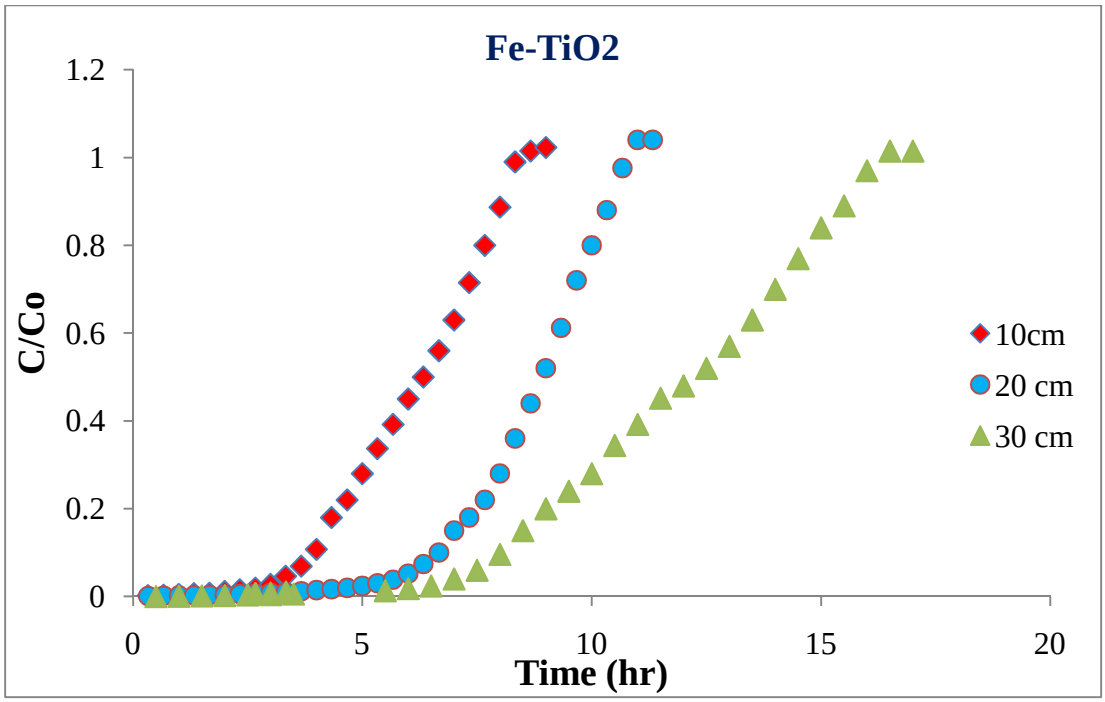

Fig. 4.60: Effect of bed height on the column parameters for Fe-TiO_2 coated glass beads

Table 4.12: Effect of bed height on the column breakthrough and exhaustion time

Nanoparticles coated on GB	Breakthrough Time (hr) (WHO / PDWQS.)			Exhaustion Time (hr)		
	10 cm	20 cm	30 cm	10 cm	20 cm	30 cm
TiO_2	1.67 / 2.3	3.67 / 5.3	4.5 / 6.5	6.67	9	14
Ag-TiO_2	2.3 / 3	4.3 / 6	6 / 7.5	7.67	9.67	16
Fe-TiO_2	3 / 4	5 / 6.67	6.5 / 8.5	8.33	10.67	16

From the data above it is clear that with an increase in bed height the arsenic removal efficiency of column increases, this is because of greater contact time plus more adsorbent for the adsorption of As (III).

4.6.4.3 Effect of Flow Rate

For this purpose a column of each nanoparticle (pure, Ag-Doped and Fe-Doped Titania) was selected. The columns were charged at flow rates of 5 and 10 ml/min. The influent As(III) concentration was maintained at 0.25 mg/L. The bed depth and column diameters were 10 cm and 1.5 cm respectively. The column breakthrough and exhaustion time, at flow rates of 5 and 10 ml/min, for all the three types of nanoparticles (Fig. 4.61-4.63) are given in the Table 4.13.

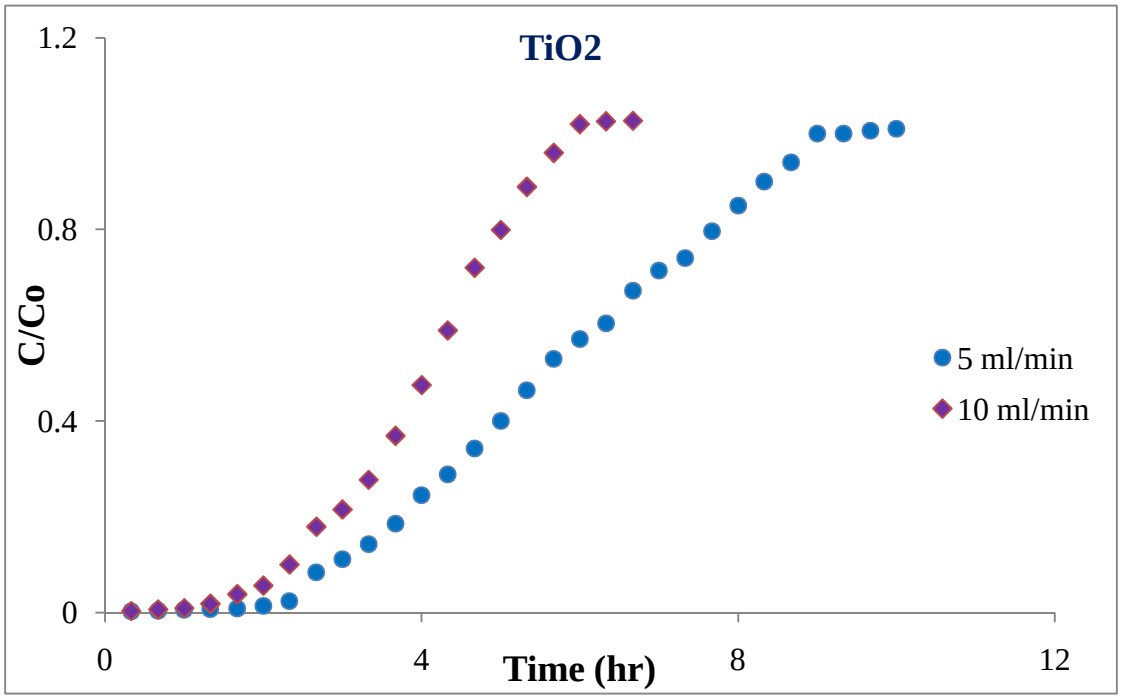

Fig. 4.61: Effect of Influent flow rate on column parameters for TiO_2 coated glass beads

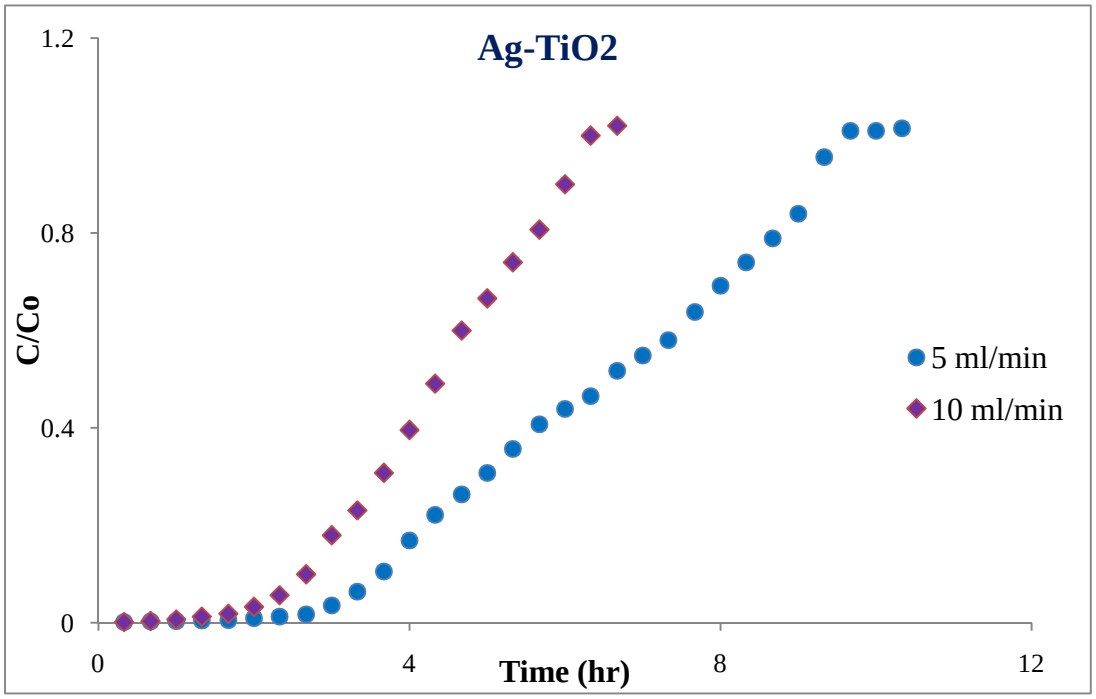

Fig. 4.62: Effect of Influent flow rate on column parameters for Ag-TiO_2 coated glass beads

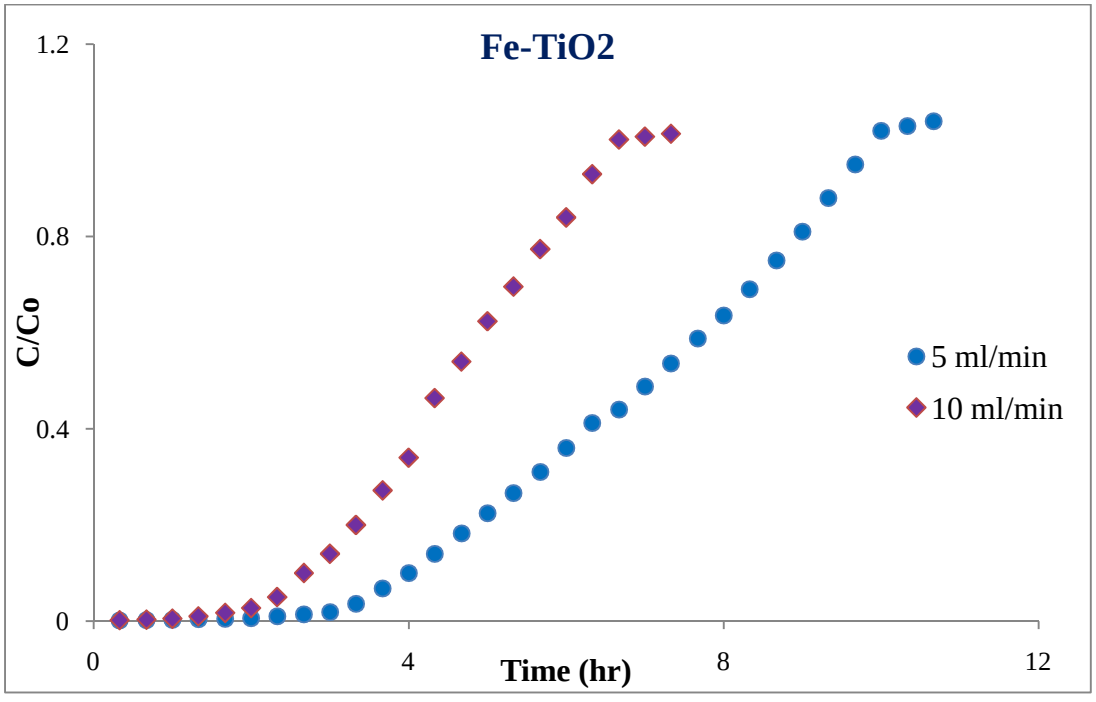

Fig. 4.63: Effect of Influent flow rate on column parameters for Fe-TiO_2 coated glass beads

Table 4.13: Effect of flow rate on the column breakthrough and exhaustion time

Nanoparticles coated on GB	Breakthrough Time (hr) (WHO / PDWQS.)		Exhaustion Time (hr)	
	5 ml/min	10 ml/min	5 ml/min	10 ml/min
TiO_2	2.33 / 3.67	0.67 / 1.67	7.67	2.83
Ag-TiO_2	3 / 4.67	1 / 1.5	8.67	3.33
Fe-TiO_2	3.67 / 5.33	1.33 / 2	9	3.67

From the results it is clear that with the increase in flow rate, residence time decrease, which in turn decrease the removal efficiency. As the flow rate is lowered an increase in the removal efficiency is observed due to the increase in residence time.

4.6.4.4 Effect of Influent Concentration

To determine the effect of influent arsenic concentration on the performance of our columns, four influent arsenic concentrations (i.e. 0.25, 0.5, 1 and 1.5 ppm) were selected. Bed depth and column diameter were maintained at 20 cm and 1.5 cm respectively, and flow rate was maintained at 5ml/min. All the three types of coated nanoparticles were used. The results found are tabulated as under.

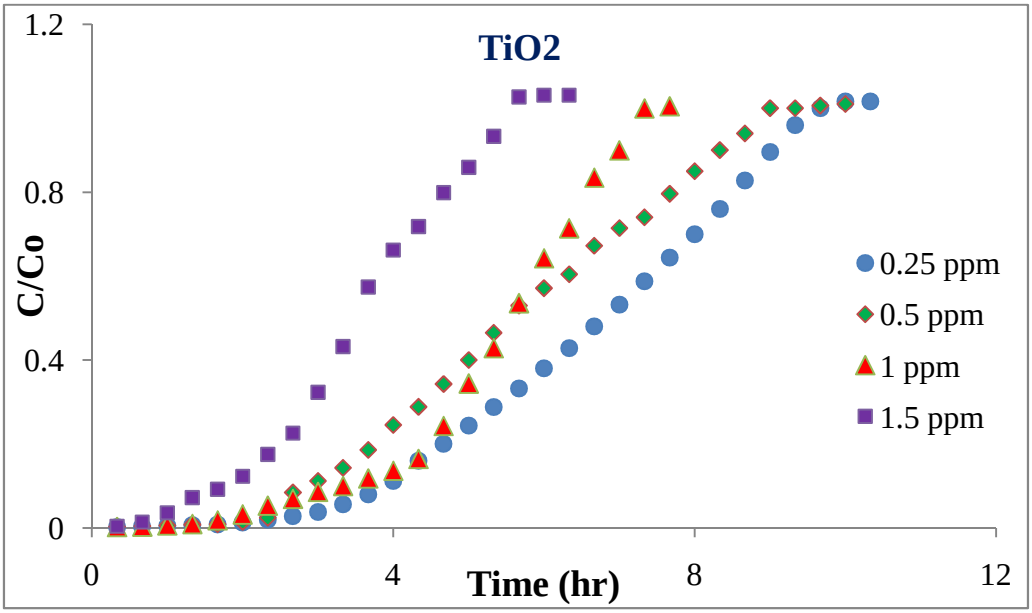

Fig. 4.64: Effect of Influent concentration on column parameters on TiO_2 coated glass beads

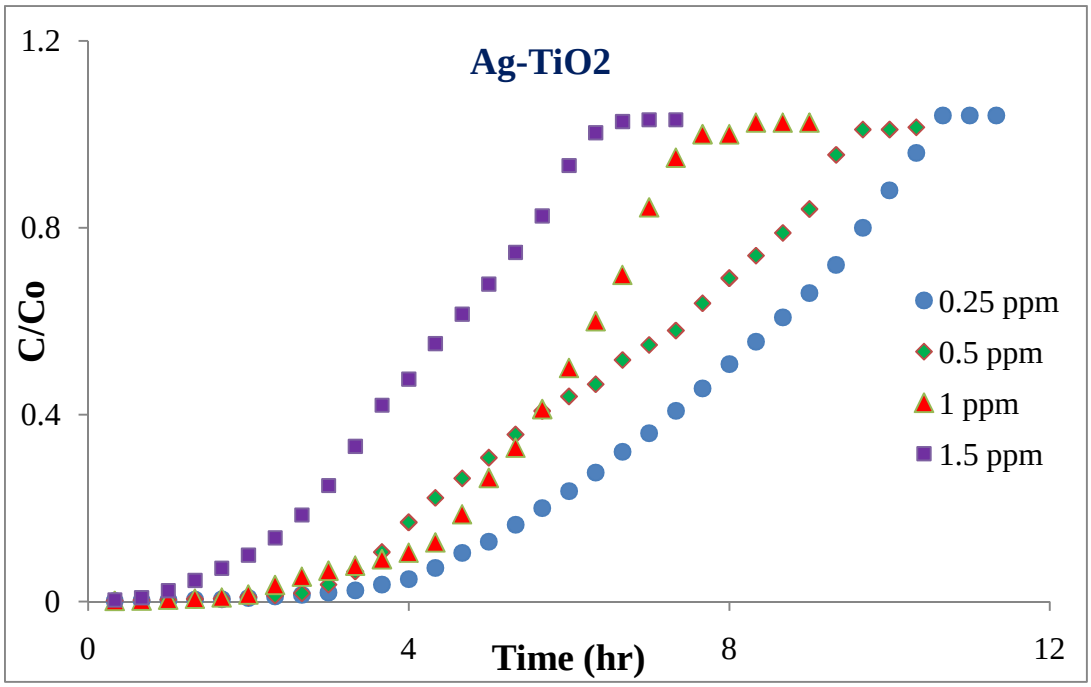

Fig. 4.65: Effect of Influent concentration on column parameters on Ag-TiO_2 coated glass beads

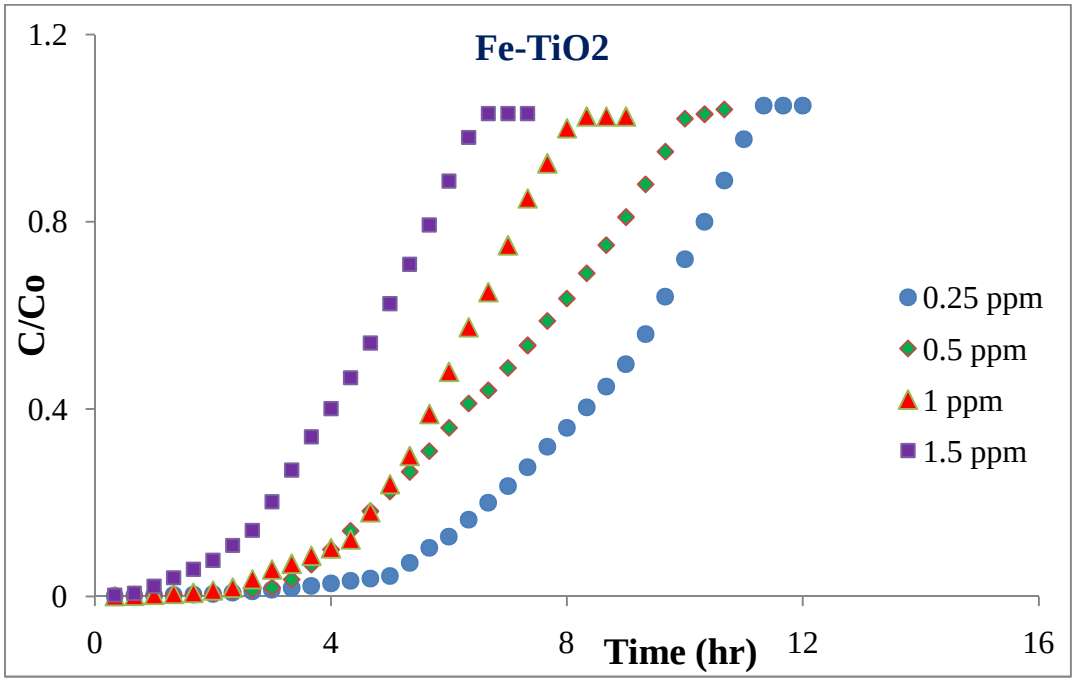

Fig. 4.66: Effect of Influent concentration on column parameters on Fe-TiO_2 coated glass beads

Table 4.14: Effect of influent concentration on the column breakthrough and exhaustion time

Nanoparticles coated on GB	Breakthrough Time (hr) (WHO / PDWQS.)				Exhaustion Time (hr)			
	0.25 ppm	0.5 ppm	1 ppm	1.5 ppm	0.25 ppm	0.5 ppm	1 ppm	1.5 ppm
TiO_2	4.7/ 6.3	3.7/5.3	2 / 3	0.67/ 1	10	9	7.3	5.3
Ag -TiO_2	5.7 /7.7	4.3/ 6	2.3/ 3.3	0.7/1.3	11.3	9.7	8.3	6
Fe -TiO_2	6 / 7.7	5 / 6.7	2.7/3.7	0.7/1.3	11.7	10.7	8.7	6.3

As expected with increase in influent arsenic concentration the column breakthrough and column exhaustion times were decreased. This shows that the lower the influent arsenic concentration the more will be the efficiency and life of the column.

4.6.5 Column Regeneration and Reuse

For a viable sorption process, easy regeneration and reuse of the column media is very important. The exhausted 20 cm bed volume column (for all the three Nanoparticles coated glass beads) after exhaustion was regenerated with 10% NaOH solution. The arsenic recovery profile during desorption process is shown in the Fig. 4.67. It was found that 10 bed volumes were sufficient for 99% arsenic recovery from the column. Initially in the first 2-3 bed volumes almost 86% of the adsorbed arsenic was eluted, the rest got desorbed in 7 further bed volumes. This clearly shows that the sorption sites of glass beads coated with Nanoparticles are easily accessible and it also shows that adsorption-desorption process is a reversible one. After regeneration, the column was rinsed with mild warm deionized water to remove any traces of NaOH and lower the pH to normal, as in basic range the adsorption is less efficient. The column was then dried and was subjected to the next sorption cycle. Fig. 4.68 shows both the consecutive sorption cycles, from which it is clear that the removal efficiency during the second cycle Is decreased by about 10%. Hence, it is clear from Fig.68 that As(III) removal capacities of different Nanoparticles coated glass beads during the two consecutive cycles, that the regeneration and reuse of these coated glass beads offers an economical approach for As(III) removal from water.

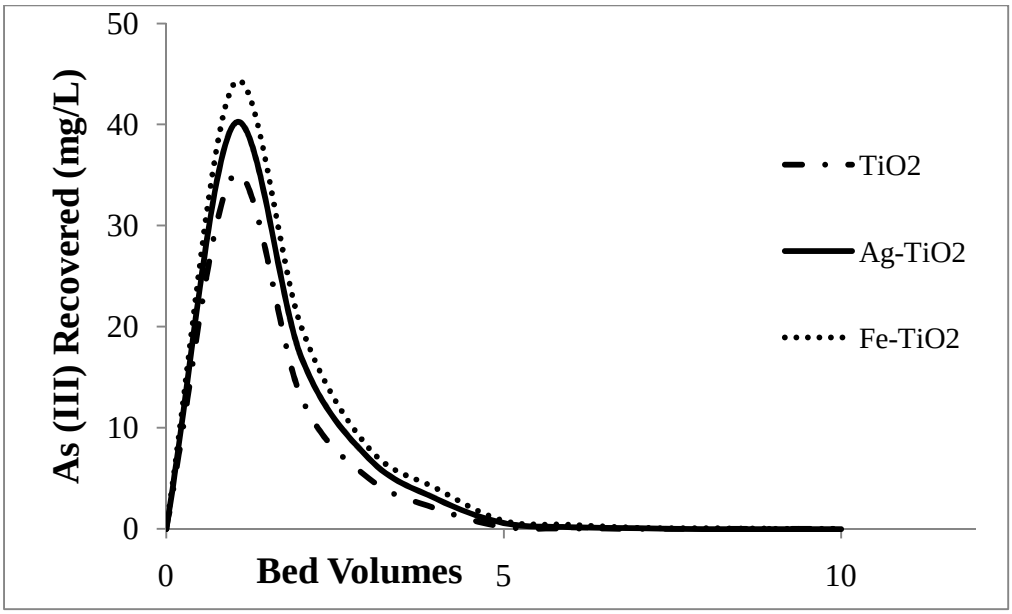

Fig. 4.67: As (III) concentration profile during column regeneration

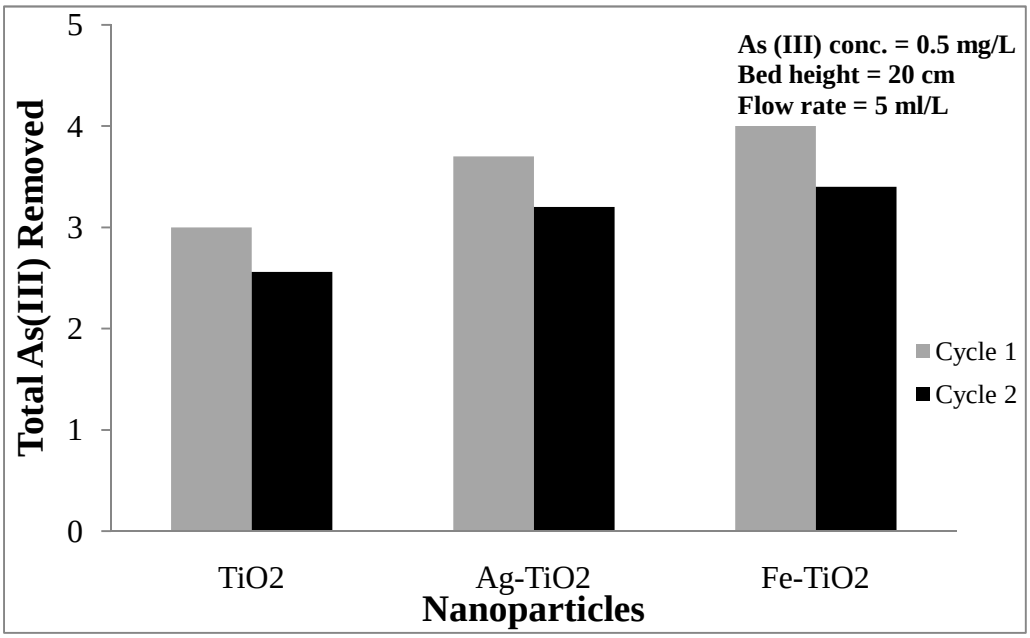

Fig. 4.68: Capacities of different Nanoparticles for As (III) removal during two successive cycles

Chapter 5

CONCLUSIONS AND RECOMMENDATIONS

5.1 CONCLUSIONS

This study showed that our synthesized pure and metal doped Titania nanoparticles showed excellent arsenic removal efficiency both in powder and coated form.

The following conclusions can be drawn from this study.

- The synthesized pure and metal doped Titania nanoparticles showed excellent arsenic removal efficiency (up to 95%) both in powder and coated form.
- Among metal doped Titania, Fe and Cr doped particles gave the highest arsenic removal efficiency.
- The removal efficiency is dependent on pH, it is maximum at neutral pH and decrease by moving on either side of the neutral pH.
- Metal doping shifted the band gap value from UV to visible region as proved by the band gap analysis.
- The adsorption data gave a good fit with Langmuir and Freundlich isotherms.
- The adsorption was found to conform to pseudo second order kinetics.
- Column studies also proved that metal doping increased the arsenic removal efficiency of Titania nanoparticles.
- The breakthrough curves shift to the right with increase in bed height, while decrease with the increase in influent concentration and flow rate.
- Thomas and Yoon-Nelson model applied to evaluate column parameters gave results in clear agreement with the practical results.
- The columns once exhausted can easily be regenerated in a cost effective way.
- Only 10 bed volumes of the regenerant (10% NaOH) were sufficient for column regeneration.

- The efficiency of the column was not much affected during the two consecutive cycles.

5.2 RECOMMENDATIONS

The following are some recommendations for further studies

- As among metal doped Titania Fe-TiO_2 is giving higher arsenic removal fficiency. We only checked the efficiency of 1% Fe-TiO_2. So the effect of variation in Iron percentage should be looked at.
- Effect of competing species like nitrate, chromate, chloride, sulfate, acetate, and phosphate ions on the arsenic removal efficiency of Titania should be checked.
- Effect of turbidity and hardness on the removal efficiency should be checked.
- The immobilization of Titania on other adsorbent should be checked for column studies.
- Determination of proper disposal method for the disposal of arsenic effluent.

REFERENCES

- Abernathy, C. and Morgan, A. (2001).'Exposure and health effect. In: UN (2001). UN synthesis report on arsenic in drinking water. Geneva, Switzerland, World Health Organization. Chapter 3. Available at: http://www.who.int/water_sanitation_health/dwq/arsenic3/en/ http://www.who.int/water_sanitation_health/dwq/arsenicun3.pdf
- Ahmad, T., Kahlown, M.A., Tahir, A. and Rashid, H. (2004). Arsenic an emerging issue: Experiences from Pakistan. 30th WEDC International conference. Vientiane, Laos.
- Aksu, Z. and G¨onen, F. (2004). Biosorption of phenol by immobilized activated sludge in a continuous packed bed: prediction of breakthrough curves, Process Biochemistry, 39 (5): 599–613.
- Akurati, K.K (2008). Synthesis of titania based nanoparticles for photocatalytic applications, Cuvillier Verlag Gottingen, pp.51-53.
- Asahi, R., Morikawa, T., Ohwaki, T., Aoki, K. and Taga, Y. (2001). Visible-light photocatalysis in nitrogen-doped titanium dioxide. Science, 293: 269-271.
- Ashutosh S.Vakharkar (2005). Adsorption Studies for Arsenic Removal Using Modified Chabazite. Master thesis, University of South Florida.
- Bang, S., Patel, M., Lippincott, L. and Meng, X. (2005). Removal of Arsenic from Groundwater by granular titanium dioxide adsorbent. Chemosphere., 60: 389-397.
- Baes, A.U., Okuda, T., Nishijima, W., Shoto, E. and Okada, M. (1997). Adsorption and ion exchange of some groundwater anion contaminants in an amine modified coconut coir, Water Science and Technology, 35, 89–95.
- Bailey, S.E., Olin, T.J., Bricka, R.M. and Adrian, D.D. (1999). A review of potentially low-cost sorbents for heavy metals. Water Research, 33, 2469–2479.

- Balaji, T. and Matsunaga, H. (2002). Adsorption characteristics of As(III) and As(V) with titanium dioxide loaded with amberlite XAD-7 resin. Analytical Science., 18: 1345- 1349.
- Behnajady, M.A., Modirshahla, N., Shokri, N. and Rad, B. (2008). Enhancement of photocatalytic activity of tio2 nanoparticles by silver doping: photodeposition versus liquid impregnation methods, Global Nest Journal, 10 (1): 1-7.
- Bissen, M., Vieillard-Baron, M.M., Schindelin, A.J. and Frimmel, F.H. (2001). TiO2-catalyzed photooxidation of arsenite (III) to arsenate (V) in aqueous samples. Chemosphere 44, 751–757.
- Bissen, M. and F.H. Frimmel. (2003). Arsenic- A Review; Part II: Oxidation of Arsenic and its removal in water treatment. Acta hydrochim. hydrobiol. 31(2): 97-107.
- Bodek, I., Lyman, W.J., Reehl, W.F. and Rosenblatt, D.H. (1998). Environmental Inorganic Chemistry: Properties, Processes and Estimation Methods. Pergamon Press, USA.
- Brewstar M. D. (1994) Removing arsenic from contami- nated water. Water Environ. & Tech 4, 54±57.
- Buswell, A.M. (1943). “War problems in analysis and treatment.” American Water Works Assosiation, 35 (10), 1303.
- Carollo Engineers. (2006). Statement of Qualifications: Drinking water with emphasis on arsenic treatment.
  http://www.carollo.com/404/section.aspx/download/72.
- Chen, H., Ye, Z., Fang, S. and Liu, X. (1998). The study on adsorption of As(III) from wastewater by different types of MnO2, China Environmental Science, 18, 126.
- Chiu, V.Q. and Hering, J.G. (2000) Arsenic adsorption and oxidation at manganite surfaces. 1. Method for simultaneous determination of adsorbed and dissolved arsenic species, Environmental Science and Technology, 34, 2029–2034.

- Chowdhury, S.R., and Yanful, E.K. (2010). Arsenic and chromium removal by mixed magnetite maghemite nanoparticles and the effect of phosphate on removal. Journal of Environmental Management, 91: 2238-2247.
- Clifford, D. and C.C. Lin (1995). "Ion Exchange, Activated Alumina, and Membrane Processes for Arsenic Removal from Groundwater," Proceedings of the 45th Annual Environmental Engineering Conference, University of Kansas, February 1995.
- Deedar, N., Irfan A. and Ishtiaq, Q.A. (2009). Evaluation of the adsorption potential of Titanium dioxide nanoparticles for arsenic removal. Journal of Environmental Sciences., 21:402–408.
- Deniz F. and Karaman S. (2011). Removal of an azo-metal complex textile dye from colored aqueous solutions using an agro-residue. Microchemical journal, 99: 296-302
- Dong, L., Pavel, V., James, Z., Cowen, P. and Ming, L.C (2009). Iron coated pottery granules for arsenic removal from drinking water, Journal of Hazardous Materials, 168 (2-3) 626-632.
- Driehaus, W., Jekel, M., Hildebrandt, U. (1998). Granular ferric hydroxide-a new adsorbent for the removal of arsenic from natural water. Water Supply Research and Technology-Aqua. 47(1): 30-35.
- EC, Council Directive 98/83/EC/3-11-1998/ on the quality of water intended for human consumption, Off. European journal of Communication L330 (1998) 42.
- Elizalde-Gonz´alez, M.P., Mattusch, J., Wennrich, R. and Morgenstern, P. (2001). Uptake of arsenite and arsenate by clinoptilolite-rich tuffs, Microporous Mesoporous Materials, 46 (2–3) 277–286.
- Evdokimov, D.Y., Kogan, E.A. and Sheikina, Z.P. (1973). Sorption of Ge(IV) and As(III) in a fluidized bed of activated carbon modified with ferric hydroxide and tartaric acid, Zhurnal Prikladnoi Khimii, 46, 1938–1942.
- Ferguson, M.A., Hoffman, M.R. and Hering, J.G., (2005). TiO2 – photocatalysed As(III) oxidation in aqueous suspensions; reaction kinetics and effect of adsorption., Environmental Science Technologies 39: 1880-1886.

- Gaya, U.I. (2011). Comparative analysis of ZnO-catalyzed photo-oxidation of p-chlorophenols, European journal of chemistry, 2 (2) 163-167.
- Ghimire, K.N., Inoue, K., Makino, K. and Miyajima, T. (2002). Adsorptive removal of arsenic using orange juice residue, Separation Science and Technology, 37, 2785–2799.
- Gimbel, R. and Hobby R. (2000). Discharge of arsenic and heavy metals from activated carbon filters during drinking water treatment, BBR, Wasser Rohrbau, 51, 15–16
- Gonzalez, M.P.E., Mattusch, J., Einicke, W.D. and Wennrich, R. (2001). Sorption on natural solids for arsenic removal. Chemical Engineering Journal, 81: 187–195.
- Guan, H., Du, J., Meng, X., Sun, Y., Sun B. and Hu, Q. (2012). Application of titanium dioxide in arsenic removal from water: A review. Journal of Hazardous Materials 215-216(2012) 1-16.
- Ho, Y.S. and Mckay, J. (1998). A comparison of chemisorption kinetic models applied to pollutant removal on various sorbents. Institution of Chemical Engineers Trans IChemE, 76(4): 332-340.
- Ho, Y.S and ofomaja, A.E. (2006). Pseudo-second-order model for lead ion sorption from aqueous solution onto palm kernel fiber. Journal of Hazardous Materials, 129: 137-142.
- Huang, C.P. and Fu, P.L.K. (1984). Treatment of arsenic (V) containing water by the activated carbon process, Water Pollution Control Federation, 56, 233–242.
- Ihara, T., Miyoshi, M., Triyama, Y., Marsumato, O. and Sugihara, S. (2003). Visible-light-active titanium oxide photocatalyst realized by an oxygen-deficient structure and by nitrogen doping. Applied Catalysis B, 42: 403-409.
- Irie, H., Watanabe, Y. And Hashimoto, K. (2003). Nitrogen-concentration dependence on photocatalytic activity of TiO2-xNx powders. Journal of Physical Chemistry B., 107: 5483-5486.
- Islam, M. and Patel, R.K. (2007) .Evaluation of Removal efficiency of fluoride from aqueous solution using quick lime, J. Hazard. Mater. 143, 303–310.

- Jain, C. K. and Ali, I. (2000). Arsenic; occurrence, toxicity and speciation techniques. Wat. Res., 34 (17): 4304- 4312.
- Jang et al. (2006). Removal of arsenite and arsenate using hydrous ferric oxide incorporated into naturally occurring porous diatomite. Environmental Science and Technology, 40 (5): 1636-1643.
- Kabata-Pendias, A. and Pendias, H. (2000). Trace elements in soils and plants. CRC Press, Boca Raton, FL.
- Kanel, S.R., Manning, B., Charlet, L. and Choi, H. (2005). Removal of arsenic (III) from groundwater by nanoscale zero-valent iron. Environ. Sci. Technol., 39 (5) 1291– 1298.
- Kartinen, E.O. & Martin, C.J. (1995). An overview of arsenic removal processes. Desalination 103: 79–88.
- Katsoyiannis, A.I. and Zouboulis, A.I. (2002). Removal of arsenic from contaminated water sources by sorption onto iron oxide-coated polymeric materials, Water Research. 36, 5141-5155.
- Kazuo, H. and Toshio, A. (1998). Development of activated alumina for water purification, Sumitomo Kagaku, 2, 4 10.
- Kesraoui-Ouki, S., Cheeseman, C.R. and Perry, R. (1994). Natural zeolite utilization in pollution control: a review of application to metal's effluents, Journal of Chemical Technology and Biotechnology, 59, 121–126.
- Khandaker, N.R., Krumhansl, J., Neidel, L. and Siegel, M. (2006). Performance evaluation of ALCAN-AAFS-50 ferric coated activated alumina and granular ferric hydroxide (GFH) for arsenic removal in the presence of competitive ions in an active well: Kirtland field trial- initial studies. SAND2005-7693. Sandia National Laboratories.
- Khalid, N., Ahmad, S., Toheed, A. and Ahmed, J. (1998). Immobilization of arsenic on rice husk, Adsorption Science and Technology, 16: 655–666.
- Kumaresan, M. and Riyazuddin, P. (2001). Overview of speciation chemistry of arsenic. Current science, 80 (7) 837-846.
- Kunzru, S. and Chaudhuri, M. (2005). Manganese amended activated alumina for adsorption/oxidation of arsenic. J. Environ. Eng., 131(9): 1350-1353.

- Kurniawan, T.A., Chan, G.Y.S., Lo, W. and Babel, S. (2006). Comparisons of low-cost adsorbents for treating wastewaters laden with heavy metals. Science of the Total Environment. 366(2–3): 409–426.
- Lee, C.K., Low, K.S., Liew, S.C. and Choo, C.S. (1999). Removal of arsenic (V) from aqueous solution by quanternized rice husk, Environmental Technology, 20, 971–978.
- Lee, H. and Choi, W. (2002). Photocatalytic oxidation of arsenite in TiO2 suspension: kinetics and mechanisms. Environ. Sci. Technol. 36, 3872–3878.
- Leupin, O. and Hu, S.J. (2005). Oxidation and removal of arsenic (III) from aerated groundwater by filtration through sand and zero-valent iron. Water Research, 39, 1729–1740.
- Liu G. L., Zhu D. W., Liao S. J., Ren L. Y., Cui J. Z. and Zhou W. B., (2009). Solid-phase photocatalytic degradation of polyethylene–goethite composite film under UV-light irradiation, Journal of Hazardous Materials, 172 (2-3): 1424-1429.
- López, S., Castillo, S., Chávez J. and Díaz K.(2003). Síntesis y caracterización óptica, eléctrica y estructural de películas delgadas de CS2 depositadas por el método PECVD. Materia, 8: 341-9.
- Lorenzen, L., van Deventer, J.S.J. and Landi, W.M. (1995). Factors affecting the mechanism of the adsorption of arsenic species on activated carbon, Min. Eng., 8, 557–569.
- Maiti, A., DasGupta, S., Basu, J.K, and Sirshendu De (2007). Adsorption of arsenite using natural laterite as adsorbent. Separation and Purification Technology 55: 350–359.
- Mampton, F.A. (1997). Mineralogy and Geology of Natural Zeolities, Southern Printing Company, Blacksburg, VA.
- Mandal, B.K. and Suzuki, K.T. (2002). Arsenic round the world: a review. Talanta., 58 (35): 201–235.
- Manning, B.A., Fendorf, S.E., Bostick, B. and Suarez, D.L. (2000). Arsenic (III) oxidation and arsenic (V) adsorption reactions on synthetic birnessite, Environmental Science and Technology, 36 (5) 976–981.

- Manju, G.N., Raji, C. and Anirudhan, T.S. (1998). Evaluation of coconut husk carbon for the removal of arsenic from water, Water Research, 32, 3062–3070.
- Matis, K.A., Papadoyannis, I.N. and Zouboulis, A.I. (1987). Separation of germanium and arsenic ions from effluents by flotation techniques, International Journal of Mineral Processing, 21, 83–92.
- McNeill, L., Edwards, M. (1994). ” Arsenic Removal via softening “Critical Issues in Water and Wastewater treatment: National Conference on Environmental Engineering. pp 640-645.ASCE .New York.1994.
- Meng, X., Bang, S. and Korfiatis, G.P. (2000). Effects of silicate, sulfate, and carbonate on arsenic removal by ferric chloride, Water Research, 34, 1255–1261.
- Mohan, D., Charles, U. and Pittman, Jr. (2007). Arsenic removal from water/wastewater Using adsorbents—A critical review. Journal of hazardous Materials, 142: 1–53.
- Mondal, P., Majumder, C.B. and Mohanty, B. (2006). Laboratory based approaches for arsenic remediation from contaminated water: recent developments, Journal of Hazardous Material, 137: 464–479.
- Moore, J.N., Walker, J.R., Hayes, T.H. (1990). Reaction scheme for the oxidation of As(III) to arsenic(V) by birnessite, Clays and Clay Minerals, 38, 549– 555.
- Murugesan, G.S., Sathishkumar, M. and Swaminathan, K. (2006). Arsenic removal from groundwater by pretreated waste tea fungal biomass, Bioresource Technology, 97, 483–487.
- MWH 2005, Water treatment: Principal and Design, Second Edition.
- Nakamura, R., Tanaka, T. and Nakato, Y. (2004). Mechanism for visible light responses in anodic photocurrents at Ndoped TiO2 film electrodes, Journal of Physical Chemistry B., 108, 10617 – 10620.
- National Research Council (2000). Arsenic in drinking water. Washington, DC, USA, National Academy press.

- Nery JG, Mascarenhas YP & Cheetham AK (2003) A study of the highly crytelline, low silica, fully hydrated zeolite P ion exchanged with Mn, Cd, Pb, Sr, Ba) cations. Microporous and Mesoporous Materials, 57: 229–248.
- Nesbitt, H.W., Canning, G.W. and Bancroft, G.M. (1998). Geochimica et Cosmochimica Acta, 62, 2097–2110.
- Ng, K.S., Ujang, Z and Le-Clech, P. (2004). Arsenic removal technologies for drinking water treatment. Environmental Science and Bio/Technology, 3, 43-53.
- Ng, J.C., J. Wang, and A. Shraim. (2003). A global health problem caused by arsenic from natural sources. Chemosphere, 52: 1353-1359.
- Oehmen, A., Valerio, R., Llanos, J., Frandinho, J., Serra, S., Reis, A.M., Crespo, J.G and Velizarov, S. (2011). Arsenic removal from drinking water through a hybrid ion exchange membrane – Coagulation process**.** Separation and Purification Technology, 83, 137-143.
- Onishi, H., (1969). Arsenic, in: K.H. Wedepohl (Ed.), Handbook of Geochemistry, Springer Verlag, New York, Vol. II-2, Chapter-33.
- Osamu, S., Yusuke, I. and Shinji, T. (2000). Removal of arsenic by activated alumina, Suido Kyokai Zasshi, 69, 22–29.
- öztürk, N. and Kavak, D. (2005). Adsorption of boron from aqueous solutions using fly ash: Batch and column studies. Journal of Hazardous Materials, 127(1-3): 81–88.
- Pal, (2001). In Technologies for Arsenic Removal from Drinking Water; Bangladesh University of Engineering and Technology, Dhaka, The United Nations University, Tokyo: Tokyo, 2001; pp 59-68.
- Pauling, L. (1929). The principles determining the structure of complex ionic crystals. Journal of American society, 51, 1010-1026.
- Pena, M., Meng, X., Korfiatis, G.P. and Jing, C. (2006). Adsorption mechanism of arsenic on nanocrystalline Titanium dioxide. Environmental Science and Technology, 40: 1257-1262.

- Pena, M.E., Karfiatis, G.P., Patel, M., Lippincott, L. and Meng, X. (2005). Adsorption of As(V) and As(III) by nanocrystalline Titaniumdioxide. Water research, 39 2327-2337.
- Pierce, M.L. and Moore, C.B. (1982). Adsorption of arsenite and arsenate on amorphous iron hydroxide, Water Research, 16, 1247–1253.
- Pollard, S.J.T., Fowler, G.F., Sollars, C.J. and Perry, R. (1992). Low cost adsorbents for waste and wastewater treatment: A review. Science Total Environment, 116, 31– 52.
- Pulido, L.L., Hata, T., Imamura, Y., Ishihara, S. and Kajimoto, T. (1998). Removal of mercury and other metals by carbonized wood powder from aqueous solutions of their salts. Wood Science, 44, 237–243.
- Quamruzzaman Q., Rahman, M. and Asad, K.A. (2003). Effects of arsenic on health in arsenic contamination: Bangladesh perspective. Dhaka, Bangladesh, ITN-Bangladesh
- Quan, C., Khoe, G. and Bangster, D. (2001). Adsorption of sodium lauryl sulfate onto arsenic-bearing ferrihydrite, Water Research, 35, 478–484.
- Rajakovic, L.V. (1992) The sorption of arsenic onto activated carbon impregnated with metallic silver and copper, Separation Science and Technolology, 27, 1423–1433.
- Raji, C. and Anirudhan, T.S. (1999). Sorption characteristic of As(III) on surface-modified sawdust carbon, Ind. Environmental Health, 41, 184–193.
- Rasmussen, L. and Anderson, K.J. (2002). Environmental health and human exposure assessment. Available at: http://www.who.int/water_sanitation_health/dwq/arsenicun2.pdf
- Rietkerk, P. (2007). Latest Arsenic Removal Technologies for Drinking Water Applications.
- Sahoo C., Gupta A.K. and Pal A. (2005). Photocatalytic degradation of Crystal Violet (C.I. Basic Violet 3) on silver ion doped TiO2, Dyes Pigments, 66: 189-196.
- Sato Y, Kang M, Kamei T & Magara Y (2002). Performance of nanofiltration for arsenic removal. Water. Res. 36: 3371–3377.

- Shih, M.-C. (2005). An overview of arsenic removal by pressure-driven membrane processes. In: Desalination, 172 (1), p. 85-97
- Smedley, P.L., Nicolli, H.B., Macdonald, D.M.J., Barros, A.J. and Tullio, J.O. (2002). Hydrogeochemistry of arsenic and other inorganic constituents in groundwaters from La Pampa, Argentina, Applied Geochemistry, 17 (3) 259–284.
- Smedley, P.L., Edmunds, W.M., Pelig-Ba, K.B., Appleton, J.D., Fuge, R. and McCall, G.J.H. (Eds.) (1996). Environmental Geochemistry and Health, vol. 113, Geological Society Special Publication, London, 153 p.
- Smith, A.H., Hopenhayn-Rich, C., Bates M.N., Goeden, H.M., Hertz-Picciotto, I., Duggan, H.M., Wood, R., Kosnett, M.J. and Smith, M.T. (1992), Cancer risks from Arsenic in Drinking Water. Environmental Health Perspectives, 97: 259-567.
- Smith, A.H., Lingas, E.O, Rahman, M. (2000). Contamination of drinking-water by arsenic in Bangladesh: a public health emergency. Bulletin of the WHO. 78(9):1093-1103.
- Smit, B. and Krishna, R. (2003). Molecular simulation in zeolite process design. Chemical Engineering Science, 58: 557–568.
- Sorg, T. J. and Logsdon, G. S. (1978). Treatment Technology to Meet the Interim Primary Drinking Water Regulations for Inorganics: Part 2. American Water Works Association, 70 (7), 379-393.
- Sutherland, D., Kabir, M. O., Chowdhury, N. A. (2001). In Technologies for Arsenic Removal from Drinking Water; Bangladesh University of Engineering and Technology, Dhaka, The United Nations University, Tokyo; pp 190-200.
- Suzuki, T.M., Bomani, J.O., Matsunaga, H. and Yokoyama, T. (2000). Preparation of porous resin loaded with crystalline hydrous zirconium oxide and its application to the removal of arsenic, Reactive and Functional Polymer, 43, 165–172.
- Suzuki, T.M., Bomani, J.O., Matsunaga, H. and Yokoyama, T. (1997)., Removal of As(III) and As(V) by a porous spherical resin loaded with monoclinic hydrous zirconium oxide, Chemistry Letters, 26, 1119..

- S.H. Lin, C.S. Wang, (2002). Treatment of high-strength phenolic wastewater by a new two-step method, Journal of Hazardous Materials, 90: 205– 216.
- Tandon, S. and Gupta, J. (1970). Measurement of forbidden energy gap of semiconductor by diffuse reflectance technique, physica status solidi (b), 38, 363-367.
- The International Agency for Research on Cancer (1980). Monographs on the evaluation of the carcinogenic risk to humans and their supplements: Some metals and metallic compounds, vol. 23. IARC, Lyon.
- The U.S. Environmental Protection Agency (1988). Special Report on Ingested Inorganic Arsenic. Skin Cancer; Nutritional essentiality. EPA 625-3-87-013, USEPA, Washington, DC.
- Thirunavakkarasu, O.S., Viraraghavan, T. and Subramanian, K.S. (2003). Arsenic removal from drinking water using iron oxide-coated sand, Water, Air and Soil Pollution, 142, 95–111.
- Thomas, S.Y., Choong, T.G., Chuah, Y., Robiah, F.L., Koay, G. and Azni, I. (2007). Arsenic toxicity, health hazards and removal techniques from water: an overview, Desalination, 217, 139-166.
- U N (2001). UN synthesis report on arsenic in drinking water. Available at:
    - http://www.who.int/water_sanitation_health/dwq/arsenic3/en/
- UNICEF (2006). Arsenic mitigation in Bangladesh Fact Sheet. Available at:
    - http://www.unicef.org/bangladesh/Arsenic.pdf
- Valencia, S., Marin, J.M. and Restrepo, G. (2010). Study of the bandgap of synthesized Titanium dioxide nanoparticles using the sol-gel method and a hydrothermal treatment. The open material science journal, 4, 9-14.
- Wang, L., Chen, A., Fields, K. (2000). Arsenic removal from drinking water by ion exchange and activated alumina plants. EPA/600/R-00/088. United States Environmental Protection Agency, Water Supply and Water Resources Division, National Risk Management Research Laboratory, Cincinnati, Ohio.
- 'Water Quality Status' Third Report 2003-2004, Pakistan Council of Research in Water Resources (PCRWR), 2005.

- Westerhoff, P., Highfield, D., Badruzzaman, M. and Yoon, Y. (2005). Rapid small-scale column tests for arsenate removal in iron oxide packed bed columns. J. Environ. Eng. 131 (2): 262-271.
- Xu, Y.H., Nakajima, T. and Ohki (2002). Adsorption and removal of arsenic (V) from drinking water by aluminum-loaded shirasuzeolite. Journal of Hazardous Material, 92(3): 275–287.
- Yang, H., Lin, W.Y. and Rajeshwar, K. (1999). Homogeneous and heterogeneous photocatalytic reactions involving As(III) and As(V) species in aqueous media. J. Photochem. Photobiol. 123, 137–143.
- Zeng, L. (2003). A method for preparing silica-containing iron (III) oxide adsorbents for arsenic removal, Water Research, 37, 4351–4358.
- Zhang, Y., Yang, M., Dou, X.M., He, H. and Wang, D.S. (2005). Arsenate adsorption on a Fe–Ce bimetal oxide adsorbent: role of surface properties, Environmental Science and Technolology, 39 (18) 7246–7253.
- Zhang, Y., Yang, M. and Huang, X. (2003). Arsenic (V) removal with a Ce(IV)-doped iron oxide adsorbent, Chemosphere, 51, 945–952.
- Zheng, H., Han, L., Ma, H., Zheng, Y., Zhang, H., Liu, D. and Liang, S. (2008). Adsorption characteristics of ammonium ion by zeolite 13X. Journal of Hazardous Materials 158 (2-3):577–584.

APPENDICES

Appndix-I

REMOVAL EFFICIENCY OF PURE AND METAL DOPED TITANIA NANOPARTICLES

Removal efficiency

Nanoparticles	Initial conc. (mg/L)	Final Conc. (mg/L)	Amount adsorbed (mg)	Percentage removal
TiO_2	0.5	0.175	0.325	65
Ag-TiO_2	0.5	0.05	0.45	90
Cr-TiO_2	0.5	0.025	0.475	95
Fe-TiO_2	0.5	0.02	0.48	96

(Adsorbent Dose = 0.5g)

Effect of pH on Removal efficiency

Nanoparticles	pH	Initial Conc. (mg/L)	Final Conc. (mg/L)	Amount Adsorbrd (mg)	Percentage Removal
TiO2	4	0.5	0.325	0.175	35
	7	0.5	0.175	0.325	65
	10	0.5	0.425	0.075	15
Ag-T	4	0.5	0.175	0.325	65
	7	0.5	0.05	0.45	90
	10	0.5	0.315	0.185	37
Cr-TiO2	4	0.5	0.14	0.36	72
	7	0.5	0.025	0.475	95
	10	0.5	0.31	0.19	38
Fe-TiO2	4	0.5	0.125	0.375	75
	7	0.5	0.02	0.48	96
	10	0.5	0.3	0.2	40

(Adsorbent Dose = 0.5g)

Appendix-II

ADSORPTION ISOTHERMS

1. Langmuir Adsorption Isotherms

TiO_2

Initial Conc. (C_0) (mg/L)	Final Conc. (C_e)(mg/L)	Amount Adsorbed/100ml	Amount Adsorbed /L	Adsorbent Amount (g)	qe (mg/g)	Ce/qe
0.1	0.033	0.067	0.0067	0.3	0.022	1.5
0.2	0.072	0.128	0.0128	0.3	0.043	1.67
0.4	0.15	0.25	0.025	0.3	0.083	1.81
0.8	0.31	0.49	0.049	0.3	0.163	1.9
1.5	0.633	0.867	0.0867	0.3	0.289	2.19
3	1.42	1.58	0.158	0.3	0.527	2.69
6	3.3	2.7	0.27	0.3	0.9	3.67

Ag-TiO_2

Iinitial Conc. (C_o) (ppm)	Final conc. (C_e) (ppm)	Amount Adsorbed/100ml	Amount Adsorbed /L	Adsorbent Amount (g)	qe (mg/g)	Ce/qe
0.1	0.015	0.085	0.0085	0.3	0.028	0.53
0.2	0.035	0.165	0.0165	0.3	0.055	0.636
0.4	0.07	0.33	0.033	0.3	0.11	0.636
0.8	0.17	0.63	0.063	0.3	0.21	0.81
1.5	0.32	1.18	0.118	0.3	0.393	0.81
3	0.85	2.15	0.215	0.3	0.717	1.186
6	2.4	3.6	0.36	0.3	1.2	2

Cr-TiO_2

Iinitial Conc. (C_o) (ppm)	Final conc. (C_e) (ppm)	Amount Adsorbed/100ml	Amount Adsorbed/L	Adsorbent Amount (g)	qe (mg/g)	Ce/qe
0.1	0.004	0.096	0.0096	0.3	0.032	0.125
0.2	0.01	0.19	0.019	0.3	0.063	0.158
0.4	0.025	0.375	0.0375	0.3	0.125	0.2
0.8	0.055	0.745	0.0745	0.3	0.248	0.22
1.5	0.12	1.38	0.138	0.3	0.46	0.261
3	0.3	2.7	0.27	0.3	0.9	0.333
6	1	5	0.5	0.3	1.67	0.6

Fe-TiO_2

Iinitial Conc. (C_o) (ppm)	Final conc. (C_e) (ppm)	Amount Adsorbed/100ml	Amount Adsorbed/L	Adsorbent Amount (g)	qe (mg/g)	Ce/qe
0.1	0.004	0.096	0.0096	0.3	0.032	0.125
0.2	0.009	0.191	0.0191	0.3	0.0637	0.141
0.4	0.02	0.38	0.038	0.3	0.127	0.158
0.8	0.04	0.76	0.076	0.3	0.253	0.158
1.5	0.08	1.42	0.142	0.3	0.4733	0.17
3	0.2	2.8	0.28	0.3	0.933	0.2143
6	0.6	5.4	0.54	0.3	1.8	0.333

2. Freundlich Adsorption Isotherm

TiO_2

Initial Conc. (C0) (mg/L)	Final Conc. (Ce)(mg/L)	Amount Adsorbed/100ml	Amount Adsorbed/L	Adsorbent Amount (g)	qe (mg/g)	ln Ce	ln qe
0.1	0.033	0.067	0.0067	0.3	0.022	-3.41	-3.82
0.2	0.072	0.128	0.0128	0.3	0.043	-2.63	-3.15
0.4	0.15	0.25	0.025	0.3	0.083	-1.8971	-2.5
0.8	0.31	0.49	0.049	0.3	0.163	-1.171	-1.81
1.5	0.633	0.867	0.0867	0.3	0.289	-0.4573	-1.24
3	1.42	1.58	0.158	0.3	0.527	0.351	-0.64
6	3.3	2.7	0.27	0.3	0.9	1.194	-0.11

Ag-TiO_2

Iinitial Conc. (Co) (ppm)	Final conc. (Ce) (ppm)	Amount Adsorbed /100ml	Amount Adsorbed /L	Adsorbent Amount (g)	qe (mg/g)	ln Ce	ln qe
0.1	0.015	0.085	0.0085	0.3	0.0283	-4.2	-3.564
0.2	0.035	0.165	0.0165	0.3	0.055	-3.35	-2.9
0.4	0.07	0.33	0.033	0.3	0.11	-2.66	-2.21
0.8	0.17	0.63	0.063	0.3	0.21	-1.772	-1.561
1.5	0.32	1.18	0.118	0.3	0.3933	-1.14	-0.933
3	0.85	2.15	0.215	0.3	0.717	-0.163	-0.333
6	2.4	3.6	0.36	0.3	1.2	0.8755	0.182

Cr-TiO_2

Iinitial Conc. (Co) (ppm)	Final conc. (Ce) (ppm)	Amount Adsorbed /100ml	Amount Adsorbed/L	Adsorbent Amount (g)	qe (mg/g)	ln Ce	ln qe
0.1	0.004	0.096	0.0096	0.3	0.032	-5.52	-3.442
0.2	0.01	0.19	0.019	0.3	0.063	-4.61	-2.76
0.4	0.025	0.375	0.0375	0.3	0.125	-3.7	-2.08
0.8	0.055	0.745	0.0745	0.3	0.248	-2.9	-1.4
1.5	0.12	1.38	0.138	0.3	0.46	-2.12	-0.78
3	0.3	2.7	0.27	0.3	0.9	-1.2	-0.11
6	1	5	0.5	0.3	1.67	0	0.51

Fe-TiO_2

Iinitial Conc. (Co) (ppm)	Final conc. (Ce) (ppm)	Amount Adsorbed /100ml	Amount Adsorbed/L	Adsorbent Amount (g)	qe (mg/g)	lnCe	lnqe
0.1	0.004	0.096	0.0096	0.3	0.032	-5.521	-3.442
0.2	0.009	0.191	0.0191	0.3	0.064	-4.711	-2.754
0.4	0.02	0.38	0.038	0.3	0.127	-3.912	-2.066
0.8	0.04	0.76	0.076	0.3	0.253	-3.219	-1.373
1.5	0.08	1.42	0.142	0.3	0.473	-2.526	-0.748
3	0.2	2.8	0.28	0.3	0.93	-1.609	-0.069
6	0.6	5.4	0.54	0.3	1.8	-0.511	0.588

Appendix-III

ADSORPTION KINETICS

Pseudo-second Order Kinetics

TiO_2

Initial Conc. (ppm)	Time (mins)	Final Conc (ppm)	Amount adsorbed/500ml	Amount adsorbed/L	qt	t/qt
0.5	1	0.465	0.035	0.0175	0.035	28.57
0.5	3	0.4315	0.0685	0.03425	0.0685	43.8
0.5	6	0.4	0.1	0.05	0.1	60
0.5	9	0.3675	0.1325	0.06625	0.1325	67.92
0.5	12	0.342	0.158	0.079	0.158	75.95
0.5	15	0.3165	0.1835	0.09175	0.1835	81.74
0.5	20	0.2855	0.2145	0.10725	0.2145	93.24
0.5	30	0.25	0.25	0.125	0.25	120
0.5	40	0.215	0.285	0.1425	0.285	140.35
0.5	50	0.185	0.315	0.1575	0.315	158.73
0.5	60	0.16	0.34	0.17	0.34	176.47
0.5	70	0.16	0.34	0.17	0.34	205.88
0.5	80	0.155	0.345	0.1725	0.345	231.88
0.5	90	0.155	0.345	0.1725	0.345	260.87

Ag-TiO_2

Initial Conc. (ppm)	Time (mins)	Final Conc (ppm)	Amount adsorbed/500ml	Amount adsorbed/L	qt	t/qt
0.5	1	0.455	0.045	0.0225	0.045	22.22222
0.5	3	0.4	0.1	0.05	0.1	30
0.5	6	0.35	0.15	0.075	0.15	40
0.5	9	0.32	0.18	0.09	0.18	50
0.5	12	0.295	0.205	0.1025	0.205	58.53659
0.5	15	0.265	0.235	0.1175	0.235	63.82979
0.5	20	0.235	0.265	0.1325	0.265	75.4717
0.5	30	0.1825	0.3175	0.15875	0.3175	94.48819
0.5	40	0.145	0.355	0.1775	0.355	112.6761
0.5	50	0.105	0.395	0.1975	0.395	126.5823
0.5	60	0.0625	0.4375	0.21875	0.4375	137.1429
0.5	70	0.038	0.462	0.231	0.462	151.5152
0.5	80	0.0325	0.4675	0.23375	0.4675	171.123
0.5	90	0.0325	0.4675	0.23375	0.4675	192.5134

Cr-TiO_2

Initial Conc. (ppm)	Time (mins)	Final Conc (ppm)	Amount adsorbed/500ml	Amount adsorbed/L	qt	t/qt
0.5	1	0.45	0.05	0.025	0.05	20
0.5	3	0.395	0.105	0.0525	0.105	28.57
0.5	6	0.346	0.154	0.077	0.154	38.96
0.5	9	0.31	0.19	0.095	0.19	47.37
0.5	12	0.2675	0.2325	0.11625	0.2325	51.6
0.5	15	0.24	0.26	0.13	0.26	57.7
0.5	20	0.2	0.3	0.15	0.3	66.67
0.5	30	0.15	0.35	0.175	0.35	85.7
0.5	40	0.11	0.39	0.195	0.39	102.56
0.5	50	0.0725	0.4275	0.21375	0.4275	116.96
0.5	60	0.035	0.465	0.2325	0.465	129
0.5	70	0.03	0.47	0.235	0.47	148.94
0.5	80	0.02	0.48	0.24	0.48	166.67
0.5	90	0.0175	0.4825	0.24125	0.4825	186.53

Fe-TiO_2

Initial Conc. (ppm)	Time (mins)	Final Conc (ppm)	Amount adsorbed/500ml	Amount adsorbed/L	qt	t/qt
0.5	1	0.455	0.045	0.0225	0.045	22.22222
0.5	3	0.4	0.1	0.05	0.1	30
0.5	6	0.35	0.15	0.075	0.15	40
0.5	9	0.31	0.19	0.095	0.19	47.36842
0.5	12	0.27	0.23	0.115	0.23	52.17391
0.5	15	0.24	0.26	0.13	0.26	57.69231
0.5	20	0.2	0.3	0.15	0.3	66.66667
0.5	30	0.15	0.35	0.175	0.35	85.71429
0.5	40	0.1075	0.3925	0.19625	0.3925	101.9108
0.5	50	0.0675	0.4325	0.21625	0.4325	115.6069
0.5	60	0.0325	0.4675	0.23375	0.4675	128.3422
0.5	70	0.03	0.47	0.235	0.47	148.9362
0.5	80	0.02	0.48	0.24	0.48	166.6667
0.5	90	0.0108	0.4892	0.2446	0.4892	183.9738

Appendix-IV

COLUMN STUDIES

Effect of Nanoparticles Used

Time (min)	Time (hr)	C/C_o		
		TiO2	Ag	Fe
20	0.33	0.0058	0.00386	0.0022
40	0.67	0.0086	0.00574	0.0034
60	1	0.012	0.008	0.0046
80	1.33	0.017	0.01134	0.0066
100	1.67	0.0204	0.0136	0.0078
120	2	0.048	0.01866	0.0116
140	2.33	0.1	0.03466	0.0154
160	2.67	0.1286	0.06666	0.0192
180	3	0.156	0.104	0.0276
200	3.33	0.2	0.15384	0.0462
220	3.67	0.26	0.2	0.0692
240	4	0.3426	0.26354	0.1076
260	4.33	0.4036	0.31046	0.18
280	4.67	0.48	0.36924	0.22
300	5	0.56	0.43076	0.28
320	5.33	0.65	0.5	0.3372
340	5.67	0.7416	0.57048	0.392
360	6	0.8	0.6154	0.45
380	6.33	0.845	0.67	0.5
400	6.67	0.941	0.74	0.56
420	7	1	0.79	0.63
440	7.33	1.001	0.85	0.715
460	7.67	1.004	0.9	0.8
480	8	1.01	1	0.887
500	8.33		1.01	0.99
520	8.67		1.015	1.015
540	9			1.023

Effect of Bed Height

Time (min)	Time (hr)	10 cm				20 cm		30 cm		
		C/Co			C/Co			C/Co		
		TiO2	Ag	Fe	TiO2	Ag	Fe	TiO2	Ag	Fe
20	0.33	0.0058	0.00386	0.0022	0.0016	0.0013	0.001	0.0016	0	0
40	0.67	0.0086	0.00574	0.0034	0.0026	0.0174	0.0016	0.0024	0.0014	0.0006
60	1	0.012	0.008	0.0046	0.0034	0.0024	0.002	0.004	0.002	0.0016
80	1.33	0.017	0.01134	0.0066	0.0044	0.003	0.0026	0.0056	0.0026	0.0024
100	1.67	0.0204	0.0136	0.0078	0.006	0.0038	0.0032	0.007	0.0036	0.0034
120	2	0.048	0.01866	0.0116	0.008	0.0044	0.004	0.0086	0.0048	0.0042
140	2.33	0.1	0.03466	0.0154	0.0094	0.0058	0.0052	0.0126	0.006	0.0056
160	2.67	0.1286	0.06666	0.0192	0.0122	0.0076	0.0064	0.019	0.008	0.007
180	3	0.156	0.104	0.0276	0.0158	0.009	0.008	0.026	0.011	0.008
200	3.33	0.2	0.15384	0.0462	0.018	0.0116	0.01	0.04	0.014	0.0106
220	3.67	0.26	0.2	0.0692	0.026	0.015	0.012	0.06	0.018	0.0134
240	4	0.3426	0.26354	0.1076	0.036	0.0172	0.0144	0.084	0.03	0.018
260	4.33	0.4036	0.31046	0.18	0.044	0.022	0.0168	0.12	0.054	0.024
280	4.67	0.48	0.36924	0.22	0.058	0.032	0.0196	0.16	0.08	0.04
300	5	0.56	0.43076	0.28	0.0794	0.04	0.024	0.24	0.12	0.06
320	5.33	0.65	0.5	0.3372	0.114	0.054	0.03	0.2882	0.188	0.096
340	5.67	0.7416	0.57048	0.392	0.158	0.0774	0.038	0.3428	0.24	0.15
360	6	0.8	0.6154	0.45	0.192	0.108	0.052	0.4	0.3	0.2
380	6.33	0.845	0.67	0.5	0.232	0.156	0.074	0.4644	0.36	0.24
400	6.67	0.941	0.74	0.56	0.3	0.188	0.1	0.52972	0.4	0.28
420	7	1	0.79	0.63	0.36	0.228	0.15	0.571	0.46	0.344
440	7.33	1.001	0.85	0.715	0.442	0.3	0.18	0.604	0.52	0.392
460	7.67	1.004	0.9	0.8	0.536	0.364	0.22	0.672	0.549	0.452
480	8	1.01	1	0.887	0.628	0.44	0.28	0.7143	0.58	0.48
500	8.33		1.01	0.99	0.744	0.528	0.36	0.74	0.638	0.52
520	8.67		1.015	1.015	0.86	0.62	0.44	0.796	0.692	0.57
540	9			1.023	0.936	0.72	0.52	0.85	0.72	0.63
560	9.33				1.048	0.84	0.612	0.9	0.76	0.7
580	9.67				1.048	0.92	0.72	0.94	0.8	0.77
600	10				1.048	1.04	0.8	1	0.85	0.84
620	10.33					1.048	0.88	1	0.89	0.89
640	10.67					1.048	0.976	1.006	0.94	0.97
660	11						1.04	1.01	1.015	1.015
680	11.33						1.04		1.015	1.015

Effect of Flow rate

Time (min)	Time (hr)	5 ml/min			10 ml/min		
		C/C_0			C/C_0		
		TiO2	Ag	Fe	TiO2	Ag	Fe
20	0.33	0.0025	0.0016	0.0012	0.003	0.002	0.002
40	0.67	0.004	0.0026	0.002	0.006	0.004	0.003
60	1	0.0056	0.0038	0.0028	0.009	0.007	0.005
80	1.33	0.0074	0.005	0.0038	0.018	0.013	0.01
100	1.67	0.0086	0.0058	0.0044	0.038	0.019	0.017
120	2	0.014	0.0094	0.006	0.056	0.033	0.027
140	2.33	0.024	0.0126	0.01	0.1	0.057	0.05
160	2.67	0.084	0.0174	0.014	0.179	0.1	0.1
180	3	0.1116	0.036	0.0186	0.215	0.18	0.14
200	3.33	0.14286	0.064	0.036	0.277	0.231	0.2
220	3.67	0.18572	0.1054	0.068	0.369	0.308	0.272
240	4	0.2448	0.1692	0.1	0.475	0.396	0.34
260	4.33	0.2882	0.2216	0.14	0.589	0.491	0.464
280	4.67	0.3428	0.2636	0.182	0.72	0.6	0.54
300	5	0.4	0.3076	0.224	0.799	0.666	0.624
320	5.33	0.4644	0.3572	0.266	0.889	0.74	0.696
340	5.67	0.52972	0.4076	0.31	0.96	0.807	0.774
360	6	0.571	0.439	0.36	1.02	0.9	0.84
380	6.33	0.604	0.465	0.412	1.026	1	0.93
400	6.67	0.672	0.517	0.44	1.027	1.02	1.002
420	7	0.7143	0.549	0.488			1.008
440	7.33	0.74	0.58	0.536			1.014
460	7.67	0.796	0.638	0.588			
480	8	0.85	0.692	0.636			
500	8.33	0.9	0.74	0.69			
520	8.67	0.94	0.789	0.75			
540	9	1	0.84	0.81			
560	9.33	1	0.956	0.88			
580	9.67	1.006	1.01	0.95			
600	10	1.01	1.01	1.02			
620	10.333		1.015	1.03			

Effect of Influent Concentration

Time (hr)	0.25 ppm			0.5 ppm			1 ppm		
	C/C_o			C/C_o			C/C_o		
	TiO2	Ag	Fe	TiO2	Ag	Fe	TiO2	Ag	Fe
0.333	0.0007	0.00032	0.00032	0.0016	0.0013	0.001	0.0021	0.0014	0.001
0.667	0.001	0.0005	0.00048	0.0026	0.0174	0.0016	0.0032	0.0022	0.0018
1	0.00304	0.0008	0.00076	0.0034	0.0024	0.002	0.0044	0.003	0.0026
1.333	0.0036	0.001	0.00092	0.0044	0.003	0.0026	0.0058	0.004	0.0038
1.667	0.0052	0.00268	0.00216	0.006	0.0038	0.0032	0.008	0.0057	0.005
2	0.0072	0.0038	0.0034	0.008	0.0044	0.004	0.012	0.008	0.007
2.333	0.0084	0.0044	0.004	0.0094	0.0058	0.0052	0.023	0.014	0.0095
2.667	0.0104	0.0056	0.0052	0.0122	0.0076	0.0064	0.04	0.028	0.013
3	0.0128	0.0068	0.0064	0.0158	0.009	0.008	0.058	0.04	0.028
3.333	0.0156	0.008	0.008	0.018	0.0116	0.01	0.078	0.055	0.042
3.667	0.02	0.01	0.0096	0.026	0.015	0.012	0.1	0.068	0.056
4	0.026	0.0132	0.012	0.036	0.0172	0.0144	0.12	0.083	0.069
4.333	0.0348	0.0172	0.0148	0.044	0.022	0.0168	0.15	0.104	0.084
4.667	0.048	0.0244	0.02	0.058	0.032	0.0196	0.228	0.156	0.102
5	0.072	0.032	0.0248	0.0794	0.04	0.024	0.32	0.216	0.14
5.333	0.104	0.038	0.0308	0.114	0.054	0.03	0.405	0.273	0.213
5.667	0.144	0.056	0.036	0.158	0.0774	0.038	0.501	0.336	0.27
6	0.176	0.088	0.048	0.192	0.108	0.052	0.59	0.4	0.325
6.333	0.208	0.104	0.08	0.232	0.156	0.074	0.675	0.46	0.39
6.667	0.248	0.124	0.112	0.3	0.188	0.1	0.77	0.515	0.45
7	0.3	0.152	0.136	0.36	0.228	0.15	0.855	0.585	0.5
7.333	0.36	0.18	0.16	0.442	0.3	0.18	0.95	0.65	0.565
7.667	0.44	0.22	0.2	0.536	0.364	0.22	1.005	0.75	0.63
8	0.528	0.268	0.244	0.628	0.44	0.28	1.005	0.85	0.7
8.333	0.6	0.304	0.288	0.744	0.528	0.36		0.95	0.8
8.667	0.672	0.348	0.328	0.86	0.62	0.44		1.025	0.95
9	0.76	0.388	0.376	0.936	0.72	0.52		1.025	1.025
9.333	0.8	0.44	0.424	1.048	0.84	0.612		1.025	1.025
9.667	0.88	0.48	0.464	1.048	0.92	0.72			1.025
10	0.96	0.52	0.504	1.048	1.04	0.8			
10.333	1.016	0.576	0.56		1.048	0.88			
10.667	1.016	0.68	0.64		1.048	0.976			
11	1.032	0.8	0.736			1.04			
11.333		0.928	0.848			1.04			
11.667		1	0.928			1.056			
12		1	1.016						
12.333		1.008	1.016						

COLUMN MODELS

THOMAS MODEL

Thomas Model parameters for TiO_2 Coated Glass beads

Initial conc. C_o (ppm)	Bed Volumes	Time (min)	Time (hr)	Final Conc. C (ppm)	C/Co	ln(Co/Ce-1)
0.5	5	30	0.5	0.0008	0.0016	6.44
0.5	10	60	1	0.0012	0.0024	6.03
0.5	15	90	1.5	0.002	0.004	5.52
0.5	20	120	2	0.0028	0.0056	5.18
0.5	25	150	2.5	0.0035	0.007	4.95
0.5	30	180	3	0.0043	0.0086	4.75
0.5	35	210	3.5	0.0063	0.0126	4.36
0.5	40	240	4	0.0095	0.019	3.94
0.5	45	270	4.5	0.013	0.026	3.62
0.5	50	300	5	0.02	0.04	3.18
0.5	55	330	5.5	0.03	0.06	2.75
0.5	60	360	6	0.042	0.084	2.39
0.5	65	390	6.5	0.06	0.12	1.99
0.5	70	420	7	0.08	0.16	1.66
0.5	75	450	7.5	0.12	0.24	1.15
0.5	80	480	8	0.1441	0.2882	0.9
0.5	85	510	8.5	0.1714	0.3428	0.65
0.5	90	540	9	0.2	0.4	0.41
0.5	95	570	9.5	0.2322	0.4644	0.14
0.5	100	600	10	0.26486	0.52972	-0.12
0.5	105	630	10.5	0.2855	0.571	-0.29
0.5	110	660	11	0.302	0.604	-0.42
0.5	115	690	11.5	0.336	0.672	-0.72
0.5	120	720	12	0.35715	0.7143	-0.92
0.5	125	750	12.5	0.37	0.74	-1.05
0.5	130	780	13	0.398	0.796	-1.36
0.5	135	810	13.5	0.425	0.85	-1.73
0.5	140	840	14	0.45	0.9	-2.2
0.5	145	870	14.5	0.47	0.94	-2.75

Thomas Model parameters for Ag-TiO_2 Coated Glass beads

Initial conc. Co (ppm)	Bed Volumes	Time (min)	Time (hr)	Final Conc. C (ppm)	C/Co	ln(Co/Ce-1)
0.5	5	30	0.333	0	0	#DIV/0!
0.5	10	60	0.667	0.0007	0.0014	6.569882061
0.5	15	90	1	0.001	0.002	6.212606096
0.5	20	120	1.333	0.0013	0.0026	5.949640448
0.5	25	150	1.667	0.0018	0.0036	5.623214938
0.5	30	180	2	0.0024	0.0048	5.334327804
0.5	35	210	2.333	0.003	0.006	5.109977737
0.5	40	240	2.667	0.004	0.008	4.820281566
0.5	45	270	3	0.0055	0.011	4.498799059
0.5	50	300	3.333	0.007	0.014	4.254599025
0.5	55	330	5.5	0.009	0.018	3.99921955
0.5	60	360	6	0.015	0.03	3.47609869
0.5	65	390	6.5	0.027	0.054	2.863258522
0.5	70	420	7	0.04	0.08	2.442347035
0.5	75	450	7.5	0.06	0.12	1.992430165
0.5	80	480	8	0.094	0.188	1.463058377
0.5	85	510	8.5	0.12	0.24	1.15267951
0.5	90	540	9	0.15	0.3	0.84729786
0.5	95	570	9.5	0.18	0.36	0.575364145
0.5	100	600	10	0.2	0.4	0.405465108
0.5	105	630	10.5	0.23	0.46	0.16034265
0.5	110	660	11	0.26	0.52	-0.080042708
0.5	115	690	11.5	0.285	0.57	-0.281851152
0.5	120	720	12	0.305	0.61	-0.447312218
0.5	125	750	12.5	0.33	0.66	-0.663294217
0.5	130	780	13	0.36	0.72	-0.944461609
0.5	135	810	13.5	0.38	0.76	-1.15267951
0.5	140	840	14	0.4	0.8	-1.386294361
0.5	145	870	14.5	0.425	0.85	-1.734601055
0.5	150	900	15	0.445	0.89	-2.090741097
0.5	155	930	15.5	0.47	0.94	-2.751535313

Thomas Model parameters for Fe-TiO_2 Coated Glass beads

Initial conc. Co (ppm)	Bed Volumes	Time (min)	Time (hr)	Final Conc. C (ppm)	C/Co	ln(Co/C -1)
0.5	5	30	0.5	0	0	7.417980723
0.5	10	60	1	0.0003	0.0006	6.436150368
0.5	15	90	1.5	0.0008	0.0016	6.029883657
0.5	20	120	2	0.0012	0.0024	5.680574054
0.5	25	150	2.5	0.0017	0.0034	5.468461909
0.5	30	180	3	0.0021	0.0042	5.179372942
0.5	35	210	3.5	0.0028	0.0056	4.954820515
0.5	40	240	2.667	0.0035	0.007	4.820281566
0.5	45	270	3	0.004	0.008	4.536244698
0.5	50	300	3.333	0.0053	0.0106	4.299009982
0.5	55	330	5.5	0.0067	0.0134	3.99921955
0.5	60	360	6	0.009	0.018	3.705408756
0.5	65	390	6.5	0.012	0.024	3.17805383
0.5	70	420	7	0.02	0.04	2.751535313
0.5	75	450	7.5	0.03	0.06	2.242481169
0.5	80	480	8	0.048	0.096	1.815289967
0.5	85	510	8.5	0.07	0.14	1.50285565
0.5	90	540	9	0.091	0.182	1.265666373
0.5	95	570	9.5	0.11	0.22	0.944461609
0.5	100	600	10	0.14	0.28	0.645519132
0.5	105	630	10.5	0.172	0.344	0.438913042
0.5	110	660	11	0.196	0.392	0.192593107
0.5	115	690	11.5	0.226	0.452	0.080042708
0.5	120	720	12	0.24	0.48	-0.16034265
0.5	125	750	12.5	0.27	0.54	-0.405465108
0.5	130	780	13	0.3	0.6	-0.663294217
0.5	135	810	13.5	0.33	0.66	-0.944461609
0.5	140	840	14	0.36	0.72	-1.208311206
0.5	145	870	14.5	0.385	0.77	-1.658228077
0.5	150	900	15	0.42	0.84	-2.090741097
0.5	155	930	15.5	0.445	0.89	-3.47609869
0.5	160	960	16	0.485	0.97	
0.5	165	990	16.5	0.5075	1.015	
0.5	170	1020	17	0.5075	1.015	

YOON-NELSON MODEL

Yoon-Nelson Model parameters for TiO_2 Coated Glass beads

Initial conc. Co (ppm)	Bed Volumes	Time (min)	Time (hr)	Final Conc. C (ppm)	C/Co	ln(Ce/(Co-Ce))
1	10	10	0.167	0.00697	0.00697	-4.95914565
1	20	20	0.333	0.01046	0.01046	-4.54968173
1	30	30	0.5	0.05	0.05	-2.944438979
1	40	40	0.667	0.08	0.08	-2.442347035
1	50	50	0.833	0.13	0.13	-1.900958761
1	60	60	1	0.2	0.2	-1.386294361
1	70	70	1.167	0.3	0.3	-0.84729786
1	80	80	1.333	0.44	0.44	-0.241162057
1	90	90	1.5	0.6	0.6	0.405465108
1	100	100	1.667	0.75	0.75	1.098612289
1	110	110	1.833	0.84	0.84	1.658228077
1	120	120	2	0.95	0.95	2.944438979
1	130	130	2.167	1	1	
1	140	140	2.333	1.06	1.06	
1	150	150	2.5	1.09	1.09	
1	160	160	2.667	1.09	1.09	

Yoon-Nelson Model parameters for Ag-TiO_2 Coated Glass beads

Initial conc. Co (ppm)	Bed Volumes	Time (min)	Time (hr)	Final Conc. C (ppm)	C/Co	ln(Ce/(Co-Ce))
1	10	10	0.167	0.00465	0.00465	-5.366227215
1	20	20	0.333	0.00697	0.00697	-4.95914565
1	30	30	0.5	0.025	0.025	-3.663561646
1	40	40	0.667	0.054	0.054	-2.863258522
1	50	50	0.833	0.095	0.095	-2.254058052
1	60	60	1	0.147	0.147	-1.758326961
1	70	70	1.167	0.22	0.22	-1.265666373
1	80	80	1.333	0.3077	0.3077	-0.810894105
1	90	90	1.5	0.45	0.45	-0.200670695
1	100	100	1.667	0.54231	0.54231	0.169645695
1	110	110	1.833	0.65	0.65	0.619039208
1	120	120	2	0.76	0.76	1.15267951
1	130	130	2.167	0.86	0.86	1.815289967
1	140	140	2.333	0.932	0.932	2.61782511
1	150	150	2.5	1.05	1.05	
1	160	160	2.667	1.0505	1.0505	
1	170	170	2.833	1.055	1.055	

Yoon-Nelson Model parameters for Fe-TiO_2 Coated Glass beads

Initial conc. Co (ppm)	Bed Volumes	Time (min)	Time (hr)	Final Conc. C (ppm)	C/Co	ln(Ce/(Co-Ce))
1	10	10	0.167	0.0041	0.0041	-5.492659877
1	20	20	0.333	0.0062	0.0062	-5.076986687
1	30	30	0.5	0.024	0.024	-3.705408756
1	40	40	0.667	0.05	0.05	-2.944438979
1	50	50	0.833	0.085	0.085	-2.376272809
1	60	60	1	0.12	0.12	-1.992430165
1	70	70	1.167	0.18	0.18	-1.516347489
1	80	80	1.333	0.25	0.25	-1.098612289
1	90	90	1.5	0.315	0.315	-0.776846199
1	100	100	1.667	0.39	0.39	-0.447312218
1	110	110	1.833	0.5	0.5	0
1	120	120	2	0.6	0.6	0.405465108
1	130	130	2.167	0.69	0.69	0.8001193
1	140	140	2.333	0.795	0.795	1.355332136
1	150	150	2.5	0.875	0.875	1.945910149
1	160	160	2.667	0.945	0.945	2.843851742
1	170	170	2.833	1.005	1.005	
1	180	180	3	1.016	1.016	
1	190	190	3.167	1.016	1.016	
1	200	200	3.333	1.016	1.016	